Structure prediction of lithium, calcium carbide, and (per)nitride compounds at ambient and high pressure on the ab-initio level

Aniket Kulkarni

Max-Planck-Institut für Festkörperforschung

Stuttgart

Dissertation an der Universität Stuttgart
Stuttgart

July 2012

Structure prediction of lithium, calcium carbide, and (per)nitride compounds at ambient and high pressure on the ab-initio level

Von der Fakultät Chemie der Universität Stuttgart
zur Erlangung der Würde eines
Doktors der Naturwissenschaften (Dr. rer. nat.)
genehmigte Abhandlung

Vorgelegt von
Aniket Kulkarni
aus Maharashtra, Indien

Hauptberichter:	Prof. Dr. Martin Jansen
Mitberichter:	Priv.-Doz. Dr. Klaus Doll
Prüfungsvorsitzender:	Prof. Dr. Thomas Schleid

Tag der mündlichen Prüfung: 23.07.2012

Max-Planck-Institut für Festkörperforschung, Stuttgart 2012

To my loving family and friends

Acknowledgements

This thesis would not be possible without the help and support of many people. Firstly, I would like to thank my supervisor, ***Prof. Dr. Dr. h. c. M. Jansen****, for giving me the opportunity to work in his research group, providing me with the necessary financial support and his keen interest in my research. I have greatly been influence by his way of presenting basic chemical concepts and deep and wide scientific knowledge. I am grateful to get involved with him for short discussion sessions during basic seminars on Solid State Chemistry.*

I have worked under the guidance of ***Priv.-Doz. Dr. Klaus Doll*** *and* ***Prof. Dr. J. C. Schön*** *during my Ph. D. I would like to thank them whole-heartedly for their support, patience, finding interesting projects for me, their feedback on my research and readiness for discussions, as well as for a careful reading of my dissertation. Furthermore, I thank* ***Prof. Dr. Thomas Schleid*** *and* ***Prof. Dr. K. Doll*** *for being coexaminers.*

I would like to thank Dr. D. V. K. Prasad for his help in theoretical calculations and discussions on various scientific problems.

I became fascinated about computer programming, when I was doing my bachelor degree. I want to give thanks to those lectures, ***Dr. Alvani*** *and* ***Dr. Mahamuni*** *(Fergusson college, Pune). During my master, I was attracted towards theoretical physics because of* ***Prof. Dr. D. G. Kanhere****,* ***Prof. Dr. Kshirsagar****, and* ***Prof. Dr. Pathak*** *(Pune University). And I would like to thank* ***Prof. Dr. P. S. Joag*** *who guided me during my master's project. I want to thank* ***Prof. Dr. Swapan K. Pati*** *with whom I worked as a research and development assistant at JNCASR, Bangalore.*

I thank my friends who encouraged me all the time. Thanks belong to friends from Pune University: ***Sandip****,* ***Hemant Dixit****,* ***Parimal****,* ***Chai-***

tanya, ***Mandar***, ***Kshemina***, ***Hemant Rajopadhye***, ***Harshal***, ***Vilas***, ***Prasanna***, ***Pallavi***, ***Pradeep***, *&* ***Gayatri***. *Thanks also belong to friends from the MPI:* ***Dr. Wedig***, ***Nico***, ***Philippe***, ***Vinod***, ***Sridhar***, ***Andreas***, ***Benjamin***, ***Manish***, ***Dejan***, ***Jelena***, ***Ilya***, ***Naveed***, ***Avijit***, ***Katerina***, ***Vania***, ***Ralph***, ***Ramli***, ***Kiran***, ***Roby***, ***Sairam***, ***Ulrike***, ***Gayatri***, *&* ***Nitin***. *Special thanks go to* ***Sabine*** *for assistance with dealing with bureaucracy. And thanks belong to friends from Stuttgart:* ***Vishal***, ***Amod***, ***Milind***, ***Ajay***, ***Deepa***, ***Aditi***, ***Hemant***, ***Bageshree***, ***Sushant***, ***Amogh***, ***Amol***, ***Sonali***, ***Rainer***, ***Nick***, ***David***, *&* ***Sebastian***.

*I have to say special thanks to my family for their enormous patience and constant support. Many thanks to my father (****Arvind****), my mother (****Asawari****), my brother (****Asit****) and his family (****Medha***, ***Soham***, *&* ***Simran****) for their support and encouragement.*

Contents

List of Figures xi

List of Tables xiii

Notation xv

Zusammenfassung xxi

I Introduction 1

1 Introduction 3
- 1.1 Introduction . . . 3
  - 1.1.1 Outline . . . 5

II Theoretical background 7

2 Exploration of the Energy Landscape for solids 9
- 2.1 Energy Landscape . . . 9
  - 2.1.1 Introduction . . . 9
  - 2.1.2 Algorithms for global optimization . . . 14
    - 2.1.2.1 Exploration of local minima . . . 15
    - 2.1.2.2 Simulated annealing . . . 17
    - 2.1.2.3 Taboo search . . . 18
    - 2.1.2.4 Lid-based optimization . . . 18
    - 2.1.2.5 Gradient-based methods . . . 19
    - 2.1.2.6 Genetic algorithms . . . 19
  - 2.1.3 Exploration of the barrier structure . . . 20
    - 2.1.3.1 Threshold algorithm . . . 20
    - 2.1.3.2 Saddle point analysis . . . 20
    - 2.1.3.3 Free energy . . . 21

3 Electronic structure calculations **23**
3.1 Quantum mechanics . . . 23
3.1.1 Introduction . . . 23
3.1.2 Hamiltonian . . . 24
3.2 Hartree-Fock method . . . 25
3.2.1 Hartree-Fock algorithm . . . 26
3.3 Density Functional Theory (DFT) . . . 28
3.3.1 Exchange-Correlation Functional . . . 30
3.4 Basis sets . . . 30
3.4.1 Basis sets types . . . 31
3.4.1.1 Slater and Gaussian Type Orbitals . . . 31
3.4.2 Plane Waves . . . 32
3.4.2.1 Orthogonalized plane waves (OPW) . . . 32
3.4.2.2 The Muffin-tin potential . . . 33
3.4.2.3 The Augmented plane-wave method (APW) . . . 33
3.4.3 Effective Core Potentials . . . 34
3.5 Methods used to estimate atomic charges in crystal structures . . . 35
3.5.1 Mulliken population analysis . . . 35
3.5.2 Bader charge analysis . . . 36
3.6 Lattice dynamics and thermodynamic properties . . . 36
3.6.1 Lattice Dynamics . . . 36
3.6.1.1 Theoretical formulation of Lattice Dynamics . . . 36
3.6.2 Phonons . . . 38

III Methods **41**

4 Method **43**
4.1 Introduction . . . 43
4.2 The modular approach . . . 43
4.3 Exploration procedures . . . 44
4.3.1 The global landscape: Global optimization using stochastic simulated annealing . . . 44
4.3.2 Ab-initio energy calculations . . . 46
4.3.2.1 CRYSTAL . . . 46
4.3.2.2 VASP . . . 47
4.3.3 Properties related to the total energy . . . 47
4.3.3.1 Equation of state (EOS) and phase transitions . . . 48
4.3.3.2 Transition pressure . . . 49
4.3.3.3 Phonon Calculations . . . 50
4.3.3.4 Theory: Finite displacement method for computing force constants . . . 52

5 New Developments **53**
5.1 Introduction . . . 53
5.1.1 Calculation using VASP . . . 54

IV Application to binary and elemental solids 55

6 Lithium 57
6.1 Introduction 57
6.2 Methods 60
6.2.1 Details of the energy calculation at standard pressure 60
6.2.2 Details of the energy calculation at high pressure 61
6.3 Results and Discussion 61
6.3.1 Standard pressure 61
6.3.2 High pressure 67
6.4 Conclusion 68

7 Calcium carbide 69
7.1 Introduction 69
7.2 Details for the global search 70
7.2.1 Description of basis set and pseudopotential 71
7.2.2 Local optimization 71
7.2.2.1 Energy calculations 71
7.3 Results 72
7.3.1 Standard pressure 72
7.3.2 Global search on elevated pressure 77
7.4 Discussion 78
7.4.1 Comparison with experiment 78
7.4.2 Analyses of the barrier structures 81
7.4.3 Comparison with CaC_2 candidates derived from common $A(X_2)$-structure types 81
7.5 Analysis of the performance of the global optimization procedure . . . 83
7.6 Conclusions 87

8 Pernitride compounds 89
8.1 Introduction 89
8.2 Method 91
8.3 Results 92
8.3.1 SrN_2 92
8.3.2 BaN_2 93
8.3.3 CaN_2 99
8.3.4 LaN_2 99
8.3.5 TiN_2 110
8.4 Discussion 110
8.4.1 Information gained from local optimizations of structure candidates derived from known AX_2-structure types 110
8.4.2 Comparison among Metal Pernitrides 113
8.4.2.1 Bond length of the N_2-unit 116
8.4.2.2 Trends of binding energies 116
8.4.2.3 Electronic density of states for the TiN_2 modifications 118
8.5 Conclusions 119

V Summary 121

9 Summary 123

References 127

VI Appendix 147

A Ionic radii 149

B Basis set for lithium and carbon 151

C Pseudopotential for Calcium 153

D List of publications 155

VII Formalia 157

List of Figures

2.1 Schematic representation of the energy landscape for a simple system with one species of atom 10
2.2 Topographical representation of 3N-dimensional landscape projected on two dimension. 13
2.3 Classification of optimization algorithms 16
2.4 Saddle point on a cut through the configuration space. 21

3.1 Simplified Hartree-Fock procedural flowchart. 27

4.1 Modular approach - procedural flowchart. 45
4.2 Flowchart for phonon calculation using Phonopy 51

6.1 (Proposed) Phase diagram of lithium over a wide pressure-temperature range. 59
6.2 The diagram shows the different modifications in the pressure range 50 - 120 GPa. 59
6.3 Enthalpy as a function of the diffuse sp exponent of the basis set for the fcc structure versus the pressure. The calculations were performed on the LDA level. 61
6.4 A15 structure for lithium. Light green spheres correspond to Li1 atoms and dark green spheres to Li2 atoms. 62
6.5 $E(V)$ curves for the structures in table 7.1, on the LDA level 65
6.6 Phonon dispersion spectrum for lithium-A15 structure 66
6.7 Calculated band structure and electronic density of states of lithium-A15 modification, on the LDA level 66
6.8 E(V) for known modification and cI16. The calculations were performed on the LDA level 67
6.9 Change of fractional coordinate as a function of the lattice constant for the cI16 structure. The calculations were performed on the LDA level . 68

7.1 Experimentally known low-temperature modifications of CaC_2. (a) CaC_2-I (experimental + predicted), (b) CaC_2-II, and (c) CaC_2-III. Blue (big) spheres correspond to calcium, yellow (small) spheres to carbon atoms, respectively. The lines indicate the unit cells, with the z-axis pointing upwards. The label 'side-on' ('end-on') marks the C_2-dimer which is a side-on (end-on) neighbor of the central Ca atom. 72

7.2 Newly predicted low-temperature modifications of CaC_2. For notation c.f. Fig. 7.1. Modifications (a) CaC_2-V and (b) CaC_2-VI are low-pressure modifications; (c) CaC_2-VII is a high-pressure modification. . . 75
7.3 E(V)-curves of the most relevant structures, at the LDA and B3LYP level. Energies per formula unit are given in hartree (E_h). 79
7.4 Enthalpies per formula unit of the most relevant structures, at the LDA and B3LYP level. Inset upper left: high pressure range; inset lower right: standard pressure range. 80
7.5 (a) Definition of the tilt angles θ and ϕ. (b) Rotation of the C_2-unit starting in the CaC_2-I-configuration. The curve shows the energy per formula unit after tilting the C_2-dumbbell by an angle ϕ (ϕ=0°, 10°, 20°, 30°, 40° and 45°) and rotating by an angle θ through 180°, and subsequently performing a local optimization. Three ranges of θ can be distinguished, [0°, 2°], [10°, 50°] and [60°, 90°], belonging to the basins of the CaC_2-I-, CaC_2-VI- and the CaC_2-V-modification. Note that the value of ϕ does not influence the outcome of the local minimization. . . 82
7.6 Enthalpy per formula unit of the three most relevant structures found during the global search and three additional ones based on well-known structure types, at the LDA level. Inset: upper left: 3 to 6 GPa; middle: 6 to 8 GPa; lower right: 23 to 26 GPa. 85

8.1 Experimentally known modifications of AN_2, where A is the cation (Sr, Ba, Ca, La, and Ti). (a) CaC_2-I and (b) CaC_2-II. Green (big) spheres correspond to metal, blue (small) spheres to nitrogen atoms, respectively. The lines indicate the unit cells, with the z-axis pointing upwards. 94
8.2 Predicted modifications for AN_2, where A is the cation (Sr, Ba, Ca, La, and Ti). (a) MgC_2-I and (b) CaC_2-V. Green (big) spheres correspond to metal, blue (small) spheres to nitrogen atoms, respectively. The lines indicate the unit cells, with the z-axis pointing upwards. 95
8.3 $E(V)$-curves of SrN_2 at (a) GGA and (b) PBE level. Energies per formula unit are represented in eV. 97
8.4 $H(p)$-curves of SrN_2 at (a) GGA and (b) PBE level. Energies per formula unit are represented in eV. 98
8.5 (a) E(V) and (b) H(p)-curves for the important structures of BaN_2 at PBE level. Energies per formula unit are represented in eV. 102
8.6 (a) E(V) and (b) H(p)-curves for the important structures of CaN_2 at PBE level. Energies per formula unit are represented in eV. 105
8.7 (a) E(V) and (b) H(p)-curves for the important structures of LaN_2 at PBE level. Energies per formula unit are represented in eV. 109
8.8 Predicted modifications for TiN_2. In the text, it is termed as TiN_2-I. Green (big) spheres correspond to titanium, blue (small) spheres to nitrogen atoms, respectively. 113
8.9 Density of states for TiN_2 at PBE level for (a)TiN_2-I and (b)CaC_2-V-modification. The total density of states is indicated by the red curve. And the contribution of the titanium atom is given as a shaded green area whereas nitrogen is displayed by the blue curve. 114
8.10 (a) E(V) and (b) H(p)-curves for the important structures of TiN_2 at PBE level. Energies per formula unit are represented in eV. 115

List of Tables

4.1 First and second order derivatives of the total energy. 48

6.1 Total energies at zero pressure of the relaxed structures of the most relevant modifications found and their statistics of occurrence during the global optimization. Energies are in hartree units (1 E_h=27.2114 eV), per atom. For comparison, the 9R^a structure is also shown. 62
6.2 Statistics of structures found at standard and high pressure 63
6.3 Interatomic Li-Li distances [Å] and volumes [Å^3] per atom of the known modifications and A15 at ambient conditions after local optimization on the LDA level. Energy and volume are given per atom. 64

7.1 Total energies at zero pressure of the relaxed structures of the most important modifications found and their statistics of occurrence during the global optimization. Energies are in hartree units (1 E_h=27.2114 eV), per formula unit. A run is termed as successful, if it reaches a stable local minimum structure. Out of 227 runs at standard pressure 54 were successful. Similarly, among the 104 runs at elevated pressures, there were 39 successful runs. 73
7.2 The energetically most favorable structures in the CaC_2-system, plus several structures at higher energy derived from well-known structure types. 74
7.3 Interatomic C-C distances[Å] and volumes[Å^3] per formula unit of the most relevant modifications after local optimization on the LDA level, at standard pressure. 75
7.4 Interatomic distances[Å] between Ca and C atoms in the CaC_2-I, -II, -III, -V, -VI, and -VII modifications, with different types of coordination of Ca by C_2-dumbbells at zero pressure after local optimization on the LDA level. 76
7.5 Optimization of crystal structures taken from ICSD. Complex anions and cations were replaced by C_2-units and Ca-atoms, respectively. These modified structures were locally optimized using LDA. It was checked, whether the relaxed structure exhibited Ca_6-octahedra around the C_2-dumbbells. 84
7.6 Statistical analysis at different pressures 86

8.1 Energetically most stable structures which are derived from well-known structure types for SrN_2 on the PBE level. 93

8.2 Optimization of crystal structures taken from ICSD for SrN_2 with AB_2 structure type on the PBE level. The lowest energies are displayed by boldfaces. 96
8.3 Energetically most stable structures which are derived from well-known structure types for BaN_2 on the PBE level. 100
8.4 Optimization of crystal structures taken from ICSD for BaN_2 with AB_2 structure type on the PBE level. The lowest energies are displayed by boldfaces. 101
8.5 The statistics of the most relevant modifications during the global optimization at various pressures. 103
8.6 Optimization of crystal structures taken from ICSD for CaN_2 with AB_2 structure type on the PBE level. The lowest energies are displayed by boldfaces. 104
8.7 Energetically most stable structures in CaN_2 and some more structures which are derived from well-known structure types on the PBE level. . 106
8.8 Energetically most stable structures in LaN_2 and some more structures which are derived from well-known structure types on the PBE level. . 107
8.9 Optimization of crystal structures taken from ICSD for LaN_2 with AB_2 structure type on the PBE level. The lowest energies are displayed by boldfaces. 108
8.10 Energetically most stable structures in TiN_2 and some more structures which are derived from well-known structure types on the PBE level. . 111
8.11 Optimization of crystal structures taken from ICSD for TiN_2 with AB_2 structure type on the PBE level. The lowest energies are displayed by boldfaces. 112
8.12 Bulk modulus for various metal pernitrides on PBE and GGA level . . 117
8.13 Binding Energy in eV per formula unit on PBE level for MN_2 (where M = Sr, Ba, Ca, La, and Ti) 118

A.1 Ionic radii and ionization potential for lithium and calcium as function of charge. 149
A.2 Ionic radii and ionization potential for carbon, nitrogen, lanthanum, and titanium as function of charge. 150

B.1 Besis set for lithium in CRYSTAL09 input format 151
B.2 Besis set for carbon 152

C.1 Pseudopotential for carbon in CRYSTAL09 input format 153

Notation

Physical Constants

Symbol	Meaning	Unit
c	speed of light in vacuum	299792458 ms^{-1}
ε_0	permittivity of free space	8.854187817$\times$10^{-12} Fm^{-1}
e	elementary charge (of proton)	1.60217733(49)$\times$10^{-19} C
a_0	Bohr radius	5.29177249(24)$\times$10^{-11} m
k_B	Boltzman constant	1.380658(12)$\times$10^{-23} J/K
$\hbar = \frac{h}{2\pi}$	Planck constant divided by 2π	1.054571726(47)$\times$10^{-34} Js
R_∞	Rydberg constant	10973731.568549(83) m^{-1}
N_A	Avogadro constant	6.0221367(36)$\times$10^{23} mol^{-1}
R	molar gas constant	8.314510(70) J/K mol

Energy Equivalents

Symbol	Meaning	Unit
E_h	Hartree energy $= \frac{e^2}{4\pi\varepsilon_0 a_0} = 2R_\infty hc$	4.3597482(26)$\times$10^{-18} J
		2.6255000$\times$10^{6} J/mol
		27.211652 eV
		627.51$\times$10^{3} Calories/mol
eV	electron volt	1.60217646$\times$10^{-19} J
$\frac{eV}{k_B}$	eV divided by Boltzman's constant	11605 K

Acronyms

Symbol	Meaning
AO	Atomic Orbital
AEBS	All electron basis set
APW	Augmented plane-wave method
BF	Bloch Function
BSSE	Basis Set Superposition Error
BZ	Brillouion Zone (first)
B3LYP	Becke 3-Parameter functional, with Lee-Yang-Parr correlation
CMPZ	”CoMPare Zellen” (= compare cells)
DFT	Density Functional Theory
DOS	Density of States
ECP	Effective Core Potential
GGA	Generalized Gradient Approximation
EOS	Equation of states
GTO	Gaussian Type Orbital
KS	Kohn and Sham
HF	Hartree-Fock
LCAO	Linear Combination of Atomic Orbitals
LDA	Local Density Approximation
LYP	Lee-Yang-Parr GGA
OPW	Orthogonalized plane waves
PAW	Projector-augmented wave
PBE	Perdew-Burke-Ernzerhof exchange and correlation
PPBS	Pseudopotential basis set
PW	Plane Wave
PW91	Perdew-Wang functional
PWGGA	Perdew-Wang GGA
PZ	Perdew-Zunger correlation
QM	Quantum Mechanics
RGS	”RaumGruppenSucher” (= space group searcher)
RHF	Restricted HF
ROHF	Restricted Open-shell HF
UHF	Unrestricted HF
SCF	Self-Consistent-Field
SFND	”SymmetrieFiNDer” (= symmetry finder)
STO	Slater Type Orbital
VBH	von Barth-Hedin
VWN	Vosko-Wilk-Nusair correlation

Abstract

In recent years, new theoretical methodologies and techniques have become available to explore the energy landscape of chemical systems. Furthermore, experimental solid state chemistry has opened new opportunities by advances in controlling synthesis routes, for example by low-temperature atom beam deposition or physical vapor deposition. Furthermore, there have been advancements in measurement techniques such as in-situ measurements, scanning tunneling microscopy, scanning electron microscopy, and transmission electron microscopy at low temperature. Still, it is quite difficult to understand structural changes at standard and extreme conditions. Often, it is impossible to understand structural changes without assistance from theoretical simulations. Sometimes it is advantageous to predict structures before the actual synthesis, because it can give more insight for deciding upon the synthesis route, and by knowing the structure, one can simulate its physical properties. Due to the knowledge of the system and its interesting properties beforehand, one can synthesize the chemical compound and validate the predictions. Crystal structure prediction requires the exploration of the energy landscape of the respective system. These prediction methods are mainly based on the fact, that stable and metastable modifications of chemical systems correspond to locally ergodic regions of the energy landscape. At low temperature, individual minima can be locally ergodic, if they are separated by sufficiently high barriers. Usually, there may exist many such locally ergodic regions encompassing one or several local minima. The latter case is most important, if some of the sites in the structures are only partially occupied, or occupied in a disordered fashion.

The aim of the present research is to predict possible crystalline structures including already observed ones as well as hypothetical new ones. The structure prediction procedure consists of two steps: the first step is the global search for possible structure candidates at various pressures on the *ab-initio* level, which is followed by the second step, a local optimization. All the energies were evaluated on the *ab-initio level* (i.e. during both the global and the local optimization). Earlier, model potentials had been used, e.g. Born-Mayer potentials. These potentials have the disadvantage of being biased towards a certain chemical bond, e.g. an ionic bond, but have difficulties to describe situations such as covalent or metallic bonds. *Ab-initio* calculations are much more general, and require less empirical input. The bond type and the charge distribution are not predefined, but are determined in the calculation. The disadvantage is that these calculations are by orders of magnitude more computationally expensive than calculations with model potentials. Up to now, only few systems have been studied by employing

ab-initio energies from e.g. the CRYSTAL code which is based on Gaussian type orbitals. In this research work, we additionally created an interface for the VASP code (Vienna Ab-initio Simulation Package), where the *ab-initio* energy calculations are based on plane waves. With the interface to VASP, the choice of basis sets is simplified, and convergence problems during the self-consistent field procedure are less severe, compared to CRYSTAL.

The goal of this thesis is to use existing energy landscape algorithms and to couple them with various *ab-initio* simulation methods, in order to predict the crystal structure. When the structure of the possible (meta)stable solid compounds is determined, then subsequently their physical and electronic properties can be computed, under standard and high pressure conditions. An investigation of the stability and the transition dynamics among various crystal structures of the same chemical system is performed. The present thesis deals with theoretical structure prediction of an elemental system, lithium metal, and binary systems such as calcium carbide and (per)nitride compounds using different *ab-initio* methods.

Although lithium is a simple metallic system, various modifications are known, in particular both at low temperature and at high pressure. To gain further insight into the possible metastable or thermodynamically stable modifications of lithium at standard conditions, a global exploration of the energy landscape was performed. For the global optimization, we used simulated annealing, to identify possible structure candidates. A local optimization followed the global search, where the structure candidates were refined. We have found structures with space group $Im\bar{3}m$ (bcc), $Fm\bar{3}m$ (fcc), and $P6_3/mmc$ (hcp). Apart from these known modifications, we have predicted one interesting new structure with space group $Pm\bar{3}n$, which shows chains of lithium atoms. This newly predicted structure corresponds to the A15 structure type. To understand the thermodynamic stability of this new polymorph, energy-vs-volume curves and enthalpy-vs-pressure curves were calculated and analyzed, and in order to estimate the dynamical stability, phonon calculations were performed.

In the past, both ionic and covalent systems had been studied with simulated annealing using *ab-initio* energy calculations in all the steps. In this thesis, we considered CaC_2 as an example of a mixed covalent-ionic system. Experimentally, four different modifications had been known. From the global optimization runs at standard pressure, we obtained 10 different structure candidates for this system. Among these, three exhibited a particularly low energy. One of them is the experimentally found (CaC_2-I) structure, and a second one (CaC_2-VI) has some similarity to the observed structure (CaC_2-III). The last one is completely new (CaC_2-V), and is lowest in energy of all the structures considered. Furthermore, at high pressure, CaC_2 is predicted to stabilize in a new structure type (CaC_2-VII), analogous to the CsCl-structure. Very recently, this high pressure modification was observed in high pressure experiments on the BaC_2 system.

The successful structure prediction for the CaC_2 system suggested that binary pernitride compounds could also be a highly interesting class of systems with complex multi-minima energy landscapes. In this thesis, we considered pernitrides MN_2, where M denotes cations with different maximal valences: II (Ca, Sr, Ba), III (La), and IV (Ti), some of which have not yet been synthesized (LaN_2 and TiN_2). Experimentally, CaN_2 and SrN_2 crystallize into a tetragonal modification (CaC_2-I). BaN_2 stabilizes into the ThC_2 structure type. Here, we performed the prediction of new crystal structures with two methods: the global search as described before, and a simple database approach. In the latter approach, we considered the well-known AB_2 structure types known from databases such as the Inorganic Crystal Structure Database (ICSD), replaced the anions and cations with N_2 units and metal atoms, respectively, and performed a local optimization. We found the CaC_2-I, ThC_2, MgC_2, and CaC_2-V modifications among all pernitride systems as candidates for the stable modifications. In the case of CaN_2, the CaC_2-I and MgC_2 structure types are stable modifications at standard and negative pressure, respectively. TiN_2-I and CaC_2-V are possible modifications for the TiN_2 system at normal and high pressure, respectively. In the case of CaN_2 and SrN_2, N_2 units are surrounded by octahedrally coordinated cations, whereas a distorted octahedron is formed by the cations in BaN_2 and LaN_2 at ambient conditions. Only for the TiN_2 system, the N_2 dumbbells are surrounded by Ti in a square pyramid. All these pernitride modifications are metallic in nature except TiN_2-I. Pernitride systems have a negative binding energy with respect to the metal and elemental N_2, which suggests that these systems might be synthesized e.g. at high pressure.

Zusammenfassung

In letzter Zeit wurden neue theoretische Methoden und Techniken entwickelt, um die Energielandschaft chemischer Systeme zu untersuchen. Darüber hinaus hat die experimentelle Festkörperchemie durch Fortschritte bei der Kontrolle von Synthesewegen, z.B. mittels Atom abscheidungsverfahren bei niedrigen Temperaturen oder physikalischer Gasphasenabscheidung, neue Möglichkeiten eröffnet. Des Weiteren wurden Fortschritte bei der Entwicklung von Messtechniken wie in-situ Messungen, Rastertunnelmikroskopie, Rasterelektronenmikroskopie, und Transmissionselektronenmikroskopie bei niedrigen Temperaturen erzielt. Dennoch ist es immer noch schwierig, strukturelle Änderungen bei Standard- und Extrembedingungen zu verstehen. Oft ist es unmöglich, strukturelle Veränderungen ohne Hilfe von theoretischen Simulationen zu verstehen. Manchmal kann es auch vorteilhaft sein, Strukturen vor der Synthese vorherzusagen, um mehr Informationen für die Entscheidung für einen bestimmten Syntheseweg zu erhalten. Außerdem können durch Kenntnis der Struktur die physikalischen Eigenschaften simuliert werden. Aufgrund der Kenntnisse über das System und seine interessanten Eigenschaften im Voraus, kann man die chemische Verbindung möglicherweise leichter synthetisieren und die Prognosen validieren. Das Voraussagen von Kristallstrukturen bedeutet die Erkundung der Energielandschaft des jeweiligen Systems. Diese Vorhersage-methoden basieren vor allem auf der Tatsache, dass stabile und metastabile Modifikationen von chemischen Systemen lokal ergodischen Regionen der Energielandschaft entsprechen. Bei niedrigen Temperaturen können individuelle Minima lokal ergodisch sein, wenn sie durch ausreichend hohe Barrieren getrennt sind. Normalerweise können viele solcher lokal ergodischen Regionen existieren, die eine oder mehrere lokale Minima umgeben. Der letztere Fall ist sehr wichtig, wenn einige der Plätze in den Strukturen nur teilweise oder ungeordnet besetzt sind.

Das Ziel der vorliegenden Arbeit ist es, mögliche Kristallstrukturen einschließlich bereits beobachteter sowie hypothetische neue vorherzusagen. Das Struktur-vorhersageverfahren besteht aus zwei Schritten: Der erste Schritt ist die globale Suche nach möglichen Strukturkandidaten bei verschiedenen Drücken auf dem ab-initio Niveau. Bei dem folgenden zweiten Schritt handelt es sich um eine lokale Optimierung. Alle Energien wurden auf ab-initio Niveau berechnet (d.h. sowohl während der globalen als auch während der lokalen Optimierung). In früheren Arbeiten waren Modellpotentiale wie z. B. Born-Mayer Potentiale verwendet worden. Diese Potentiale haben den Nachteil, dass sie durch ihre Kalibrierung eine Tendenz zu einer bestimmten chemischen Bindung aufweisen. Beispielsweise können sie ionische Bindungen bevorzugen und Schwierigkeiten haben, kovalente oder metallische Bindungen zu beschreiben. Ab-initio-Rechnungen sind viel allgemeiner, und benötigen weniger empirischen Input. Der Bindungstyp und die Ladungsverteilung sind nicht vordefiniert, sondern werden bei

der Berechnung bestimmt. Der Nachteil ist, dass diese Berechnungen um Größenordnungen rechenintensiver sind als Berechnungen mit den Modellpotentialen. Bis jetzt wurden nur wenige Systeme mit Hilfe von ab-initio Energien unter Benutzung z. B. des CRYSTAL-Code, der auf Gauß-Orbitalen beruht, untersucht. In dieser Arbeit haben wir zusätzlich eine Schnittstelle für den VASP-Code (Vienna Ab-initio Simulation Package) erstellt, bei dem die ab-initio Berechnungen der Energien auf ebenen Wellen basieren. Mit der Verbindung zu VASP wird die Wahl des Basissatzes vereinfacht, und die Konvergenzprobleme während der "self-consistent field" Prozedur sind im Vergleich zu CRYSTAL geringer.

Das Ziel dieser Arbeit ist es, bestehende Algorithmen zur Berechnung von Energielandschaften zu verwenden und sie mit verschiedenen Verfahren von ab initio-Simulationen zu koppeln, um die Kristallstruktur vorherzusagen. Nachdem die Struktur der möglichen (meta)stabilen Festkörper bestimmt ist, können anschließend ihre physikalischen und elektronischen Eigenschaften unter Standard-und Hochdruck-Bedingungen berechnet werden. Eine Untersuchung der Stabilität und der Übergangsdynamik zwischen verschiedenen Kristallstrukturen des gleichen chemischen Systems kann durchgeführt werden. Die vorliegende Arbeit beschäftigt sich mit der theoretischen Struktur-vorhersage von einem elementaren System (metallischem Lithium) und binären Systemen wie Calciumcarbid und (Per-)Nitrid-Verbindungen mit verschiedenen ab-initio-Methoden.

Obwohl Lithium ein einfaches metallischen Systems ist, sind verschiedene Modifikationen bekannt, insbesondere bei niedriger Temperatur und unter hohem Druck. Um weitere Einblicke in mögliche metastabile oder thermodynamisch stabile Modifikationen von Lithium bei Standardbedingungen zu gewinnen, wurde eine globale Untersuchung der Energielandschaft durchgeführt. Für die globale Optimierung verwendeten wir Simulated Annealing, um mögliche Strukturkandidaten zu identifizieren. Der globalen Suche folgte eine lokale Optimierung, bei der die Strukturkandidaten verfeinert wurden. Wir haben Strukturen mit den Raumgruppen $Im\bar{3}m$ (bcc), $Fm\bar{3}m$ (fcc), und $P6_3/mmc$ (hcp) gefunden. Abgesehen von diesen bekannten Modifikationen, haben wir eine interessante neue Struktur mit der Raumgruppe $Pm\bar{3}n$ vorhergesagt, die Ketten der Lithium-Atome zeigt. Diese neu vorhergesagte Struktur entspricht dem A15 Struktur-Typ. Um die thermodynamische Stabilität dieses neuen Polymorphs zu verstehen, wurden Energie und Enthalpie als Funktion vom Druck berechnet und analysiert. Um die dynamische Stabilität abzuschätzen, wurden Phonon-Berechnungen durchgeführt.

In letzter Zeit wurden ionische und kovalente Systeme mit Simulated Annealing mit ab-initio Energieberechnungen in allen Schritten untersucht. In dieser Arbeit betrachteten wir CaC_2 als Beispiel für ein gemischt kovalent-ionisches System. Experimentell waren vier verschiedene Modifikationen bekannt. Aus den globalen Optimierungen bei Normaldruck erhalten wir 10 verschiedene Strukturkandidaten für dieses System. Von diesen zeigen drei eine besonders niedrige Energie. Eine von ihnen ist die experimentell gefundene (CaC_2-I)-Struktur, die zweite (CaC_2-VI) hat einige Ähnlichkeiten mit der beobachteten (CaC_2-III)-Struktur. Die dritte Struktur ist komplett neu (CaC_2-V), und ist die mit der niedrigsten Energie aller berücksichtigten Strukturen. Ferner wird vorhergesagt, dass sich CaC_2 unter hohem Druck in einem neuen Strukturtyp (CaC_2-VII, analog zur CsCl-Struktur) stabilisiert. Diese vorhergesagte Modifikation wurde kürzlich in Hochdruckexperimenten am BaC_2-System beobachtet.

Die erfolgreiche Struktur-Vorhersage für das CaC_2-System legte nahe, dass binäre Pernitrid-Verbindungen auch ein sehr interessantes System mit komplexen Multi-Minima-Energielandschaften sein könnten. In dieser Arbeit betrachten wir Pernitride MN_2, wobei M Kationen mit unterschiedlichen maximalen Valenzen bezeichnet: II (Ca, Sr, Ba), III (La) und IV (Ti), von denen einige noch nicht synthetisiert wurden (LaN_2 und TiN_2). Experimentell kristallisieren CaN_2 und SrN_2 in einer tetragonalen Modifikation (CaC_2-I), BaN_2 im ThC_2 Strukturtyp. Hierbei führten wir die Vorhersage der neuen Kristallstrukturen mit zwei Methoden durch: der globalen Suche, wie zuvor beschrieben, und einem einfachen Datenbankansatz.

Im letzteren Ansatz verwendeten wir die bekannten AB_2 Strukturtypen, die aus Datenbanken wie etwa der Inorganic Crystal Structure Database (ICSD) bekannt sind, ersetzten die Anionen und Kationen mit N_2-Einheiten bzw. Metallatomen, und führten eine lokale Optimierung durch. Wir fanden die CaC_2-I, ThC_2, MgC_2, und CaC_2-V Modifikationen unter allen Pernitridsystemen als Kandidaten für stabile Modifikationen. Bei CaN_2 sind die CaC_2-I und MgC_2 Strukturtypen stabile Modifikationen unter Standard- und Unterdruck. TiN_2-I und CaC_2-V sind mögliche Modifikationen für das TiN_2 System bei Normaldruck und bei hohem Druck. Im Fall von CaN_2 und SrN_2 sind die N_2-Einheiten von oktaedrisch koordinierten Kationen umgeben, während bei BaN_2 und LaN_2 bei Standardbedingungen durch die Kationen ein verzerrter Oktaeder gebildet wird. Nur für das TiN_2 System werden die N_2-Hanteln von quadratischen Pyramiden aus Ti umgeben. All diese Pernitridmodifikationen sind metallischer Natur außer TiN_2-I. Pernitridsysteme verfügen über eine negative Bindungsenergie in Bezug auf elementares Metall und N_2, was darauf hindeutet, dass diese Systeme unter hohem Druck hergestellt werden könnten.

Part I

Introduction

1

Introduction

1.1 Introduction

Crystal structure prediction of chemical systems is very important in theoretical and experimental solid state chemistry (1, 2, 3, 4, 5, 6, 7, 8, 9, 10). Often, it is a very difficult and time-consuming task to synthesize the chemical compounds at various conditions. To overcome this issue, several techniques (6, 7) were used by the researchers, which try to mimic the procedures employed for the synthesis of the chemical compounds. The existence of a wide range of materials, such as superconductors, semiconductors, multiferroics, alloys, catalysts, ceramics, polymers, nanomaterials, bio-materials and many more, has motivated the development of systematic approaches for the theoretical prediction of these new compounds and their physical, electronic and dynamical properties at standard and extreme conditions (6, 11).

Along similar lines, many new experimental techniques have been used to synthesize elemental solids, binary, ternary and many more compounds with the help of the concept of rational synthesis of inorganic materials. There are various articles (11, 12, 13, 14) whose objective is the synthesis of predicted and not-yet synthesized materials, with the help of chemical intuition and more rational with a priori approaches to synthesis planning.

Our knowledge about chemical systems is mostly based on the experimentally known structures which exist at ambient conditions. But the chemical system may behave differently at low temperature and pressure. At these conditions, the atoms have low coordination numbers and are relatively loosely packed. At high pressure the system may have higher coordination numbers and the atoms are more densely packed. This can lead to a change in the physical properties such as from insulating to semiconducting to metallic behavior at slightly elevated pressure. Also, the system may show superconductivity. Some systems are very sensitive to pressure, and even a slight rise in pressure makes the whole system collapse, which becomes amorphous in nature such as the crystalline-amorphous transition of α-$NaVO_3$ at 60 kbar (15). Some chemical systems can only be synthesized at high pressure and high temperature, and not at standard conditions. Understanding chemical systems at various conditions is extremely important.

There is also a strong interest in structures which can be found at low temperature. A new class of synthesis techniques is available such as sputtering deposition (physical vapor deposition) (16, 17) or the growth of crystalline structures on amorphous materials using atom beam deposition (18, 19) at very low temperature, possibly at liquid nitrogen or liquid helium temperature. Note that this is not possible with the well known molecular beam epitaxy (20, 21, 22, 23), as this method requires higher temperatures. In such cases (18, 19, 24, 25), the observed modifications have low densities which are otherwise observed at high temperature or low pressure. Such a phase is due to the formation and growth of nuclei inside the amorphous material, which is less dense than crystalline materials. The forces acting on the interface of the amorphous and the crystalline material result in a negative pressure which favors the low density polymorph (25).

Synthesizing systems at high pressure (26, 27) has recently received increased attention. This method led to the discovery of new phases of crystalline structures (28, 29, 30, 30, 31, 32, 33, 34, 35, 36, 37, 38, 39, 40). Though there is an advancement in techniques such as in-situ measurements, it is not so simple to understand the structural transformations. With the help of theory, by computing $E(V)$ and $H(p)$-curves, one gets deep insight into the structural modifications and phase transitions.

With this increase of newly observed modifications, there are also new challenges for theoreticians. Basically, all plausible structures are associated with local minima of the potential energy. For exploring all modifications of a given system, one has to study the enthalpy surface at various pressures. This is similar to structure prediction of solids at standard and extreme conditions by locating local minima on the potential surface for the chemical system (6, 11, 41, 42, 43).

In the past decade, novel and advanced theoretical and computational methods for the prediction of new materials of all kinds of systems have evolved. Furthermore, there has been an enormous growth in computational power. There are several algorithms such as simulated annealing (44, 45, 46, 47), genetic/evolutionary algorithms (42, 48, 49, 50, 51), or basin hopping (52, 53), threshold algorithm (54) or meta-dynamics (55, 56) which are used for structure prediction of solid compounds. Another possible optimization technique is particle swarm optimization (57, 58), which has been applied, e.g., to predict protein folding using a toy model (59) or to solve crystal structures from powder diffraction (58) and elemental solids such as lithium (60). Some more algorithms were also used for global exploration such as *ab-initio* random structure searching (AIRSS) (61), or data mining.

Since structure prediction is a very time-consuming task involving many millions of energy calculations, one usually attempts to reduce the computational effort by employing simplified energy functions, that are typically based on empirical potentials. Such potentials are often of sufficient quality and computationally cheap as well, but they have some in-principle shortcomings. They are system dependent, and even for a given system, it is not guaranteed that all relevant polymorphs correspond to basins around local minima. Furthermore, while these potentials are successful for ionic systems, they often encounter problems for systems with covalent or metallic bonds or mixtures thereof. As a consequence, it is much better to employ *ab-initio* based energy calculations already during the global search (62).

In this study, the main goal of energy landscape exploration of chemical systems is to find experimentally observed structures and then new modifications (not-yet synthesized). The next step is to find similarities between predicted and observed modifications on the basis of the structural analysis and physical properties. The starting point of most structure prediction methods is the fact that (meta)stable modifications of chemical systems correspond to locally ergodic regions of the energy landscape.

Several years ago, it was demonstrated that global optimization with genetic algorithms (50) and simulated annealing (63) is possible, with all energy calculations performed on the *ab-initio* level. For example, the ionic system lithium fluoride (LiF) was the first system studied with simulated annealing on the *ab-initio* level (63), in order to validate the methodology.

LiF had been studied with model potentials (47, 64) earlier, and it was found that the most relevant minima were the same on the level of empirical potentials and on the *ab-initio* level. Subsequently, boron nitride (BN), a covalent system, was successfully investigated using *ab-initio* simulated annealing as the global exploration method (65). The possibility to compute barriers was demonstrated for LiF (66) and subsequently MgF_2 (67) clusters. Meanwhile, further systems have been studied such as GeF_2 (68) and PbS (69). In this thesis, we go one step further and investigate metallic and mixed covalent-ionic systems.

1.1.1 Outline

The thesis is organized in different sections which are as follows: (I) **Introduction**, (II) **Theoretical background**, (III) **Methods**, (IV) **Application to solid and binary systems**, (V) **Summary**, (VI) **Appendix**, and (VII) **Formalia**.

Part II: Theoretical background: We analyzed different energy landscape exploration methods to model solid chemical systems on *ab-initio* level.

Part III: Methods: In this section, we first review the method which gives more insight into the stability of the chemical system, e.g., thermodynamic and dynamical.

In particular, we created an interface to VASP (Vienna Ab-initio Simulation Package) for *ab-initio* energy calculations (**Chapter 5**).

Part IV: Application to solid and binary systems: This part can be divided into three sections viz. three different systems. (1)*"Lithium"*, (2)*"Calcium carbide"*, and (3) *"(Per)nitride compounds"*.

Chapter 6: In this chapter, we studied elemental lithium. Here, we performed an energy landscape exploration at standard pressure with various numbers of atoms per unit cell. During the simulation, we found the experimentally known modifications. Furthermore, we discovered one more modification which is usually observed in binary systems. We studied its dynamical stability that supports that it can exist at ambient or low temperature.

Chapter 7: Until now, ionic systems have been very well studied using global exploration techniques which are based on simulated annealing. We went ahead and investigated CaC_2, a mixed covalent-ionic system. It is an experimentally very well known system. We performed global optimizations at standard and high pressure. As the outcome our search, several new structures were discovered of which one structure should exist at ambient condition whereas another one is predicted as a high pressure phase. For comparison, we took known AB_2 structure types from a database as a starting point for our local optimization. Among these, some show the same kind of structure types as those that are experimentally known and theoretically predicted.

Chapter 8: We took one further step ahead in the direction of covalent-ionic systems. We performed global explorations on (per)nitride compounds which have not-yet been synthesized. We took three different cations viz., calcium (Ca^{2+}), lanthanum (La^{3+}), and titanium (Ti^{4+}) with the same anion ${N_2}^{2-}$, and we performed global optimizations. The result shows interesting trends as we move from the left to the right and the top to the down in the periodic table. We compared the predicted polymorphs with the known structures of alkali earth metals e.g., SrN_2 and BaN_2.

In the **Supplementary material** we provide information about ionic radii according to the atomic charges for all systems. We also include the basis set for lithium and carbon and the pseudopotential for calcium.

Part II

Theoretical background

2

Exploration of the Energy Landscape for solids

In solid-state chemistry, two approaches are used to validate the existence (or non-existence) of a chemical compound. One is the actual synthesis of the respective chemical compound and the other is to apply some empirical rules and/or chemical intuition. But, since about twenty years there has been a new methodology that is used to predict the crystal structure before its synthesis without taking prior experimental information into account. Similarly, the amount of information gained during experiments is often not enough to determine the structure of the chemical system. In the experiment, it is hard to understand the transformation dynamics while the system goes through various (meta)stable modifications. And it is more difficult when the possible (meta)stable modifications have not yet been synthesized. In such cases, theory, especially mathematical modeling, gives some assistance (8, 9). From the theoretical point of view, the description of a chemical compound and its dynamics is incorporated in the energy, which is a function of the position of the atoms in the crystal structure (70).

2.1 Energy Landscape

2.1.1 Introduction

The positions of all the atoms in a solid or in a molecule can be described in the classical limit with the position vectors in 3D of all the N atoms which are part of the chemical system (6, 11, 41, 71, 72, 73, 74, 75, 76, 77, 78). Every configuration is represented by a point in a 3N-dimensional Euclidean space, called configurational space. For the first time, the energy landscape concept had been used to study the non-equilibrium features of glasses (71, 72). The energy landscape (see Fig. 2.1) has been used to predict new structures of crystalline compounds which can give new insight to develop different routes to their synthesis (7, 11), whereas clusters (73, 74) and big molecules such as

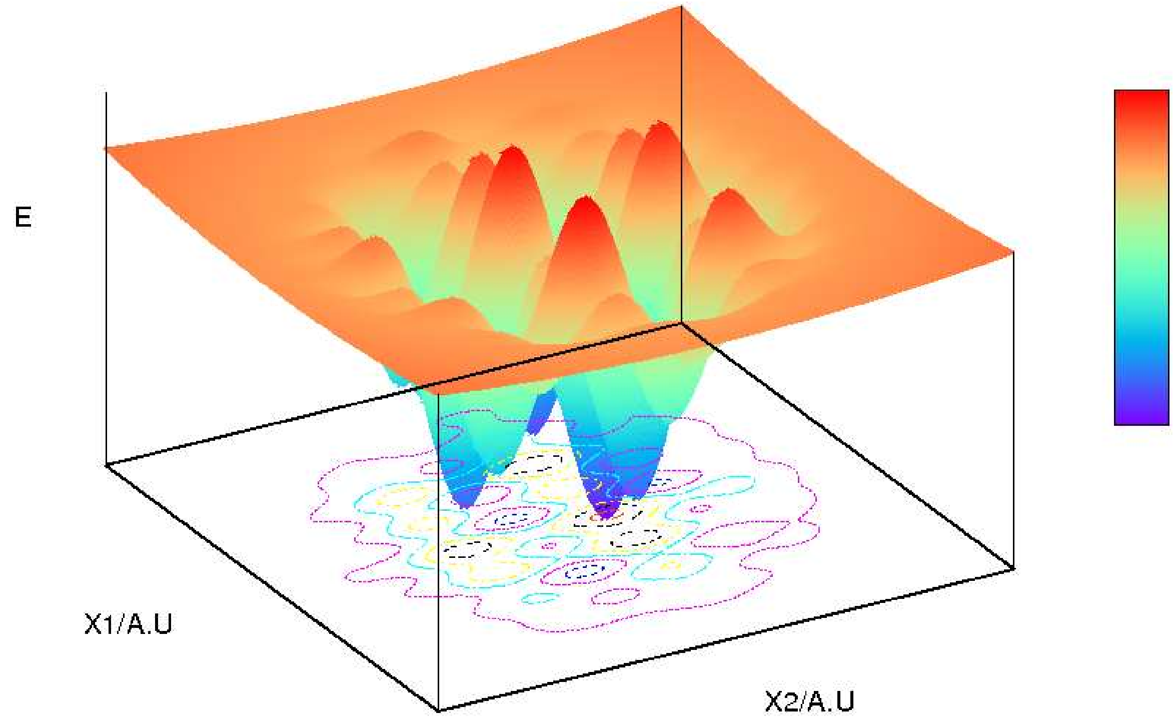

Figure 2.1: Schematic representation of the energy landscape for a simple system with one species of atom with fictive coordinates X_1 and X_2.

proteins and polymers (41, 74, 79) are both studied as model systems for complex landscapes. These models are useful to understand some of their properties, such as the existence of magic number clusters or protein folding.

The chemical system is generally represented by position and momentum vectors. The position of each atom can be denoted by $\vec{x}_i$ in a 3N-dimensional vector space $\vec{X} = (\vec{x}_1,.....\vec{x}_N)$. Similarly, the velocity of every atom is denoted by $\vec{v}_i$ in a 3N-dimensional vector space $\vec{V} = (\vec{v}_1,.....\vec{v}_N)$, or by momenta $\vec{P} = (\vec{p}_1,.....\vec{p}_N)$, $\vec{p}_i = m_i\vec{v}_i$. This results in a 6N-dimensional space of both the N position vectors $\vec{x}_i$ and N velocity vectors $\vec{v}_i$. It is known as phase space. To simplify this, we usually replace this vector and an infinitesimal cube in phase space around it by a state i (8, 9) and the integral over phase space by summation over i. Using classical mechanics, the energy can be defined as

$$E = E(\vec{X}, \vec{P}) = E_{kin}(\vec{P}) + E_{pot}(\vec{X}) \tag{2.1}$$

where $E_{kin}(\vec{P}) = \sum_i \vec{p_i}^2/2m_i$ is the kinetic energy and $E_{pot}(\vec{X})$ is the potential energy. Newton's equations give the time evolution of such a system as follows:

$$\frac{d\vec{x}_i}{dt} = \frac{\vec{p}_i}{m_i} = \vec{v}_i \tag{2.2}$$

$$\frac{d\vec{p}_i}{dt} = \vec{F}_i = -\frac{\partial E_{pot}(\vec{X})}{\partial \vec{x}_i} \tag{2.3}$$

The above set of equations can be solved and gives a unique solution (trajectories $(\vec{X}(t),\, \vec{V}(t))$) for all physically valid choices of initial conditions $(\vec{X}_0,\, \vec{V}_0)$. If we have to analyze the dynamics of the chemical system, the simplest approximation is to keep the system at zero Kelvin. The kinetic energy of the system becomes zero. Thus, the trajectory goes to the nearest local minimum of the potential energy surface which is dependent on the starting point. The system will stay there for the rest of the duration of the experiment or simulation. Hence, all minimum configurations on the energy landscape can be explored at zero Kelvin and these structures are known as kinetically stable structures. At zero Kelvin, the system is static. Classically, the system can stay at a stable configuration for infinite time, but in the case of quantum mechanics, it is not possible because of tunneling.

It is very difficult to consider the system at non-zero temperature, because it has many degrees of freedom, that are highly likely to lead to a complicated trajectory in configurational space. One can not get the actual essence of the system from experimental observations and not even through a molecular dynamics simulation, that simulates how the system evolves from a gaseous state to a more ordered form, i.e. a crystalline structure. Usually, lattice vibrations and thermal excitations are associated with a crystal structure. The structure is called stable when the number of atoms corresponds to some thermal (Boltzmann) average, not when a single atom or several atoms correspond with one formula unit. When the crystal structure is thermodynamically stable, then it should satisfy ergodicity. Ergodicity can be defined as the equivalence of time-average (the average of the simulated trajectory over the whole simulation time) and the ensemble average. This also holds for metastable compounds with some constraints, because the existence of metastable compounds is limited in time. Hence, we are interested in identifying all locally ergodic regions for metastable compounds of a chemical system at a reasonable time scale.

In the next section, we have to translate these qualitative considerations into a mathematical definition of an energy landscape and local ergocity. Three important factors are required to define an energy landscape mathematically: A configuration space of states (or solutions of an optimization problem), energy (or cost) function given as a real function over configuration space, and a neighborhood relation (topology). Usually, an energy landscape of an atomic arrangement has some surroundings given by the topology of $\Re^{3N}$, but for optimization problems we have to explicitly define such a neighborhood relation (called move-class). While performing a global energy landscape exploration, in the present work we used *ab-initio* calculations for the energy calculation which is enormously expensive as compared to empirical potentials. Initially, there is no information provided about the cell geometry and no atom positions are given. The configurational space that needs to be explored is greatly enlarged due to the necessary variation of the simulation cell compared to only an adjustment of atomic positions, which affects the speed and accuracy of the energy calculation. In such a case, we are interested in an approximate calculation of energy functions. The outcome of the global optimization yields local minima, which need to be checked using the local optimization on *ab-initio* level. The analysis of the thermodynamical stability of these locally optimized structures can be investigated (6, 80, 81) employing algorithms that provide 'topographic' (see Fig. 2.2) facts about the structure of the energy barriers around these minima, and the local density of states near the minimum (54, 82). In classical mechanics, the time evolution can be decided by the positions and velocities of all the atoms at some initial time t_1. This time evolution is coupled with the laws of motion and the energy function of the system, from which the forces on the atoms can be calculated. A physical measurement consists of the average of some observable O,

$$\langle O \rangle = \frac{1}{t_{obs}} \int_{t_1}^{t_2} O(\mathbf{X}(t^{'}), \mathbf{V}(t^{'})\, \mathrm{d}t^{'} \tag{2.4}$$

over a time interval $[t_1, t_2]$ of the length t_{obs}=t_2-t_1 along this trajectory. Usually the physical properties are independent of the initial point t_1 of the trajectory in phase space $\langle O \rangle_{t_1,t_2} = \langle O \rangle_{t_{obs}=t_1-t_2}$. In particular, if a system can reach equilibrium, with respect to the observable O, faster than we perform measurements, $t_{obs} > t_{eq}(O)$, the so-called ensemble average,

$$\langle O \rangle_{ens}(T) = \frac{\int O(\mathbf{X}(\mathbf{t}), \mathbf{V}(\mathbf{t})) e^{\frac{-E(\mathbf{V},\mathbf{X})}{k_B T}}\, \mathrm{d}\mathbf{V} d\mathbf{X}}{\int e^{\frac{-E(\mathbf{V},\mathbf{X})}{k_B T}}\, \mathrm{d}\mathbf{V} d\mathbf{X}} \tag{2.5}$$

equals the time average within an accuracy a_m,

$$|\langle O \rangle_{t_{obs}} - \langle O \rangle_{t_{ens}}| < a_m \tag{2.6}$$

If this condition holds, then we can say that the system is ergodic with respect to the observable $\langle O \rangle$ on the time scale t_{obs} and up to accuracy a_m. It is not a trivial task to prove that a system can be termed ergodic. But in many cases, the ergodicity assumption turns out to be justified.

Apart from t_{obs} and t_{eq}, there is another time scale, termed as the escape time t_{esc}. The average time spent by the system in a locally ergodic region $\mathscr{R}$ (81, 84) is given by the escape time. The local ergodicity is a weaker version of the (global) ergodicity approach which relates to the fact that only a subset of $\mathscr{R}$ of the energy landscape may be ergodic. If we can get a reproducible diffractogram of a modification associated with $\mathscr{R}$ before the substance disintegrates or transforms to another modification, $t_{esc}(\mathscr{R}; O) > t_{obs} > t_{eq}(\mathscr{R}; O)$, then we are dealing with a metastable compound on our observation scale t_{obs}. If we are working on a system that is not an isolated solid, but a system in contact with an external heat bath at constant temperature, then the temperature serves as an indicator that the solid is isothermal with the surrounding. We cannot reproduce the above experiment on a time scale that is shorter than the equilibration time t_{eq}^{T}.

The equilibration time and escape time are temperature dependent. Especially, the escape time may vary by many orders of magnitude, according to the Arrhenius law,

$$t_{esc} \propto e^{\frac{E_{barrier}}{k_B T}} \tag{2.7}$$

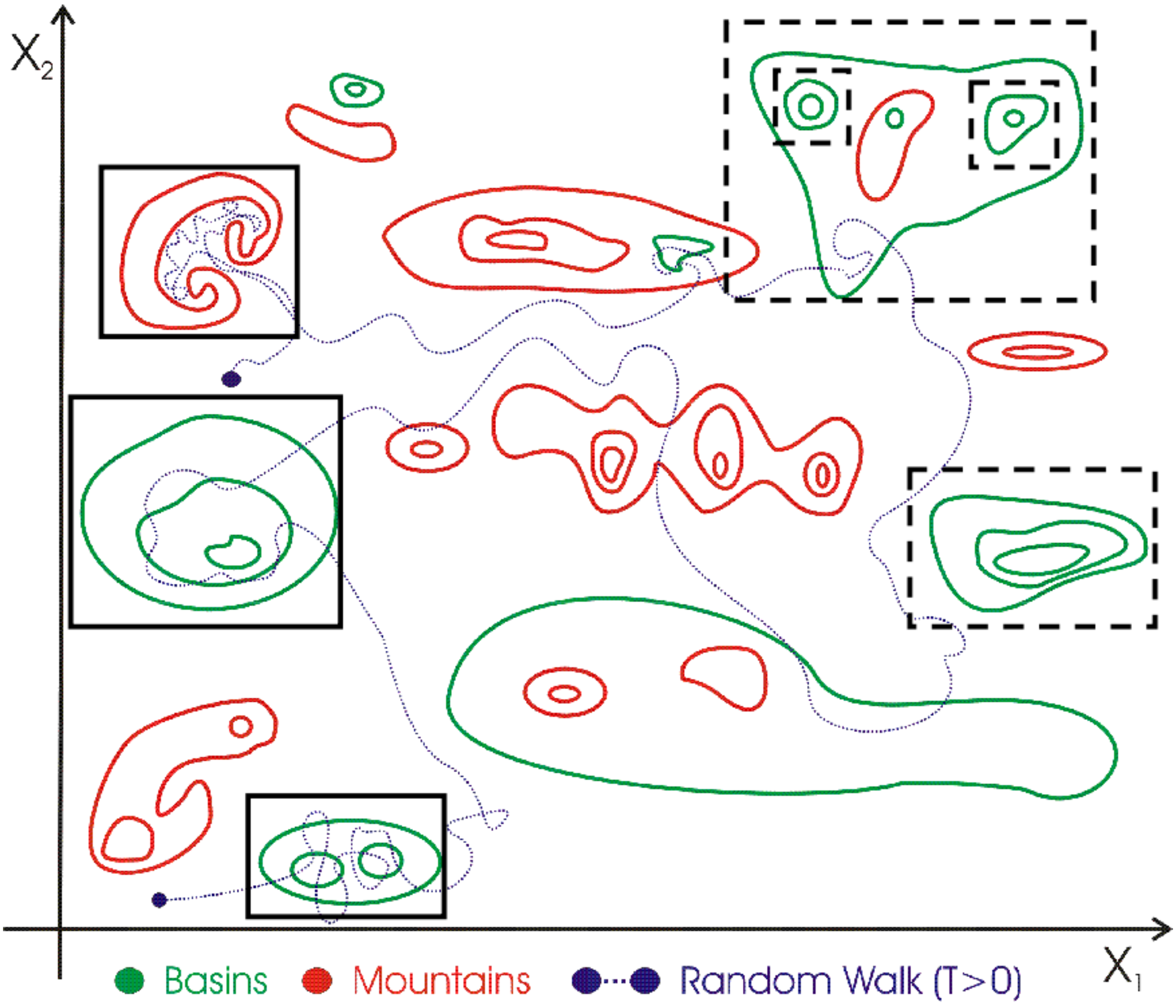

Figure 2.2: Topographical representation of 3N-dimensional landscape projected on two dimensions (83). The blue line suggests the trajectory of time evolution of a system on the landscape. The red and green curves show the basins and mountains on the energy landscape, respectively. Regions enclosed by black rectangles were observed during Monte-Carlo simulation and the dashed rectangles contain local minima but which are not explored in this simulation run.

As the locally ergodic regions $\mathscr{R}_i$ have been discovered (for a given temperature and t_{obs}), one can figure out the local free energy of each region (see Section 2.1.3.3). The kinetic stability of the modification one associates with such a region is given by the escape time t_{esc}.

The energy landscape depends on several factors such as temperature and other thermodynamic parameters like pressure, and external fields (electric $\vec{E}$, magnetic $\vec{B}$, etc.). Temperature, for example, changes the dynamics of the landscape in a stochastic fashion via the average kinetic energy ($\langle E_{kin} \rangle = 3/2Nk_BT$). The pressure p modifies the energy function itself:

$$E\left(p = 0, \vec{E}{=}\vec{0}, \ldots\right) = E_{pot} \rightarrow E\left(p \neq 0, \vec{E}{\neq}\vec{0}, \ldots\right) = E_{pot} + pV + \vec{E}\vec{P} + \ldots . \quad (2.8)$$

Since these external parameters are time-independent, we are dealing with a fixed time-independent energy landscape, and these modifications do not pose any real difficulties. We can perform the exploration of this modified landscape $E\,(p \neq 0, \ldots)$ analogously to the one of the potential energy landscape $E\,(p = 0, \ldots)$.

The first step is the determination of the locally ergodic regions. At low temperatures (usually $T \approx 0$), escape times are controlled by energy barriers, and will increase exponentially according to the Arrhenius law (Eqn. 2.7). It is observed that in many cases these barriers are actually high enough for local ergodicity to hold even at much higher temperatures (8, 9).

2.1.2 Algorithms for global optimization

In science and technology, there are several problems which can be systematically specified in terms of the minimum or maximum of a cost function, over a space of acceptable solutions. There are many methods available to (approximately) solve this problem. For simplicity, they can be divided into global and local approaches, usually termed as *global optimization* (GO) and *local optimization* (LO) methods.

Global optimization deals with the optimization of a function. The main goal of global optimization is to find the best possible (or feasible) solution of (nonlinear) models, in case of the (possible) existence of multiple local optima. Initially, optimization techniques were used to solve real world problems such as transport management and the organization of sales personnel. Formally, there is a simple technique to solve these problems, by searching the minimum cost with all constraints to be satisfied. The simplest form is the minimization of one real-valued function $f\left(\vec{x}\right)$ in the configuration/solution space. In addition, the states $\vec{x}$ may have to fulfill one or several constraints $C\left(\vec{x}\right) = 0$. In reality, the cost function of many variables may have a large number of local minima and maxima. To locate an arbitrary local minimum is relatively simple as compared to the global maximum or minimum of a function. To find the global minimum is barely possible for many problems up till now. The maximization of a real-valued function $g(x)$ can be regarded as the minimization of the transformed function $f\,(x) = (-1) \cdot g\,(x)$ (85, 86, 87). Application of the global optimization techniques in various fields include: Structure prediction (minimize the energy/free energy function), traveling salesman problem and circuit design (minimize the path length), chemical engineering (e.g. analyzing the Gibbs free energy), calibration of radio propagation models, safety verification, safety engineering (e.g. mechanical structures, buildings), worst case analysis, mathematical problems (e.g. the Kepler conjecture), spin glasses, curve fitting (e.g. non-linear least squares) and many more.

Optimization algorithms (88) can be divided in two basic classes: deterministic and probabilistic algorithms (see Fig. 2.3). Deterministic algorithms are most often used if there is a clear relation between the characteristics of the possible solutions. The search space can efficiently be explored using simple techniques such as a divide and conquer scheme which works by iteratively breaking the problem into two or more sub-problems of the same or related kind, until these become simple problems to be solved directly. The solution of the original problem is the combination of solutions of all sub-problems. If the connection between a solution candidate and solution of its subproblems is complicated, or the search space is high-dimensional, then under these conditions it is harder to deterministically find a solution to the problem.

If deterministic solutions are not practicable, then probabilistic algorithms come into the picture. They contain stochastic, heuristics and metaheuristic optimization methods. Mostly, probabilistic algorithms are based on the Monte-Carlo simulation method. The performance of these algorithms is very good on the simulation time scale but this does not imply that the results obtained using them are incorrect - they may just not be the global optima. At the same time, a solution is not the best possible solution if another solution is better, even if it needs 10^{100} years to be found. Several Monte-Carlo-based algorithms exist: simulated annealing (SA), direct Monte-Carlo sampling, stochastic tunneling, parallel tempering, Monte-Carlo with minimization, and basin hopping techniques. A heuristic algorithm (88, 89, 90) is a part of an optimization algorithm which uses the details of a system currently gathered by the algorithm to help to decide which solution candidate should be tested next or how the next individual can be produced. Usually, heuristics problems are class dependent. A metaheuristic algorithm (88, 91, 92) combines objective functions or heuristics in an abstract and hopefully efficient way, usually without utilizing deeper insight into their structure, i. e. by treating them as black-box-procedures. It is a method used for solving very general classes of problems. Recent developments employ heuristic tactics to explore the search space, including evolutionary algorithms (e.g. genetic algorithms and evolution tactics) (44, 45, 85, 86, 87, 93, 94, 95, 96, 97, 98, 99), swarm-based optimization algorithms (e.g., particle swarm optimization and ant colony optimization) (57), memetic algorithms (100), and algorithms combining global and local search tactics, reactive search optimization (i.e. integration of sub-symbolic machine learning techniques into search heuristics) (101).

The energy landscape of a chemical system is a special case of cost functions which requires a clever combination of GO and LO methods. The energy landscape may possess many minima and a very complicated barrier structure (see Fig. 2.2).

2.1.2.1 Exploration of local minima

A number of methods has been developed to locate the local minima on the energy landscape, to solve discrete and continuous optimization problems in physics, mathematics, biology, technology, economics, and computer science. These optimization algorithms have been implemented and are used to find structure candidates in chemical systems,

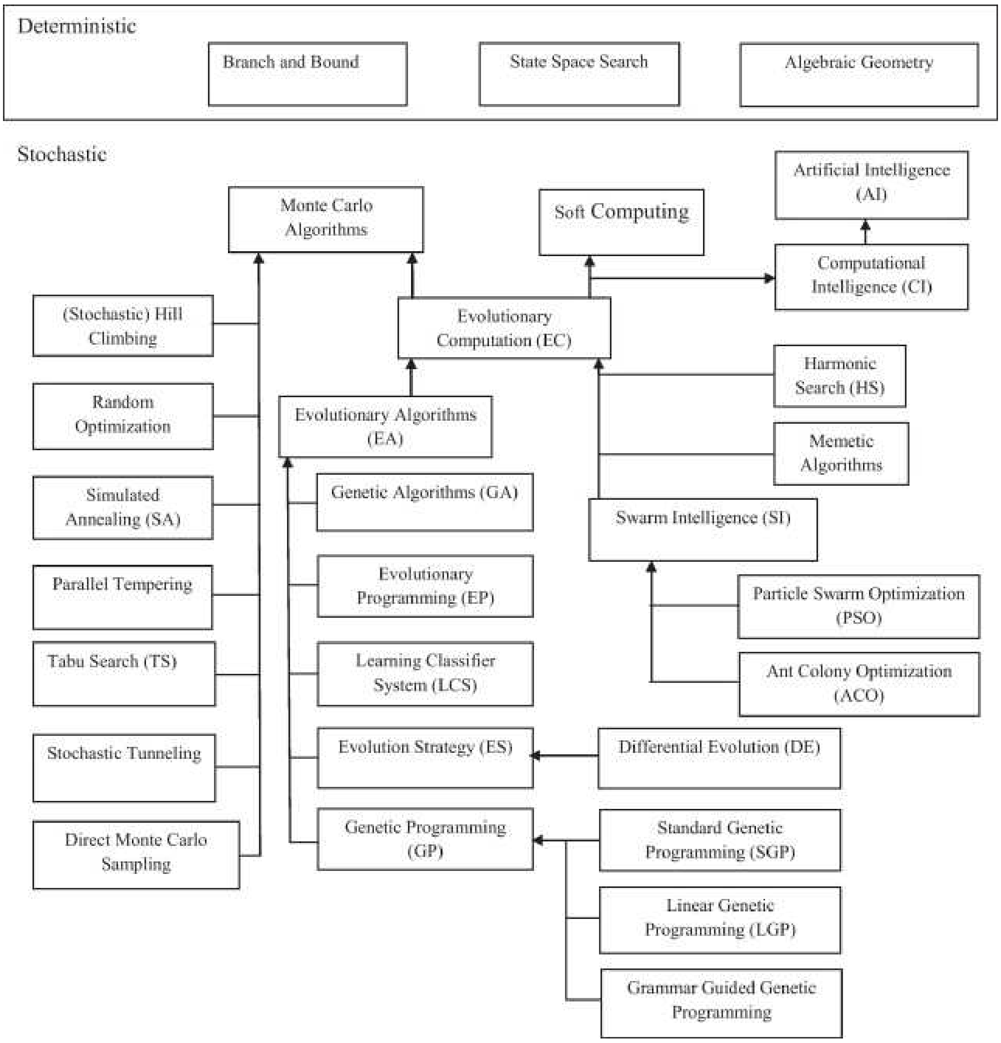
Deterministic
Branch and Bound
State Space Search
Algebraic Geometry
Stochastic
Monte Carlo Algorithms
Soft Computing
Artificial Intelligence (AI)
Computational Intelligence (CI)
(Stochastic) Hill Climbing
Evolutionary Computation (EC)
Harmonic Search (HS)
Random Optimization
Evolutionary Algorithms (EA)
Memetic Algorithms
Simulated Annealing (SA)
Genetic Algorithms (GA)
Swarm Intelligence (SI)
Parallel Tempering
Evolutionary Programming (EP)
Particle Swarm Optimization (PSO)
Tabu Search (TS)
Learning Classifier System (LCS)
Ant Colony Optimization (ACO)
Stochastic Tunneling
Evolution Strategy (ES)
Differential Evolution (DE)
Direct Monte Carlo Sampling
Genetic Programming (GP)
Standard Genetic Programming (SGP)
Linear Genetic Programming (LGP)
Grammar Guided Genetic Programming

Figure 2.3: Classification of optimization algorithms. (88)

as a tool for the rational planning of syntheses (6, 11). In these simulations, there are critical issues viz. the efficiency of the search, and the effect of approximations and modifications of the energy landscape to speed up the search. In the global exploration, we are not only interested in the global minima but also in the minima with low energies and sufficiently high barriers surrounding them. These low-energy minima are also important because they represent possible metastable compounds.

The global optimization/exploration methods can be split into two parts viz. stochastic optimization and deterministic approaches. A random walker (or a set of such walkers) is the fundamental concept behind stochastic methods. The trajectory of the random walker on the landscape traces the time evolution of the chemical systems. In the case of a Monte Carlo simulation with the Metropolis algorithm (102), one (or many) walker at the configuration with energy E_i chooses one of the neighboring configurations as test configuration with energy E_j. It is accepted if $\Delta E = E_j$-$E_i < 0$ or if exp(-ΔE/T) $>$ r for a random number $0 \leq$ r < 1. The variation in the configuration can be generated randomly and with non-physical rules. These random moves may allow us to take large steps on the landscape. In the case of molecular dynamics simulations, the physical trajectory reproduces the system in a deterministic way. By applying an external heat bath to the system, a certain degree of stochasticity is imitated. On the other hand, the classic deterministic global optimization approaches were able to search for minima on the landscape with heuristic or exhaustive rules. These methods are advantageous when the landscape can be divided into a hierarchy of regions each containing several local minima, hence one employs a divide-and-conquer approach.

2.1.2.2 Simulated annealing

A Monte-Carlo method for calculating the properties of any substance which may be considered as composed of interacting individual molecules was developed by Metropolis and coworkors (102) in 1953. Using the Metropolis algorithm, the way in which configurational atoms reconfigure and reach the equilibrium state, is simulated. This process has been described above. Later, in early 1980, Kirkpatrick (44) developed a simulated annealing algorithm (95, 103) for the global optimization (88, 104). V. Černý (45) used the same approach to solve the traveling salesman problem (105, 106). It is quite handy to use this for arbitrary search and problem spaces. Simulated annealing requires a single initial individual as the starting point and a unary search operation. The implementation of this algorithm is quite simple, and corresponds to a lowering of temperature during the Metropolis walk.

Annealing, in metallurgy, is a process where heat is applied to the system above a critical temperature, maintaining a suitable temperature, and then cooling. This process can change ductility and hardness. Usually, the bulk metal materials have small defects, such as dislocations. By heating the bulk metal, these dislocations and defects are removed and the crystal structure is more ordered as the material cools down. The system reaches the equilibrium state. The cooling rate is the crucial factor in this process. If the cooling process is sufficiently slow it is avoids the system getting stuck in a meta-stable, non-crystalline, state, which would represent a local minimum of energy.

Sometimes simulated annealing appears to be slow. Speeding up the cooling process will improve its performance, but on the other hand it results in difficulties to locate the minima. Such speeded-up algorithms are called Simulated Quenching (SQ) (107, 108, 109). Simulated annealing with ”large” moves (moves which strongly change the configuration), combined with a quench after such a move, is termed as basin hopping (53, 110, 111).

Besides the move-class, there are some other parameters of simulated annealing, that have to be fine-tuned so that the efficiency of the algorithm (95, 112) can be improved. The temperature schedule T(n) is used to keep the system at equilibrium for some time, where n is the number of moves along the trajectory, which can be optimized. Usually, schedules are exponentially or linearly decreasing with n. These schedules may have temperature cycles (113, 114), where the temperature periodically rises and then decreases again, or they may be adaptive schedules (115, 116) which take care of how the landscape is explored up till now. Some other useful methods are available, such as multi-walker methods (112, 117), the Demon-algorithm (118), or methods that generate an averaged landscape (103, 119, 120, 121, 122), including methods such as conformation-family Monte Carlo (123), the particle swarm optimization (124), superposition state molecular dynamics (125), or multi-overlap dynamics (126, 127, 128, 129), parallel tempering (130), and J-walking (131). To overcome barriers, all walkers run at different temperatures as well as sometimes switch positions (or temperatures). Lastly, the acceptance criterion can be selected between the classical Metropolis distribution (102), the Tsallis distribution (132, 133) or based on a temperature dependent acceptance threshold (134). Further descriptions of these methods are found in the literature (103, 135).

2.1.2.3 Taboo search

In mid 1980s (136), Glover (137) developed the Taboo search, based on a trajectory optimization. Later, this method was formalized by Hansen (138), Glover (139, 140), de Werra and Hertz (141), as well as by Battiti and Tecchiolli (142) and Cvijović (143, 144) and Klinowski (145), independently. The meaning of the word “Taboo” is a sacred place or object. So, things that are taboo may not be visited or touched. It is an extension of hill climbing. The solution candidates which have already been visited during landscape exploration, are called taboo states. Hence, they must not be visited again and the optimization process is less likely to get stuck in a local optimum. In this approach, one uses a taboo list which stores all the solution candidates that have already been visited. This avoids repeatedly visiting the same solution candidate. Due to technical reasons, the list cannot grow infinitely but has a finite maximum length n. To overcome this issue, the $n + 1^{st}$ solution candidate is added, and the first one must be removed. Alternatively, the combination of Taboo search with the quenches and long moves like in basin hopping can resolve the problem of memory (146). Apart from this, there are other methods designed to gain a more efficient barrier crossing such as locally elevating visited areas (147) (a precursor of meta-dynamics), by lowering barriers relative to the local minima (148), stochastic tunneling (149, 150, 151, 152), dynamic lattice searching (153), or changing the potential between the atoms (154). We can find a close relationship of Taboo search with adaptive MC/MD simulations.

2.1.2.4 Lid-based optimization

There are some algorithms which are based on lid methods for the stochastic global exploration of continuous energy landscapes such as the deluge algorithm (155) and the threshold algorithm (54). In the first algorithm, the energy lid keeps the system below a certain value during the Monte Carlo simulation and all moves are accepted, i.e., as if $T = \infty$. The system is slowly lowered from very high energy lid values. In the threshold algorithm, the walker can make some moves below an ascending sequence of energy lids. One keeps an eye on new local minima that have been reached by performing quench runs from stopping points along the trajectories.

2.1.2.5 Gradient-based methods

The stochastic optimization methods are useful for the exploration of discrete and continuous energy landscapes. These algorithms have some drawbacks, e.g., they do not take into consideration local information such as the derivatives of the cost function. This information is used in those algorithms which use gradients such as the gradient descent method. Gradient descent is a first-order optimization algorithm. To find a local minimum of a function using gradient descent, one takes steps proportional to the negative of the gradient (or of the approximate gradient) of the function at the current point. If one takes steps proportional to the positive of the gradient, one approaches a local maximum of that function. This procedure is then known as gradient ascent or steepest descent (86, 87). There are several algorithms which consider second derivatives of the cost function such as simple conjugate gradient, biconjugate gradient, and nonlinear conjugate gradient. The conjugate gradient method is an algorithm for finding the nearest local minimum of a function of n variables which presuppose that the gradient of the function can be computed. It uses conjugate directions instead of the local gradient for going downhill. If the vicinity of the minimum has the shape of a long, narrow valley, the minimum is reached in far fewer steps than would be the case using the method of steepest descent. For handling large sparse systems, the performance of an iterative method such as conjugate gradient is better than direct methods, such as Newton-Raphson, Gauss-Newton, Quasi-Newton etc. (86, 87).

2.1.2.6 Genetic algorithms

A genetic algorithm (GA) (48, 156) is a search heuristic that imitates the process of natural evolution. It is a search technique which is used to find approximate solutions to optimization and search problems. These algorithms are a distinct class of evolutionary algorithms that adopt techniques inspired by evolutionary biology such as inheritance, mutation, natural selection, and recombination (or crossover) (157).

Genetic algorithms are implemented in a computer simulation which has its own terminology such as population of abstract representations (known as chromosomes) of candidate solutions (termed as individuals) to an optimization problem, and which evolves toward better solutions. Usually, solutions are formulated in binary format as strings of 0s and 1s, but a representation is possible in other formats as well. The system evolves from a completely random individual to an ordered one in generations. In every generation, the fitness of the whole population is calculated, multiple individuals are stochastically selected from the current population (based on their fitness), and modified (mutated or “crossed“) to form a new population, which becomes the current in the next iteration of the algorithm (157).

When applied in the framework of the exploration of energy landscapes, this means that an ensemble of configurations with the lowest energy survives preferentially from one generation to the next. The selection criteria can vary between two extremes: only those configurations with the lowest energy survive, or all new configurations always survive (at least for one generation). Between these two extremes one uses probabilistic criteria analogous to the Metropolis criterion.

2.1.3 Exploration of the barrier structure

Usually, the main aim of energy landscape exploration is to find all local minima which correspond to low-lying states. However, for structure prediction it is also very important to know to which extent the local minima found exhibit a high degree of stability. The knowledge of the barrier structure around minima gives some useful information to judge the stability of the corresponding structure candidates. Using stochastic and deterministic optimization algorithms, one can investigate the barrier structure.

2.1.3.1 Threshold algorithm

The threshold algorithm (54, 82) is a stochastic approach for the exploration of the barrier structure. After locating a local minimum one can choose a sequence of energy lids L_k ($L_k > \mathrm{E}_{min}$) where E_{min} is the energy which corresponds to the local minimum structure. For a given lid L_k one performs long Monte Carlo (MC) walks, where every move is accepted, unless it exceeds the energy of the lid. Every n_q moves, one or many quenches into the closest local minimum are performed. This procedure is repeated for other lids as well. From the energy lids where new minima are first found during one of the quenches, one deduces an estimate for the barrier height between the starting minimum and other minima. From the distribution of energies encountered during the runs at various lids, one can deduce the local density of states within the basin of the starting minimum. Next, one can repeat the whole procedure for all other local minima observed. With the help of all this information, we can construct a tree graph for the energy landscape.

The transition probabilities determined by this algorithm between the local minima include both energetic, entropic and kinetic contributions. As a result, we identify the lowest energy lids, at which a transition between two minima can occur, yielding an estimate of the (free)energy barrier between the minima.

2.1.3.2 Saddle point analysis

In computational physics or chemistry, there are many problems which can be described as an optimization of a multidimensional function. With the help of the optimization one can usually find a stationary point of a function, where the first derivative is zero. In most of the cases the required stationary point is a minimum, i.e., all the second derivatives should be positive. In some cases the desired point is a first-order saddle point, i.e., the second derivative is negative in one, and positive in all other, directions (see Fig. 2.4).

Because the gradient at a saddle point vanishes, an alternative to explore regions around saddle points is to follow a downhill path, or to deform the landscape in such a way as to make the detection of the saddle points easier.

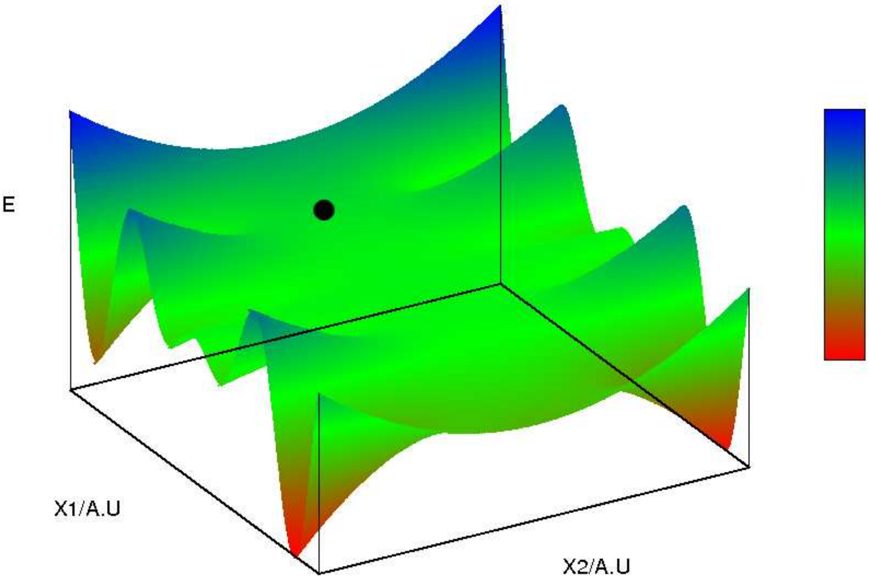

Figure 2.4: Saddle point on a cut through the configuration space.

2.1.3.3 Free energy

The most commonly observed structures in the experiments are the ones which have the lowest free energy (Eqn. 2.9).

$$F\left(\mathscr{R}\right) = -k_B T ln Z\left(\mathscr{R}\right) \tag{2.9}$$

Hence, we have to perform a minimization of the local free energy over all locally ergodic regions which correspond to metastable modifications. The configurational space of locally ergodic regions consists of many isolated local minima, surrounded by high energetic and entropic barriers (see Fig. 2.2). If we consider mathematically the local free energy, it is not a continuous function of $\mathscr{R}$. Consider a continuous order parameter $\vec{M}$ which describes the full solution space. Then we can calculate the free energy as a function of the order parameter. But there is one shortcoming in this assumption, that the region of the landscape which corresponds to a given value of this parameter $\vec{M}$ is usually not locally ergodic. In the best possible case we can divide the coordinates into two parts: a first one which depends upon the degrees of freedom that equilibrate very quickly, and the rest that vary more slowly (so-called reaction coordinates). We can approximate the full free energy on short time scales, by computing F only with respect to the fast degrees of freedom.

At very low temperatures, in the case of insulators, only the lattice vibrations (phonons) contribute to the local free energy, whereas in metals, the electrons at the Fermi level are more important than the phonons.

3

Electronic structure calculations

In this chapter, we present a short overview on the electronic structure calculations for the ideal crystalline solid. This is also applicable for various systems such as molecules, glasses, and biological systems. The aim of the present research is to study the ideal periodic solid. First, we discuss different methods used for solving the Schrödinger equation. Later, the calculation of physical properties using *ab-initio* simulation methods is presented. This chapter is mainly based on the text books by Jensen (158), Cramer (159), Chaplot (160) and resources such as Wikipedia (161), articles by C. D. Sherrill (162), and on different methods of charge analyses (163, 164).

3.1 Quantum mechanics

3.1.1 Introduction

From the beginning to the middle of the 20th century, the foundation and development of quantum mechanics has drastically changed the understanding of physics. Quantum mechanics has explained occurrences of various phenomena with a high accuracy, and the significance of quantum mechanics in the pure and applied science is evident.

For modeling real systems, one has to solve the Schrödinger equation. But the Schrödinger equation cannot be solved analytically for all but the most trivial systems. Out of these trivial cases, most are not applicable to realistic systems. To get more information about a realistic system, the Schrödinger equation usually has to be solved numerically.

For a detailed description of the electron distribution, there is no substitute for quantum mechanics. Electrons are very light particles and they cannot be explained correctly even qualitatively by classical mechanics. We start with the basic features of quantum mechanics. The important thing used in electronic structure calculations (159) is the wave function, Ψ. The operators which operate on Ψ return the observable properties of the system.

$$\langle \vartheta \rangle = \langle \Psi \mid \vartheta \mid \Psi \rangle$$

$$\vartheta\Psi = e\Psi \tag{3.1}$$

where ϑ is an operator and e is a value for some physical property of the system. The equation 3.1 holds good if Ψ is an eigenstate of ϑ. Ψ is called an eigenfunction and e an eigenvalue. For a bound particle, the normalized integral of $\mid \Psi \mid^2$ over all space must be unity which requires that Ψ is quadratically integrable.

3.1.2 Hamiltonian

The operator in Eqn. 3.1 that returns the system energy E as an eigenvalue, is called the Hamiltonian operator, H. Thus,

$$H\Psi = E\Psi \tag{3.2}$$

which is the time independent Schrödinger equation for a system of N particles. The nonrelativistic Hamiltonian for a chemical system is as follows:

$$\begin{aligned} H &= -\sum_i \frac{\nabla_i^2}{2} - \sum_i \frac{\nabla_A^2}{2M_A} - \sum_{A,i} \frac{Z_A}{r_{Ai}} \\ &\quad + \sum_{A>B} \frac{Z_A Z_B}{R_{AB}} + \sum_{i>j} \frac{1}{r_{ij}} \end{aligned} \tag{3.3}$$

where i and j are associated with electrons, A and B are associated with nuclei, R denotes the nuclear coordinates, and r denotes the electronic coordinates. The mass of an electron, m_e, the charge, Plancks constant h divided by 2π, the permittivity of the vacuum, are all set to unity.

The Schrödinger equation can be rewritten as:

$$H = T_{\mathrm{N}}(\mathbf{R}) + T_{\mathrm{e}}(\mathbf{r}) + V_{\mathrm{eN}}(\mathbf{r};\mathbf{R}) + V_{\mathrm{NN}}(\mathbf{R}) + V_{\mathrm{ee}}(\mathbf{r}) \tag{3.4}$$

where $\mathrm{T_N}$, $\mathrm{T_e}$, $\mathrm{V_{ee}}$, $\mathrm{V_{NN}}$, and $\mathrm{V_{eN}}$ represent the nuclear and electron kinetic energy operators and electron-electron, electron-nuclear, and nuclear-nuclear interaction potential operators, respectively. Spin-orbit effects can be incorporated using a spin-orbit operator H_{so}.

To solve the equation, some approximations are applied to reduce the complexity to a manageable level. By applying the Born-Oppenheimer approximation (165), we separate the electronic and the ionic degrees of freedom. Next, we solve the equation for the electrons in a static lattice potential of fixed ions. A separation of the Hamiltonian into a nuclear and an electronic part is not possible because of the potential term which has contributions from the electrons and the nuclei (162). Hence, the molecular wavefunction is composed of a combination of nuclear and electronic terms, $\Psi(\mathbf{r},\mathbf{R}) = \psi(\mathbf{r};\mathbf{R})\,\chi(\mathbf{R})$, where $\psi(\mathbf{r};\mathbf{R})$ and $\chi(\mathbf{R})$ is the electronic and nuclear wavefunction, respectively. By introduction of the Born-Oppenheimer approximation one can solve the equation 3.2. It is based on the fact that the nuclei are much heavier than the electrons, which allows us to assume that the nuclei are nearly stationary with respect to the electron motion. The kinetic energy of the nucleus $\mathrm{T}_N(\mathbf{R})$ can be neglected as compared to the kinetic energy of electron T_e by a fraction of $\mu_e \diagup M_A$, where μ_e and M_A is the reduced mass of an electron and mass of the nucleus, respectively. Thus, after the Born-Oppenheimer approximation, it remains:

$$\begin{aligned} H_{\mathrm{el}} &= T_{\mathrm{e}}\left(\mathbf{r}\right) + V_{\mathrm{eN}}\left(\mathbf{r};\mathbf{R}\right) + V_{\mathrm{ee}}\left(\mathbf{r}\right) \\ \text{such that} & \\ H_{\mathrm{el}}\psi\left(\mathbf{r};\mathbf{R}\right) &= E_{el}\psi\left(\mathbf{r};\mathbf{R}\right) \qquad (3.5) \end{aligned}$$

This can be termed as the ”clamped-nuclei” Schrödinger equation (162). For solids, V_{NN} is infinite. This divergence is compensated by V_{eN} and V_{ee}. H_{el} cannot be written as a sum of one electron terms due to V_{ee}. If we neglect V_{ee} or replace it by a function $\mathrm{V}_{\mathrm{ee}}\left(\mathbf{r}\right)$ which is the same for all electrons, then all electrons see the same, average, potential. Then, we can replace the many-particle equation by N identical independent one-particle equations, the so-called band-approximation. Under these circumstances, the only “remnant” of the many-body nature of the problem is the Pauli-principle, i.e. no electronic state can be occupied by two electrons.

We can additionally consider spin-orbit effects. These can be incorporated at each nuclear configuration according to

$$H_0 = H_{\mathrm{el}} + H_{\mathrm{so}} \qquad (3.6)$$

$$(3.7)$$

Usually, the first major approximation when dealing with the electrons is the one-electron approximation, which leads to the Hartree- and the Hartree-Fock approximations. This results in N one-particle equations, where each electron sees a different average potential generated by the other $N-1$ electrons. We now have to solve each one-particle equation separately, and feed the N one-particle ground state wave functions back into T_{e}, V_{ee} and V_{eN}, until self-consistency is reached.

3.2 Hartree-Fock method

The Hartree Fock method (159, 166, 167) is the simplest method to solve the many-body Hamiltonian. With this method one can determine the ground-state wave function and the ground state energy of the system. The simple assumption is that the wave-function is approximated by a Slater determinant. The variational method is used to solve a set of N coupled equations for the N spin orbitals. The exact solution of this set of N coupled equations gives the Hartree-Fock wave function and energy of the system. This is a commonly used method in quantum chemistry. The Hartree-Fock method broadly divides into two parts: Restricted Hartree-Fock (RHF) (158, 168, 169) and Unrestricted Hartree-Fock (UHF) (170).

3.2.1 Hartree-Fock algorithm

To solve the time-independent Schrödinger equation for the many-body Hamiltonian, the Hartree-Fock approximation is one of the most straightforward approaches. Since the problem is usually too difficult to be solved analytically, numerical techniques are applied. The Hartree-Fock algorithm proceeds as follows:

1. Guess the initial spin orbitals (one electron orbitals) $\psi_i = \sum_k^M c_{ik}\phi_k$ with expansion coefficient c_{ik}
2. Compute the electronic density, $n(r)$, with the recent spin orbitals.
3. Solve the single-electron equations for the spin orbitals using the electronic density from step (2)
4. If the spin orbitals are identical in step (2) and (3), then these are the solution for the HF problem. If not, then use the orbitals from step (3) and return to step (2).

As we have mentioned earlier, a set of approximate one-electron orbitals which is similar to the solutions of the hydrogen atom, is used. Both for molecular or crystalline calculations, we consider linear combinations of atomic orbitals (LCAO) (171, 172) as guess for the initial one-electron wave functions. With the LCAO method, other electrons are considered in an averaged manner. In the Hartree-Fock method, the effect of the remaining electrons is taken care using mean-field theory. The optimization of the orbitals is performed by the minimization of the expectation value of the energy of the Slater determinant. The outcome of this variational method on the orbitals is the Fock operator, which is a new one-electron operator. The orbitals corresponding to the minimum energy value have energy eigenvalues with respect to the Fock operator. The most important approximation of the Hartree-Fock method is its simplification of the Coulombic repulsion term. The repulsion energy experienced by every electron in the system is computed using a continuous distribution of negative charge which is contributed by all electrons within the chemical system.

Since the Fock operator depends on the orbitals used to construct the corresponding Fock matrix, the eigenfunctions of the Fock operator are in turn new orbitals which can be used to construct a new Fock operator (161). In this way, the Hartree-Fock orbitals are optimized iteratively until the change in total electronic energy falls below a predefined threshold. In this way, a set of self-consistent one-electron orbitals is calculated. The Hartree-Fock electronic wave function is then the Slater determinant constructed out of these orbitals. Following the basic postulates of quantum mechanics, the Hartree-Fock wave function can then be used to compute any desired chemical or physical property within the framework of the Hartree-Fock method and the approximations employed.

The flow-chart in fig. 3.1 shows that the Fock matrix is constructed from the orbitals. Then the eigenfunctions of the respective matrix give the new Fock operator and this operator returns new orbitals which are used to generate once again a new Fock operator. With this procedure, the optimization of the Hartree-Fock orbitals is performed iteratively till the energy difference between subsequent iterations falls below a minimal value. During this procedure, also the one-electron orbitals are computed

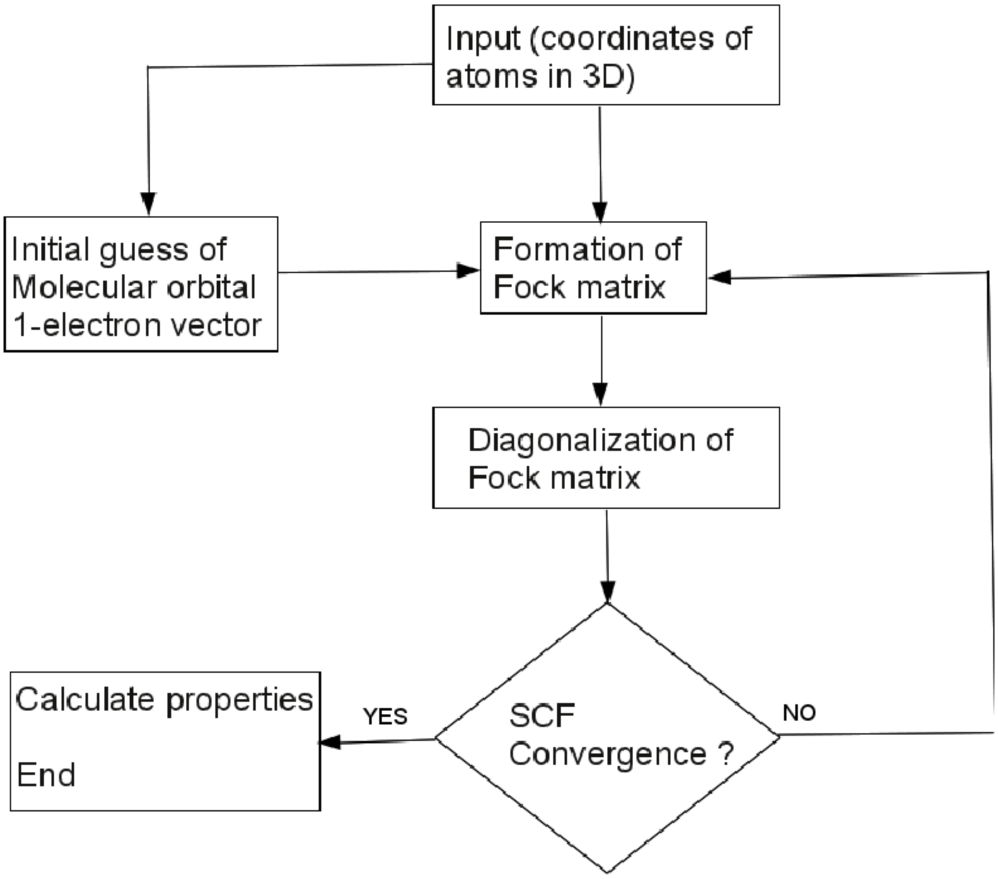
Input (coordinates of atoms in 3D)
Initial guess of Molecular orbital 1-electron vector
Formation of Fock matrix
Diagonalization of Fock matrix
SCF Convergence ?
YES
NO
Calculate properties
End

Figure 3.1: Simplified Hartree-Fock procedural flowchart.

self-consistently. With the help of the Hartree-Fock method, the Schrödinger equation is therefore approximately solved.

One important thing one should keep in mind is the stability of this method. To make this method stable, a mixing of the Fock matrix of subsequent iterations is useful. While performing Fock matrix mixing, the single electron wave function is calculated with the help of a linear combination of the present and the previous Fock operator instead of a direct calculation of the Fock matrix with the present single electron wave function. The above methodology is useful for molecular calculations and calculations on solids.

In modern Hartree-Fock calculations, the one-electron wavefunctions are approximated by a linear combination of atomic orbitals (LCAO) (171, 172), or so-called Slater-type orbitals. It is very common for the atomic orbitals (AO) to be composed of a linear combination (LC) of one or more Gaussian-type orbitals, rather than Slater-type orbitals. Various basis sets (159, 166, 167, 173, 174, 175, 176) are used in practice, most of which are composed of Gaussian functions.

The Hartree-Fock method is a crude approximation which often leads to large discrepancies with the experimental results. To overcome these shortcomings, post Hartree-Fock methods have been developed, which deal with the electron correlation part of the multi-electron wave function. There are different methods such as configurational interaction, coupled cluster, Møller-Plesset perturbation theory, quadratic configuration interaction, and quantum chemistry composite methods.

3.3 Density Functional Theory (DFT)

Density functional theory (DFT) (166, 177, 178) is another approach to solve Schrödinger's wave equation, which provides good information about the ground state properties for metals, semiconductors, and insulators. It is one more method to solve the Schrödinger equation for a many-body system. It gives precise information about the ground-state energy. This method is based on a functional (a function of another function). The functional is a function which takes a value of a variable or variables and defines a single number from those variables. Here, the function is the electron density. And thus, the name of the method is due to functionals which depend on the electron density. If we consider a system with N constituents, then the density depends only on three variables, i.e., the spatial coordinates x,y,z, instead of 3*N (where every atom has three degrees of freedom), which makes calculations easier.

In 1964, Hohenberg and Kohn published their paper on DFT (179, 180). Density functional theory is based on two fundamental mathematical theorems proved by Hohenberg and Kohn and the derivation of a set of equations by Kohn and Sham. The first theorem is: The ground-state energy of the Schrödinger equation is a unique functional of the electron density. The physical interpretation of this theorem is: there exists a one-to-one mapping between the ground-state wave function and the ground-state electron density. The importance of this result is hidden in one term, called functional. According to Hohenberg and Kohn's theorem, the ground-state energy E can be expressed as $E[n(\mathbf{r})]$, where $n(\mathbf{r})$ is the electron density. The electron density $n(\mathbf{r})$ corresponding to an N-electron wavefunction $\Psi^{(N)}$ is given by the one-electron function:

$$n(\mathbf{r}) = 2\sum_i \Psi_i(\mathbf{r})^* \Psi_i(\mathbf{r}) \tag{3.8}$$

.

The second theorem of Hohenberg-Kohn is: The electron density that minimizes the energy of the overall functional is the true electron density corresponding to the full solution of the Schrödinger equation. By knowing the true functional form, one can vary the electron density until the energy of the functional is minimized. With the help of the Hohenberg-Kohn theorem, the functional can be written in terms of the single-electron wave functions, $\Psi_i(r)$. The energy functional is given as

$$E[\Psi_i] = E_{known}[\Psi_i] + E_{XC}[\Psi_i] \tag{3.9}$$

where $E_{known}[\Psi_i]$ is a simple analytical form, which is given by

$$\begin{aligned} E_{known}[\Psi_i] &= \sum_i \int \Psi_i^* \nabla^2 \Psi_i d^3\mathbf{r} + \int V(\mathbf{r})\, n(\mathbf{r})\, d^3\mathbf{r} \\ & \iint \frac{n(\mathbf{r})\, n(\mathbf{r}')}{|\mathbf{r}-\mathbf{r}'|} d^3\mathbf{r} d^3\mathbf{r}' + E_{ion} \end{aligned} \tag{3.10}$$

In the above expression, the known energy is composed of the kinetic energy, the Coulomb interaction between electrons and the nuclei, pairs of electrons, and pairs of nuclei. $E_{XC}[\Psi_i]$ is the exchange-correlation functional. It is defined to include all the quantum mechanical effects that are not included in the known terms. Still it is difficult to solve the full Schrödinger equation for any wave function. This problem is solved by Kohn and Sham, who showed that the electron density can be represented in such a way that involves solving a set of equations in which each equation only involves a single electron.

The KohnSham equations can be written as

$$[\nabla^2 + V(\mathbf{r}) + V_H(\mathbf{r}) + V_{XC}(\mathbf{r})]\Psi_i(\mathbf{r}) = \varepsilon_i \Psi_i(\mathbf{r}) \tag{3.11}$$

There are three potentials, viz., V, V_H, and V_{XC} on the left-hand side of the Kohn-Sham equations. V is the interaction between an electron and nuclei. V_H is Hartree potential, the Coulomb repulsion between the electron and the total electron density contributed by all electrons. It is defined as

$$V_H(\mathbf{r}) = \int \frac{n(\mathbf{r}')}{\mathbf{r}-\mathbf{r}'} d^3(\mathbf{r}') \tag{3.12}$$

The Hartree potential includes the Coulomb interaction between an electron with itself which is unphysical. V_{XC} includes a correction for the self-interaction, and exchange and correlation (181, 182, 183, 184) contributions to the single electron equations.

For solving the Kohn-Sham equations, we have to specify the Hartree potential, which depends on the electron density. But, to get the electron density, we should know the single-electron wave functions, and to know these wave functions we must solve the Kohn-Sham equations. For the solution of this problem, we have to solve the Kohn-Sham equations iteratively.

The procedure is analogous to the Hartree-Fock self consistency procedure 3.2.1.

3.3.1 Exchange-Correlation Functional

Solving the many-body problem is an extremely difficult task but the theorems given by Kohn, Hohenberg, and Sham showed that the ground state can be found by minimizing the energy of an energy functional (177). This can be obtained by discovering a self-consistent solution for a set of single-particle equations. But, defining the exchange-correlation function, $E_{XC}[\Psi_i]$ in the Kohn-Sham equations is one of the difficult tasks. We can approximate this functional by considering the uniform electron gas (181, 182, 183, 184). In such a situation the electron density is constant at all points in space; i.e., $n(\mathbf{r}) = \text{constant}$. This situation is the simplest one whereas, in reality, it is quite different. The definition of the chemical bond is not possible with this condition. But, the uniform electron gas gives an easy and efficient way to solve the Kohn-Sham equations. We can define the exchange-correlation potential at every point as the known exchange-correlation potential from the uniform electron gas with the electron density observed at the same position:

$$V_{XC}[n(\mathbf{r})] = V_{XC}^{\text{electron gas}}[n(\mathbf{r})] \tag{3.13}$$

This approximation is called the local density approximation (LDA) which takes into consideration only the local density.

The next approach is to consider the local density and its gradient. This approach is known as generalized gradient approximation (GGA). It includes more physical information than the LDA, so it is usually better than LDA. But, this approach is still not always accurate.

There are different ways in which the information from the gradient of the electron density can be inserted in a GGA functional. Out of them, two commonly used functionals in *ab-initio* calculations are the Perdew-Wang functional (PW91) (177, 185, 186) and the Perdew-Burke-Ernzerhof functional (PBE) (177, 187). These are usually used for solids. Apart from these functionals, many other GGA functionals have been developed.

3.4 Basis sets

Ab-initio calculations were used to solve the Schrödinger equation without any information from the experiments. Sometimes it is very handy to compare the results with experiments for a specific problem, according to that one a computational model is developed. This procedure requires less simulation time.

A finite basis set (159, 166, 167, 173, 174, 175, 176) is one of the approximations for performing *ab-initio* calculations. This is the set of functions used to create the molecular orbitals (MO). A basis set is said to be incomplete when the set of functions is finite, or in practice, does not provide a good approximation. The full basis set (infinite size) is computationally expensive or impossible to use. In a finite basis set, only the MO components along the coordinate axes of the basis functions are considered. For a smaller basis set, the representation is insufficient, because it does not provide enough information. The accuracy depends on the type of basis functions (181, 182, 183, 184, 188) used. In the following section, some information about the different types of basis sets is presented.

3.4.1 Basis sets types

3.4.1.1 Slater and Gaussian Type Orbitals

There are two types of basis sets commonly used in *ab-initio* calculations: Slater Type Orbitals (STO) (189, 190, 191, 192, 193) and Gaussian Type Orbitals (GTO) (194, 195, 196, 197, 198, 199). The functional form of Slater type orbitals is given in eqn. 3.14

$$\chi_{\zeta,n,l,m}\left(r,\theta,\phi\right)=NY_{l,m}\left(\theta,\phi\right)r^{n-1}e^{\zeta r} \tag{3.14}$$

where N is a normalization constant and $Y_{l,m}$ are spherical harmonic functions. r is the distance between nucleus and electron. Usually, the radial node is not present in the STOs, but this can be achieved by introducing linear combinations of STOs. For a fast convergence, the exponential factor and an increasing number of basis functions are responsible. Using analytical techniques, it is difficult to calculate three- and four-center two-electron integrals. Initially, STOs were commonly used where a requirement of a high accuracy existed, e.g. for atomic and diatomic systems. Also, they can be applied in the case of semi-empirical methods where all high order integrals can be neglected. They are useful in density functional theory, when there is no exact exchange, for fitting the density with a set of basis functions in order to determine the Coulomb energy.

The representation of Gaussian type orbitals in polar and Cartesian form is as in eqn. 3.15

$$\begin{aligned}\chi_{\zeta,n,l,m}\left(r,\theta,\phi\right) &= NY_{l,m}\left(\theta,\phi\right)r^{2n-2-l}e^{\zeta r^2}\\ \chi_{\zeta,l_x,l_y,lz}\left(x,y,z\right) &= Nx^{l_x}y^{l_y}z^{l_z}e^{\zeta r^2}\end{aligned} \tag{3.15}$$

The main difference between STOs and GTOs is in the exponential factor. At the nucleus a GTO has a zero slope, whereas a STO has a cusp (discontinuous) derivative. The square of the radial term in the exponential part of GTOs is responsible for representing the proper behavior near the nucleus, but falls off too rapidly far from the nucleus as compared with an STO. And the tail of the wave function is described poorly because of this decaying factor. From this discussion, we conclude the selection of GTOs should be done carefully to achieve a similar accuracy compared with STOs.

The important factor is the number of functions to be used after deciding on the type of function (STO/GTO) and the location (nuclei). A minimum basis set consists of the smallest number of functions needed to describe all electrons. For all the electrons of the neutral atom, there must be sufficient functions. While representing first row elements of the periodic system, there should be two s-functions (1s and 2s) and one set of p-functions (2p_x, 2p_y and 2p_z). Similarly, for the higher elements one should use more functions.

The next advancement in basis set size is a doubling of all the basis functions; the Double Zeta (DZ) (200, 201) basis type. Here, Zeta (ζ) is the factor in the exponential term of the basis functions. A DZ basis has two s-functions for hydrogen (1s and 1s'). Valence orbitals take part in the formation of the chemical bond. A DZ basis type doubles the number of the valence orbitals which produces a split valence basis. Only in some special cases DZ basis sets are used in calculations. Similarly, Triple Zeta

(TZ) (200, 201, 202, 203), Quadruple Zeta (QZ) (200) and Quintuple or Pentuple Zeta (PZ or 5Z) for the next levels of basis sets are also used.

Further functions are the polarization and diffuse functions. The polarization functions have higher values of the angular quantum number (l) than the filled atomic orbitals of the respective atom (e.g., for sulphur, introduction of the d-functions are considered polarization functions). The polarization functions are important for reproducing the chemical bonding and performing simulations on correlated systems. Diffuse functions are those functions which have very small exponents and decay slowly with distance from the nucleus.

3.4.2 Plane Waves

Ideally, functions with an infinite range can be use to model periodic system. The concept of plane-waves is influenced by the way one models valence electrons in a metal in the free electron approximation. Hence, the solution of the Schrödinger equation for free electron in one-dimension is given as:

$$\begin{aligned} \phi\left(\mathbf{x}\right) &= Ae^{i\mathbf{k}x} + Be^{-i\mathbf{k}x} \\ E &= \frac{\hbar^2 k^2}{2m} \end{aligned}$$

Here, $\mathbf{k}$ is wave vector. Orbitals represented using plane waves characterize the electrons in a band. It is expressed with a complex function in 3 dimensions as:

$$\chi_{\mathbf{k}}(\mathbf{r}) = e^{i\mathbf{k}\cdot\mathbf{r}}u(\mathbf{r}) \tag{3.16}$$

where $u(\mathbf{r})$ is a periodic Bloch function. $\mathbf{k}$ is also considered a frequency factor and high $\mathbf{k}$ values signify a rapid oscillation. Usually, plane wave basis sets are larger than Gaussian ones. The size of the plane wave basis set depends upon the periodicity of the system whereas Gaussian basis sets depend upon the number of atoms in the simulation cell. With these advantages, plane wave basis sets are more applicable in large systems. Plane wave basis functions are more useful to describe delocalized, slowly varying electron densities, especially in the case of the valence bands in a metal.

3.4.2.1 Orthogonalized plane waves (OPW)

This method (204, 205) was developed by Herring in 1940. It considers the oscillations of the wave functions in the atomic core and the plane-wave-like behavior outside the core. The OPW-approximation uses a combination of localized sets taken from an atomic-like calculation, and the non-localized states are plane-waves which are orthogonalized to the core states.

The OPW state can be represented as:

$$|\phi^{OPW}_{\mathbf{k}+\mathbf{K}}\rangle = |\mathbf{k}+\mathbf{K}\rangle - \sum_c \langle\phi_c|\mathbf{k}+\mathbf{K}\rangle|\phi_c\rangle \tag{3.17}$$

where the sum runs over all core states with Bloch vector **k**. Here, the first term and the second term on the right hand side are the localized and non-localized states, respectively.

A Schrödinger equation 3.3 is satisfied by the orthogonalized plane waves with change in the potential as follows:

$$V_{OPW} = V + \sum_{c} (\epsilon - \epsilon_c) \, |\phi_c\rangle\langle\phi_c| \tag{3.18}$$

3.4.2.2 The Muffin-tin potential

The Muffin-tin potential (206, 207) is a variable potential within a sphere of radius r_0 around every atom and is constant elsewhere.

The muffin-tin potential is defined as:

$$U_{m-t}(\mathbf{r}) = \begin{cases} V(|\mathbf{r} - \mathbf{R}|) & \text{when } |\mathbf{r} - \mathbf{R}| < r_0 \\ \text{constant} & \text{when } |\mathbf{r} - \mathbf{R}| \geq r_0 \end{cases}$$

where r_0 is less than half the distance between nearest neighbors.

3.4.2.3 The Augmented plane-wave method (APW)

This method was developed (207, 208) by Slater in 1937 (207, 208). The effective crystal potential is assumed to be constant between the cores. The wave function for the wave vector **k** can be written as:

$$\psi_{\mathbf{k}}(\mathbf{r}) = \begin{cases} e^{i\mathbf{k}.\mathbf{r}} & \text{when } |\mathbf{r} - \mathbf{R}| < r_0 \\ \text{atomic function} & \text{when } |\mathbf{r} - \mathbf{R}| \geq r_0 \end{cases}$$

where r_0 is the core radius. The wave function outside the core is a plane wave as the potential is constant, whereas the function is atom-like in the core part. Such an atomic solution can be found by solving the Schrödinger equation inside the core region. The full solution is chosen in such a way that it can join such two different functions.

There is no restriction on **k** and ϵ for a plane-wave, as we have $\epsilon = \hbar^2 k^2 / 2m$. It is the boundary conditions which connect **k** with a given ϵ.

There are some disadvantages of APW: in general, the wavefunction has discontinuous derivatives on the boundary between the interstitial and atomic regions. The APW method is computationally very expensive because the augmenting function R_l corresponds to an exact muffin-tin potential eigenstate. The energy dependence of the function R_l leads to an eigenvalue problem that will be non-linear in energy and has to be solved iteratively.

3.4.3 Effective Core Potentials

A system which contains atoms from the lower part of the periodic table has more core electrons compared to a system with atoms only from the upper half of the periodic table. There are two problems regarding these atoms, which are the very large number of electrons and the proper description of relativistic effects. To overcome these problems, one can consider only the valence electrons, and the effects of the core electrons are modeled by some functions. Such modeling functions are known as Effective Core Potential (ECP) (158, 209, 210, 211) or Pseudopotential (PP). The elimination of core electrons still gives good results, with less computational time as compared to an all electron calculation. Considering relativistic effects (especially the scalar effects) is also possible and advisable.

There are four important steps for designing an ECP:

- Obtain a good-quality all-electron wave function for the atom using a Hartree-Fock, a relativistic Dirac-Hartree-Fock or a density functional calculation.
- Find the replacement of the valence orbitals by choosing an appropriate set of node-less pseudo-orbitals.
- Find a potential for the core electrons which is parameterized by an expansion in analytical functions of the distance between nucleus and electron.
- Look for the right parameters for the potential such that the solutions of the Schrödinger (or Dirac) equation gives matching results for pseudo-orbitals and the all-electron valence orbitals.

The quality of the ECP is determined by the number of valence electrons. The outer (n + 1)s-, (n + 1)p- and (n)d-orbitals denote the set of valence electrons for transition metals. The large-core potentials give reasonable geometries, but the energies are not always satisfactory. Better results can be achieved by considering the orbitals in the next lower shell in the valence space, although this comes with extra computational cost. For example, for the lanthanum atom (atomic number 57), the ECPs (in italics) and valence electrons (in bold) are given as follows:

- Large-core ECP: 9 electrons in valence space:
  $(1s)^2(2s)^2(2p)^6(3s)^2(3p)^6(4s)^2(3d)^{10}(4p)^6(5s)^2(4d)^{10}(\mathbf{5p})^{\mathbf{6}}(\mathbf{6s})^{\mathbf{2}}(\mathbf{5d})^{\mathbf{1}}$
- Small-core ECP: 27 electrons in valence space:
  $(1s)^2(2s)^2(2p)^6(3s)^2(3p)^6(4s)^2(3d)^{10}(\mathbf{4p})^{\mathbf{6}}(\mathbf{5s})^{\mathbf{2}}(\mathbf{4d})^{\mathbf{10}}(\mathbf{5p})^{6}(\mathbf{6s})^{\mathbf{2}}(\mathbf{5d})^{\mathbf{1}}$
- All-electron ECP: 57 electrons in valence space:
  $(\mathbf{1s})^{\mathbf{2}}(\mathbf{2s})^{\mathbf{2}}(\mathbf{2p})^{\mathbf{6}}(\mathbf{3s})^{\mathbf{2}}(\mathbf{3p})^{\mathbf{6}}(\mathbf{4s})^{\mathbf{2}}(\mathbf{3d})^{\mathbf{10}}(\mathbf{4p})^{\mathbf{6}}(\mathbf{5s})^{\mathbf{2}}(\mathbf{4d})^{\mathbf{10}}(\mathbf{5p})^{\mathbf{6}}(\mathbf{6s})^{\mathbf{2}}(\mathbf{5d})^{\mathbf{1}}$

Usually, the Projector Augmented Wave (PAW) method is considered an all-electron pseudopotential method (It is an effective potential built by replacing the all-electron potential). The PAW is computationally expensive compared to large-core or small-core ECP, however.

3.5 Methods used to estimate atomic charges in crystal structures

3.5.1 Mulliken population analysis

The charge or spin-density distribution is one of the important properties of a chemical system. There is no unique way to choose electrons which are connected to an atom in a molecule, based only on the electron density. The Mulliken population analysis (164, 212, 213, 214) is an easy and commonly used way to count electrons in an atom.

The number of electrons of a chemical system is related to the density matrix and the overlap integrals. It can be defined as:

$$\begin{aligned} N &= \int d\mathbf{r}\rho(\mathbf{r}) \\ &= 2\sum_{i=1}^{N/2}\left(\sum_{\mu=1}^{K} c_{\mu i}\phi_{\mu}(\mathbf{r})\right)\left(\sum_{\nu=1}^{K} c_{\nu i}\phi_{\nu}(\mathbf{r})\right) \\ &= 2\sum_{i=1}^{N/2}\sum_{\mu=1}^{K} c_{\mu i}c_{\mu i}\phi_{\mu}(\mathbf{r})\phi_{\mu}(\mathbf{r}) + 2\sum_{i=1}^{N/2}\sum_{\mu=1}^{K}\sum_{\nu=\mu+1}^{K} c_{\mu i}c_{\nu i}\phi_{\mu}(\mathbf{r})\phi_{\nu}(\mathbf{r}) \end{aligned} \tag{3.19}$$

where $\rho(\mathbf{r})$ is electron density. $c_{\mu i}$ and $c_{\nu i}$ are the coefficients of the basis functions. The density matrix can be defined as:

$$P_{\nu\mu} = 2\sum_{i=1}^{N/2} c_{\mu i}c_{\nu i} \tag{3.20}$$

Substitution in eqn. 3.19 gives

$$N = \sum_{i=1}^{K} P_{\mu\mu}S_{\mu\mu} + 2\sum_{i=1}^{K}\sum_{\nu=\mu+1}^{K} P_{\mu\nu}S_{\mu\nu} \tag{3.21}$$

where $S_{\mu\nu}$ is an overlap integral.

The eqn. 3.21 shows the relation between the density matrix and the overlap integral. The net nuclear charge can be defined as:

$$q_A = Z_A - \sum_{\mu=1;\mu \text{ on } A}^{K} P_{\mu\mu}S_{\mu\mu} - \sum_{\mu=1;\mu \text{ on } A}^{K}\sum_{\nu=1;\nu\neq\mu}^{K} P_{\nu\mu}S_{\mu\nu} \tag{3.22}$$

$$\tag{3.23}$$

The density matrix is available due to the self-consistent field procedure. Hence, Mulliken population analysis is a simple and quick calculation.

3.5.2 Bader charge analysis

This concept is used to develop an efficient way of dividing a molecule into "atoms" and was proposed by Bader (163, 215). According to this, the definition of an atom depends on the charge density. Zero flux surfaces are used to separate "atoms" in a molecule. A zero flux surface is the two-dimensional surface on which the gradient of the charge density is parallel to the surface. Usually, in a molecular system the charge density goes to a minimum value between atoms. This is an obvious and natural way to separate atoms from each other.

Here, the algorithm (216) is briefly explained: The input data required for this analysis is the electron density ρ associated with a rectangular volume V which contains the whole molecule. The volume is selected such that the electron density outside of this volume is insignificant; in mathematical terms it tends to zero. The volume is split into M parts with δV_i, where i = 1,....M. The center of each δV_i is defined as $r_i = l\Delta x\vec{\mathbf{i}} + m\Delta y\vec{\mathbf{j}} + n\Delta z\vec{\mathbf{k}}$ where l, m, and n are the different numbers associated with the mesh points and Δx, Δy, and Δz is the differential distance between mesh elements along the Cartesian directions. With this technique every volume element δV_i is assigned to a Bader volume and this volume is associated with the particular nucleus. And in some case (which rarely exists), the Bader volume is related to a local minimum of ρ, which is not a nucleus.

Using the above algorithm (217), the first nucleus is identified. Later, for locating another nucleus, the steepest descent method is applied to find the maximum value of the charge density. The steepest ascent trajectory is started from all grid points, the partitioning analysis is performed, and all grid points are assigned to a respective Bader region. Assigning the grid points to Bader regions is important because one can perform a charge analysis and compute multi-pole moments. This analysis is also used to define the hardness of atoms, which is useful to calculate the amount of energy required to remove an electron from an atom.

3.6 Lattice dynamics and thermodynamic properties

3.6.1 Lattice Dynamics

The theoretical formulation of lattice dynamics is based on the Born-Oppenheimer approximation. The assumption in this approximation is that the electronic wavefunctions change adiabatically during the nuclear motion. Electrons contribute an additional effective potential for the nuclear motions and the lattice vibrations are associated only with the nuclear motions. The theory of lattice dynamics (160) is briefly explained in this section.

3.6.1.1 Theoretical formulation of Lattice Dynamics

For small displacements of the atoms in the crystal structure, $\mathbf{u}\binom{l}{\kappa}$, from their equilibrium positions, $\mathbf{r}\binom{l}{\kappa}$, where l is the l^{th} unit cell (l = 1, 2, . . . N) and k is the k^{th} type of atom (k = 1,2, . . . n) in the unit cell, the crystal potential energy can be written as a Taylor expansion. The expansion is retained only up to the second derivative in the so-called harmonic approximation, as follows:

$$\phi = \phi_0 + \phi_1 + \phi_2 \tag{3.24}$$

where

$$\begin{aligned}
\phi_0 &= \phi\left(\mathbf{r}\begin{pmatrix} l \\ \kappa \end{pmatrix}\right) \\
\phi_1 &= \sum_{l\kappa\alpha} \phi_\alpha \begin{pmatrix} l \\ \kappa \end{pmatrix} u_\alpha \begin{pmatrix} l \\ \kappa \end{pmatrix} \\
\phi_2 &= \frac{1}{2}\sum_{l\kappa\alpha}\sum_{l'\kappa'\beta} \phi_{\alpha\beta}\begin{pmatrix} l & l' \\ \kappa & \kappa' \end{pmatrix} u_\alpha \begin{pmatrix} l \\ \kappa \end{pmatrix} u_\beta \begin{pmatrix} l' \\ \kappa' \end{pmatrix}
\end{aligned}$$

where α and β represent Cartesian coordinates.
At the equilibrium position, the forces on each atom vanish, which results into

$$\phi_\alpha \begin{pmatrix} l \\ \kappa \end{pmatrix} = 0, \text{ for every } \alpha, \kappa, \text{ and } l.$$

Hence, $\phi_1 = 0$.
The equation of motion of the $(lk)^{th}$ atom is described as

$$m_\kappa u_\alpha \begin{pmatrix} l \\ \kappa \end{pmatrix} = -\sum_{l'\kappa'\beta} \phi_{\alpha\beta}\begin{pmatrix} l & l' \\ \kappa & \kappa' \end{pmatrix} u_\beta \begin{pmatrix} l' \\ \kappa' \end{pmatrix} \tag{3.25}$$

From eqn. 3.25, it is clear that $\phi_{\alpha\beta}\begin{pmatrix} l & l' \\ \kappa & \kappa' \end{pmatrix} u_\beta \begin{pmatrix} l' \\ \kappa' \end{pmatrix}$ is the negative of the force exerted on the atom $(l\kappa)$ in the α-direction because there is a small finite displacement of the atom $(l'\kappa')$ in the β-direction. The term $\phi_{\alpha\beta}$ is called the force constant.

Due to the periodicity of the crystal, the solution of eqn. 3.25 must obey a consistency condition: the displacements of an atom in a different unit cell must be the same apart from a phase factor. The solution of eqn. 3.25 is as follows; reminiscent of the Bloch functions for electrons in periodic potentials:

$$u_\alpha \begin{pmatrix} l \\ \kappa \end{pmatrix} = U_\alpha \left(\kappa \middle| q\right) exp\left[i\mathbf{q}.\mathbf{r}\begin{pmatrix} l \\ \kappa \end{pmatrix} - \omega\left(\mathbf{q}\right) t\right] \tag{3.26}$$

where $\mathbf{q}$ is the wave vector and $\omega\left(\mathbf{q}\right)$ is the angular frequency corresponding to the wave.

Putting epn. 3.26 into eqn. 3.25 we get,

$$m_\kappa \omega^2 (\mathbf{q}) U_\alpha \left(\kappa \middle| q\right) = \sum_{\kappa' \beta} D_{\alpha\beta} \begin{pmatrix} \mathbf{q} \\ \kappa\kappa' \end{pmatrix} U_\beta \begin{pmatrix} \kappa' \\ \mathbf{q} \end{pmatrix} \tag{3.27}$$

where m_κ is the mass element and $\mathbf{r}\begin{pmatrix} l \\ \kappa \end{pmatrix}$ is position coordinate of κth atom,
The dynamical matrix is given by

$$D_{\alpha\beta} \begin{pmatrix} \mathbf{q} \\ \kappa\kappa' \end{pmatrix} = \sum_{l'} \phi_{\alpha\beta} \begin{pmatrix} l & l' \\ \kappa & \kappa' \end{pmatrix} exp \left\{ i \left(\mathbf{q}. \left[\mathbf{r} \begin{pmatrix} l' \\ \kappa' \end{pmatrix} - \mathbf{r} \begin{pmatrix} l \\ \kappa \end{pmatrix} \right] \right) \right\} \tag{3.28}$$

The frequencies of the normal modes and eigenvectors are determined by diagonalizing the dynamical matrix through a solution of the secular equation

$$det \left| m_\kappa \omega^2 (\mathbf{q})^2 \delta_{\kappa\kappa'} \delta_{\alpha\beta} - D_{\alpha\beta} \begin{pmatrix} \mathbf{q} \\ \kappa\kappa' \end{pmatrix} \right| = 0 \tag{3.29}$$

$3n$ eigenvalues are obtained by solving eqn. 3.29, $\omega_j^2 (\mathbf{q})$, $(j = 1, 2, ..., 3n)$. As the dynamical matrix is Hermitian, the eigenfrequencies are real and its eigenvectors may be chosen as orthonormal. The components of the eigenvectors $\xi_j (\mathbf{q})$ decide the prototype of displacement of the atoms in a particular mode of vibration.
The displacement due to the vibration can be given as

$$u_\alpha \begin{pmatrix} l \\ \kappa \end{pmatrix} = \xi_\alpha \left(\kappa \middle| \mathbf{q} j\right) exp \left\{ i \mathbf{q}.r \begin{pmatrix} l \\ \kappa \end{pmatrix} \right\} P \begin{pmatrix} \mathbf{q} \\ j \end{pmatrix} \tag{3.30}$$

where, $P \begin{pmatrix} \mathbf{q} \\ j \end{pmatrix}$ is the normal coordinate and $\xi_\alpha \left(\kappa \middle| \mathbf{q} j\right)$ is the normalized eigenvector of the normal mode $(\mathbf{q}j)$, where $(j = 1, 2, ...3n)$ is used to distinguish between the $3n$ normal modes at $\mathbf{q}$. Corresponding to every direction in $\mathbf{q}$-space, there are $3n$ curves $\omega = \omega_j (\mathbf{q})$, $(j = 1, 2, ...3n)$. Such curves are known as phonon dispersion relations. In a periodic crystal, there are three zero frequency modes at $\mathbf{q} = 0$, which correspond to the acoustic branches. The rest of the $(3n - 3)$ branches has finite frequencies at $\mathbf{q} = 0$, which are called optical branches.

3.6.2 Phonons

For the detailed information of any system at the microscopic level, it is important to have knowledge about the crystal structure and the lattice dynamics of the atoms (218, 219, 220, 221). From the dynamical study of the atoms one can get more insight into many important physical properties such as phase transitions, thermal expansion, specific heat, and thermal conductivity. The dynamics of an atom depends upon the lattice vibrations which are the combined movement of atoms in solids which creates traveling waves. The excited lattice vibrations can often be described as harmonic below the Debye temperature. These vibrations can be described as linear combinations of vibrational eigenfunctions with discrete energies also known as "phonon". The phonons are described by three parameters, viz., wave vector, polarization vector, and energy. The information about the vibration of atoms along all the three directions is given by the polarization vector. The dispersion relation $\mathrm{E}(\omega)$ of the phonon spectrum, is an important quantity in the study of the physical properties of a solid system.

Above the Debye temperature, the higher order terms in the expression have to be taken into account, and the lattice vibrations are no longer harmonic and interaction of phonons can occur. If there is a small anharmonicity, this can be solved using perturbation theory. But if the anharmonicity is large, other methods have to be used. The dynamical matrix is calculated brute force in the case of molecular dynamics calculations. With this technique, one can study thermodynamic properties and phase transitions.

Experimentally, there are lattice vibration measurement techniques such as Raman spectroscopy, infrared absorption, inelastic neutron scattering, inelastic X-ray scattering, and so on. But these techniques have some limitations at high pressure and temperature. To overcome these problems, accurate models for various materials are used. The performance of the models in predicting thermodynamic properties depends on their ability to describe a variety of microscopic dynamical properties (218, 219, 220, 221).

Part III

Methods

4

Method

4.1 Introduction

Usually, the structure candidates that should exist at low temperatures (at least), are associated to local minima of the enthalpy hypersurface ($H = E_{pot} + pV$) of the chemical system of interest. From our experience, there are many metastable modifications of a chemical compound that can exist at different temperatures and pressures. These modifications may not be thermodynamically stable, but they can be found as the outcome or as an intermediary product of a particular synthesis route or natural chemical process. Hence, one important goal in energy landscape exploration is to search for possible low-lying local minima. By using a global optimization method, one can identify the energetically favored candidate for a given set of thermodynamic parameters as well as find the candidates that represent metastable modifications. Here, for the global exploration, we vary atomic positions, cell parameters, and, in principle, the composition of material.

4.2 The modular approach

At low temperature, the structure prediction task is quite simple. One mainly has to identify local minima on the potential energy landscape and analyze their various properties. But, the global energy landscape exploration consists of millions of energy calculations for different atomic configurations. It requires a lot of time to perform the energy calculations on the *ab-initio* level. However, using empirical potentials has its own disadvantages. As a comparison, we usually perform *ab-initio* energy evaluations with less accuracy. Once we have found a stable structure candidate on the energy landscape, we perform a local optimization with highest accuracy. Thus, we divide our procedure into various sections (7, 7) (see Fig. 4.2):

- Perform global optimizations with less accuracy on the *ab-initio* level. The resulting configuration should be in or at least very close to a local minimum on the energy hyper-surfaces.

- Next, we compare these predicted configurations with each other to avoid duplicates.
- The distinct structure candidates are then locally optimized on *ab-initio* level. Then we compute the $E(V)$ and $H(p)$-curves for all relevant structure candidates. With this we can decide which of the possible modifications is thermodynamically stable and which are close in energy but metastable at a given pressure.
- Finally, we perform a phonon calculation in order to understand the kinetical stability of the structure.
- After understanding the stability (thermodynamical and kinetic), we compute physical and electronic properties of the given structure.

4.3 Exploration procedures

4.3.1 The global landscape: Global optimization using stochastic simulated annealing

The global optimization consists of simulated annealing (44, 45) and a subsequent stochastic quench which is based on a random walk over the energy landscape. Each step from configuration x_i to a neighbor x_{i+1} is accepted according to the Metropolis criterion (102), with a temperature schedule $T_n = T_0\gamma^n$ ($\gamma = 0.95, ..., 0.995$). During the simulated annealing stage, the energy of a newly generated structure is computed and compared with the previous one. If the energy of the new structure is lower, then the new structure is accepted. If the energy of the new structure is higher, then the new structure is accepted with a probability of $exp(-\Delta E/k_BT)$ (where ΔE is the energy difference between the two structures, T a temperature and k_B the Boltzmann constant, respectively). This corresponds to the Metropolis algorithm (102). After the simulated annealing, a quench was applied, i.e., a simulated annealing run with the temperature 0 eV. The simulated annealing and quench moves were typically selected as follows: movements of individual atoms, atom exchange, and change in lattice parameters were attempted (70%), (10%), and (20%) of the time, respectively. When applying moves that change one of the lattice constants, the probability to shrink the lattice constant was set to 60%, in order to accelerate the shrinking of the cell.

Since the structure candidates were found using *ab-initio* methods with less accuracy, we are faced with two problems. First, we note that the structure candidates will usually not show any obvious symmetries (they are always found in space group $P1$, due to the unrestricted optimization procedure). To resolve this issue, we use algorithms such as SFND (222), RGS (223) and CMPZ (224) that have been implemented in the program KPLOT (225), where SFND (222), acronym for "SymmetrieFiNDer" (= symmetry finder), identifies all symmetries of a periodic structure, where only the atomic coordinates are given as input. RGS (223), abbreviation for "RaumGruppen-Sucher" (= space group searcher) determines for a given set of symmetries the space group of the structure. Finally, CMPZ (224), short for "CoMPare Zellen" (= compare cells), performs a comparison of a given pair of periodic structures, and determines,

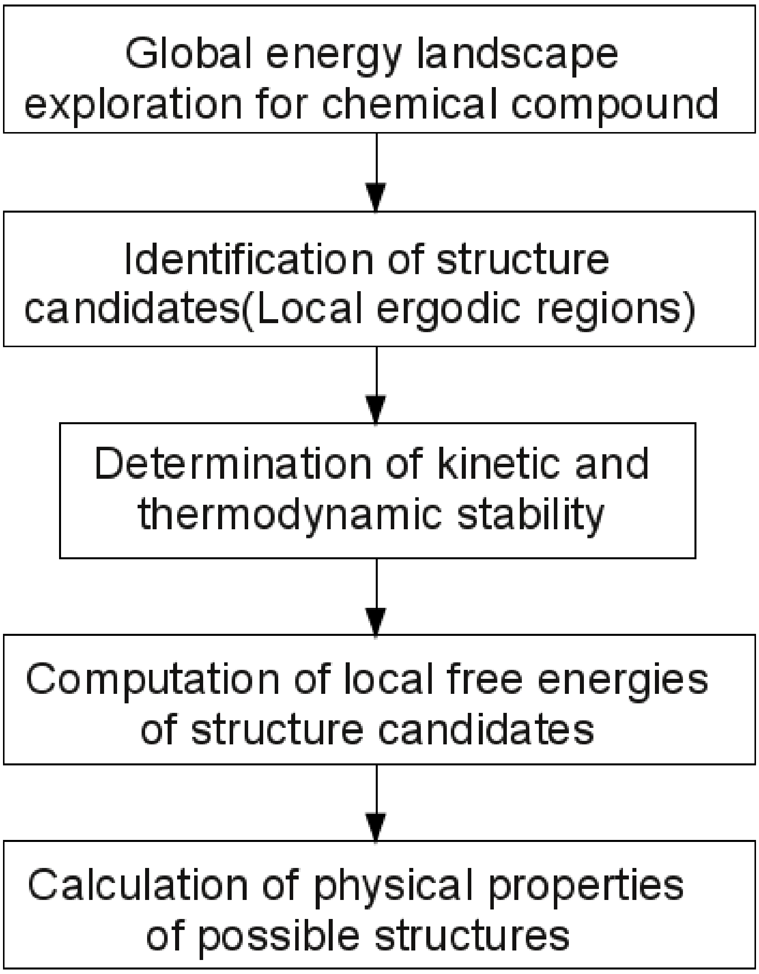
Global energy landscape exploration for chemical compound
Identification of structure candidates(Local ergodic regions)
Determination of kinetic and thermodynamic stability
Computation of local free energies of structure candidates
Calculation of physical properties of possible structures

Figure 4.1: Modular approach - procedural flowchart.

whether these structures are the same within some given set of tolerances. With the help of these algorithms one can find the symmetries and space groups of all minimum configurations of the enthalpy landscapes. We have identified, eliminated duplicates and grouped these structures. For more details on the working of these algorithms, we refer to the references given. Other important parameters are the minimum allowed distance between two atoms and the reduction of the cell size. The minimum distance between two atoms was required to be (0.5 - 0.7) times the sum of the ionic radii, in order to avoid unphysical geometries which can cause numerical instabilities in the *ab-initio* calculations. In order to estimate the atomic/ionic radii, first a Mulliken or Bader population analysis was performed. Then, the atomic and ionic radii were obtained from tabulated values of the corresponding atoms/ions, as a function of charge (226) (and employing a simple linear interpolation to obtain the radii, as the computed Mulliken charges and Bader charges are non-integer). We note that there is an ongoing discussion concerning the accuracy of the Mulliken population analysis (166, 227, 228, 229). However, we do not expect a big impact of the accuracy of the Mulliken population or Bader charges on the present calculations, as the derived charges and radii are only used to eliminate very unrealistic conformations.

4.3.2 Ab-initio energy calculations

In this thesis, we performed the *ab-initio* energy calculation using two software packages viz., CRYSTAL (230) and VASP (231, 232, 233, 234). CRYSTAL supports Gaussian type functions and pseudopotentials whereas VASP is based on plane-waves. The detailed information about these packages is as follows:

4.3.2.1 CRYSTAL

The CRYSTAL, *ab-initio* simulation package (230) is based on Gaussian type basis sets. All-electron and valence-only basis sets with effective core pseudo-potentials are allowed. CRYSTAL calculates the electronic wave function and properties of periodic systems within Hartree-Fock, density functional or hybrid approximations (184).

This program exploits the spatial symmetry to avoid redundancy of atoms which can be described by symmetry elements. It is consistent with all periodic systems. It supports the 3D periodic systems with 230 space groups, for 2D films and surfaces with 80 layered groups, for 1D polymers with the symmetry of 75 rod groups and helical symmetry, and for 0D molecules with the 32 point groups. It is possible to perform automated geometry reduction such as going from higher dimension to lower, e.g., 3D to 2D (a slab parallel to a given plane). Geometry manipulation is also possible e.g., the reduction of the symmetry, addition or deletions of atoms, and displacements.

With the CRYSTAL program, one can solve both the Hartree-Fock (see Section 3.2) and Kohn-Sham (see Section 3.3) equations with local and hybrid functionals. With the Hartree-Fock method, it can handle Restricted Closed Shell, Restricted Open Shell, and Unrestricted calculations. And with DFT, it can deal with various exchange functionals (LDA, von Barth-Hedin, Becke, PWGGA, PBE, and many more) and correlation functionals (PZ, LYP, VWN, etc.). It is useful for hybrid HF-DFT functionals such as B3PW, B3LYP, and user-defined hybrid functionals.

With the CRYSTAL program, various types of calculations are possible. Obvious ones are single-point energy calculations, and geometry optimizations which includes full optimization (cell parameters and atom coordinates), freezing atoms during the optimization, at constant volume or pressure and transition state search. One can calculate harmonic frequencies at the Gamma point, phonon dispersion with an appropriate super-cell, IR intensities, and reflectance spectra. With the newest version, the calculation of the equation of state, the elastic tensor of crystalline systems, and anharmonic frequencies for X-H bonds are also possible. Numerous physical properties are possible to calculate using this program, e.g., the band structure, density of states, Mulliken population analysis, atomic multi-poles, structure factors, dielectric properties, and many more.

4.3.2.2 VASP

The Vienna Ab-initio Simulation Package (VASP) (231, 232, 233, 234) is a package for performing *ab-initio* quantum mechanical molecular dynamics (MD) using either Vanderbilt pseudopotentials, or the Projector Augmented Wave Method, and a plane wave basis set. The basic methodology is Density Functional Theory (DFT), but the code also allows the use of post-DFT corrections such as hybrid functionals mixing DFT and Hartree-Fock exchange, many-body perturbation theory (the GW method) and dynamical electronic correlations within the random phase approximation.

Using VASP, one can use the approach implemented, which is based on the (finite-temperature) local-density approximation with the free energy as variational quantity and an exact evaluation of the instantaneous electronic ground state at each MD time step. It has an efficient matrix diagonalization scheme and an efficient Pulay/Broyden charge density mixing. These techniques avoid all problems possibly occurring in the original Car-Parrinello method, which is based on the simultaneous integration of electronic and ionic equations of motion. US-PP (and the PAW method) allow for a considerable reduction of the number of plane-waves per atom for transition metals and first row elements. Forces and the full stress tensor can be calculated with VASP and can be used to relax atoms into their instantaneous ground-state.

Here are some highlights of VASP (235):

- It uses some old techniques for the self-consistency cycle to calculate the electronic ground-state. However, these techniques are robust, efficient, and constitute a fast scheme for evaluating the self-consistent solution of the Kohn-Sham functional. For iterative matrix diagonalization, RMM-DISS and blocked Davidson are used.

- It determines the symmetry of arbitrary configurations automatically.

- For an efficient calculation of bulk materials and symmetric clusters, the symmetry code is used to set up the Monkhorst Pack special points.

4.3.3 Properties related to the total energy

The most important properties can be deduced from the ground-state total energy and its derivatives, where the energy calculations were performed using *ab-initio* quantum mechanical methods on solids. Some of the observables depend upon first- and second-order derivatives, which are displayed in Table 4.1. Many characteristics of the

Differentiating variable	Total energy derivative	Observable
nuclear coordinate	$\left(\frac{\partial E}{\partial \mathbf{u}_i}\right) = 0$	equilibrium nuclear coordinates
	$\left(\frac{\partial^2 E}{\partial \mathbf{r}_i \partial \mathbf{r}_j}\right)_{eq} = k_{ij}$	force constants
lattice parameter	$\left(\frac{\partial E}{\partial \mathbf{a}_i}\right)_{eq} = 0$	equilibrium unit cell
	$\left(\frac{\partial^2 E}{\partial \epsilon_i \partial \epsilon_j}\right)_{eq} = c_{ij}$	elastic tensor
unit cell volume	$\left(\frac{\partial E}{\partial V}\right)_S = -P$	internal pressure
	$V\left(\frac{\partial^2 E}{\partial V^2}\right)_S = B$	bulk modulus

$\mathbf{u}_i$ denotes a nuclear displacement from the equilibrium position,

ϵ_i is a component of the strain tensor, $\mathbf{a}_i$ is a lattice basis vector.

Table 4.1: First and second order derivatives of the total energy (183).

crystalline structure can be deduced when the total energy of the system is known. The total energy difference gives better insight to analyze two or more structures of the same composition. The simplest relationship between two structures can be judged using first derivatives of the total energy of the systems with respect to the volume (which gives the pressure). The elastic constants and vibrational spectrum are the properties that can be calculated using second derivatives of the energy which are the most important for our purposes.

4.3.3.1 Equation of state (EOS) and phase transitions

Usually, the behavior of crystalline systems under pressure (or change in volume) is a very important aspect. Pressure (P) and temperature (T) are the independent variables in the case of high pressure experiments. In our calculations, the volume V (and $T = 0$) is the independent variable. Minimization of the total energy of the system is performed keeping the volume constant but the other geometrical parameters are optimized such as cell parameters and fractional coordinates. The same procedure is repeated for 30 - 40 different volumes. Using an analytical function to this data the E versus V curve is fitted. Mostly, we use either a polynomial or one of the many equations of states (EOS) proposed in the literature. We have considered the Murnaghan (236) EOS,

$$E(V) = E_0 + \frac{B_0 V}{B_0'}\left(\frac{(V_0/V)^{B_0'}}{B_0' - 1} + 1\right) - \frac{B_0 V_0}{B_0' - 1} \tag{4.1}$$

where the three fit parameters B_0 and B_0' are the bulk modulus and its derivative and V_0, the equilibrium volume, respectively. We can compute the pressure by taking the first derivative of E(V):

$$P = -\left(\frac{\partial E}{\partial V}\right)_T . \tag{4.2}$$

With the above relation, it is easy to represent the pressure P as an analytic function of V, $P \equiv P(V)$ or, conversely, $V \equiv V(P)$ and $E \equiv E(P)$.

4.3.3.2 Transition pressure

In experiments, the controlled parameters are N (number of atoms), T and P, so that the thermodynamic function of interest is the Gibbs free energy:

$$G = E + PV - TS \tag{4.3}$$

On the experimental level, the syntheses are performed at constant pressure. So we adopt the same condition where pressure and temperature are applied externally and the energy E, volume V and entropy S are adjusted so as to minimize the Gibbs free energy G. The above equation gives the information about the stability of a structure: an increase in pressure with smaller specific volume may be acceptable, even if this leads to a higher internal energy.

The stability of the most stable modification of a chemical system is the one with the lowest Gibbs free energy at given values of N, P, and T. The implication of the NPT thermodynamic ensemble (where N is the number of atoms, presumed constant) is that there is no coexistence of two phases over a range of external pressures. In the case of the *static limit* which we usually consider in this work ($T = 0$, and frozen nuclear motion), G is reduced to H, the enthalpy ($H = E + PV$), and the function of interest is then:

$$H \equiv H(P) \tag{4.4}$$

which can be easily obtained because both of the functions $E \equiv E(P)$ and $V \equiv V(P)$ have been obtained using an analytic form from the fitting function.

By definition, the pressure is defined as $p = -\frac{\partial E}{\partial V}$. A condition for a pressure driven phase transition, is that the enthalpies of the two modifications must be equal. The transition pressure is given by the negative slope of the joint tangent of the two E(V)-curves.

For the determination of the transition pressure, we need the energy E as a function of the volume V for every phase involved in the transition. A set of data points is obtained from CRYSTAL or VASP calculations, and these data points are fitted by an adequate equation of state or by a fitting polynomial. As mentioned earlier, we applied the Murnaghan (236) EOS. We calculated the energy by changing the volume and keeping the symmetry of the modification fixed, in other words, a restricted geometry optimization should be performed at each volume. For calculating the bulk modulus, we used the Murnaghan EOS for fitting the E(V) data. The bulk modulus of the modifications is calculated at the equilibrium position of the energy of that chemical system.

4.3.3.3 Phonon Calculations

For phonon calculations, we used two packages, FROPHO and phonopy (237).

An atom κ in the primitive cell l, having mass m_κ, is displaced from the equilibrium by $\mathbf{u}\binom{l}{\kappa}$ as the lattice vibrates. The force on each atom is then given by

$$F_\alpha\binom{l}{\kappa} = \sum_{l'\kappa'\beta} \phi_{\alpha\beta}\begin{pmatrix} l & l' \\ \kappa & \kappa' \end{pmatrix} u_\beta\begin{pmatrix} l' \\ \kappa' \end{pmatrix} \tag{4.5}$$

where ϕ represents the interactions between pairs of atoms.

A normal mode with angular frequency ω is represented as a motion such that $\mathbf{F}(l,\kappa) = -m_\kappa\omega^2\mathbf{u}(l,\kappa)$. Phonon solutions which have two equivalent atoms with the same κ but in different primitive cells, will differ in the phase of their motion by an amount $\mathbf{q}\cdot\Delta\mathbf{r}$, where $\Delta\mathbf{r}$ is the difference in the positions of their primitive cells. Mass reduced coordinates can be defined as $\boldsymbol{\epsilon}\ \binom{l}{\kappa} = \sqrt{m_\kappa}\mathbf{u}\binom{l}{\kappa}$ and, using 4.5, the equation of motion for phonon solutions define an eigenvalue problem at each wave-vector $\mathbf{q}$:

$$-\omega^2\boldsymbol{\xi} = \mathbf{D}(\mathbf{q})\boldsymbol{\xi} \tag{4.6}$$

where the Fourier-transformed dynamical matrix is

$$D_{\alpha\beta}\begin{pmatrix} \mathbf{q} \\ \kappa\kappa' \end{pmatrix} = \sum_{l} \frac{1}{\sqrt{m_\kappa m_{\kappa'}}}\phi_{\alpha\beta}\begin{pmatrix} l & l' \\ \kappa & \kappa' \end{pmatrix} exp\left\{ i\left(\mathbf{q}.\left[\mathbf{r}\begin{pmatrix} l' \\ \kappa' \end{pmatrix} - \mathbf{r}\begin{pmatrix} l \\ \kappa \end{pmatrix}\right]\right)\right\} \tag{4.7}$$

The frequencies and eigenvectors ξ of the normal modes at each wave-vector $\mathbf{q}$ are given after evaluation and diagonalization of $\mathbf{D}(\mathbf{q})$, which may be assigned to the corresponding point of the Brillouin Zone.

We have to consider interactions between pairs of atoms at all separations up to infinity. But, it is practically impossible because only non-Coulombic contributions decay rapidly enough with distance and thus only a few atom pairs have to be considered. In addition, calculations of a dynamical matrix for all atom pairs within one super-cell are sufficient to give phonons at all wave-vectors within the super-cell. For example, phonon calculation at the Γ-point may be performed with only a single primitive cell.

Making small displacements of each atom at a time, and computing the corresponding forces experienced on all the atoms, the dynamical matrix can be computed, and the force constants can then be computed from eqn. 4.5. In addition, we can get the useful information about the force constants with the help of symmetry which exists in a system (239).

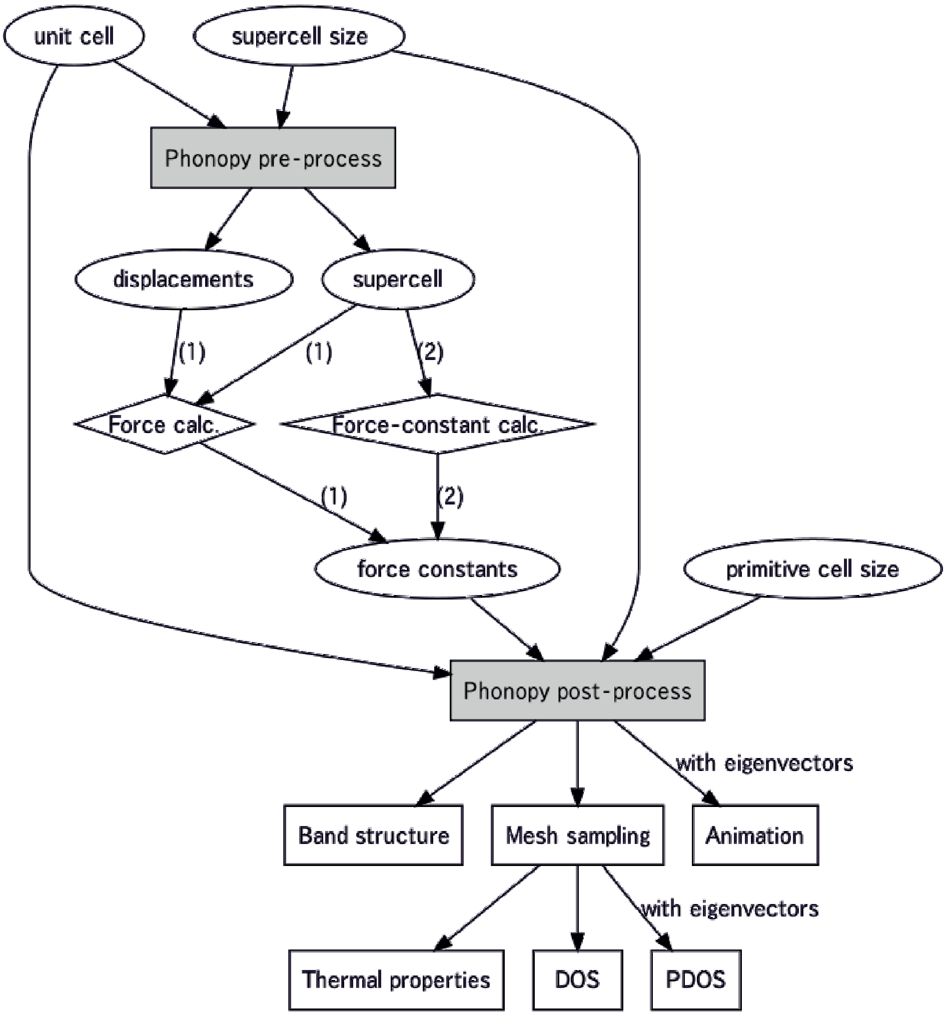
unit cell
supercell size
Phonopy pre-process
displacements
supercell
(1)
(1)
(2)
Force calc.
Force-constant calc.
(1)
(2)
force constants
primitive cell size
Phonopy post-process
with eigenvectors
Band structure
Mesh sampling
Animation
with eigenvectors
Thermal properties
DOS
PDOS

Figure 4.2: Flowchart for phonon calculation using Phonopy (238)

4.3.3.4 Theory: Finite displacement method for computing force constants

The potential energy of the phonon system is represented as functions of the atomic positions:

$$V\left[\mathbf{r}\begin{pmatrix} l_1 \\ \kappa_1 \end{pmatrix}, \ldots, \mathbf{r}\begin{pmatrix} l_n \\ \kappa_N \end{pmatrix}\right], \tag{4.8}$$

where $\mathbf{r}\begin{pmatrix} l \\ \kappa \end{pmatrix}$ is the point of the l-th atom in the κ-th unit cell and n and N are the number of atoms in a unit cell and the number of unit cells, respectively. A force and a second-order force constant $\phi(\alpha\beta)$ are given by

$$F_\alpha\begin{pmatrix} l \\ \kappa \end{pmatrix} = -\frac{\partial V}{\partial r_\alpha\begin{pmatrix} l \\ \kappa \end{pmatrix}} \tag{4.9}$$

and

$$\begin{aligned}\Phi_{\alpha\beta}\begin{pmatrix} l & l' \\ \kappa & \kappa' \end{pmatrix} &= \frac{\partial^2 V}{\partial r_\alpha\begin{pmatrix} l \\ \kappa \end{pmatrix} \partial r_\beta\begin{pmatrix} l' \\ \kappa' \end{pmatrix}} \\ &= -\frac{\partial F_\beta\begin{pmatrix} l' \\ \kappa' \end{pmatrix}}{\partial r_\alpha\begin{pmatrix} l \\ \kappa \end{pmatrix}}\end{aligned} \tag{4.10}$$

respectively, where α, β, ..., are the Cartesian indices, l, l', ..., are the indices of atoms in a unit cell, and κ, κ', ..., are the indices of unit cells. In the finite displacement method, the equation for the force constants is approximated as

$$\Phi_{\alpha\beta}\begin{pmatrix} l & l' \\ \kappa & \kappa' \end{pmatrix} \simeq -\frac{F_\beta\left(\begin{pmatrix} l' \\ \kappa' \end{pmatrix}; \Delta r_\alpha\begin{pmatrix} l \\ \kappa \end{pmatrix}\right) - F_\beta\begin{pmatrix} l' \\ \kappa' \end{pmatrix}}{\Delta r_\alpha\begin{pmatrix} l \\ \kappa \end{pmatrix}} \tag{4.11}$$

where $F_\beta\left(\begin{pmatrix} l' \\ \kappa' \end{pmatrix}; \Delta r_\alpha\begin{pmatrix} l \\ \kappa \end{pmatrix}\right)$ are the forces on the atoms with a finite displacement $\Delta r_\alpha\begin{pmatrix} l \\ \kappa \end{pmatrix} \equiv u_\alpha\begin{pmatrix} l \\ \kappa \end{pmatrix}$ and usually $F_\beta\begin{pmatrix} l' \\ \kappa' \end{pmatrix} \equiv 0$.

5

New Developments

5.1 Introduction

As we mentioned earlier, structure prediction is based on global energy landscape exploration. It is divided into two parts viz., global search and local optimization. While performing energy landscape exploration, we computed energies on *ab-initio* level. Prior to this way of exploration, the energy calculation was performed using model potentials e.g., the Born-Mayer-Huggins potential (240), the Buckingham potential (241), and many more. These model potentials require less time for energy computation as compared to *ab-initio* calculations. But, such potentials have serious short-comings. They are dependent upon the system. For a given system, it is not guaranteed that all important modifications correspond to basins around local minima. Apart from this, these potentials are useful for ionic systems whereas they have problems with covalent or metallic bonds or mixtures of covalent and ionic bonds. To overcome these problems, *ab-initio* energy calculation is the best option. Initially, some systems were studied by computing *ab-initio* energies with the CRYSTAL code (230) which is based on Gaussian type orbitals. In this work, we went one step further and created an interface to the VASP code (231, 232, 233, 234), where the *ab-initio* energy calculations are based on plane waves.

Using plane wave basis functions has several advantages over Gaussian type basis sets:

- the same basis function can be used for all atom types,
- convergence problems during the self-consistent field procedure are less severe,
- plane wave functions do not depend upon nuclear positions.
- In particular for metallic systems, the use of the plane wave method is advantageous.

5.1.1 Calculation using VASP

The general procedure for VASP energy calculations is as follows:

- It require four input files viz., INCAR, POSCAR, POTCAR, and KPOINTS.
- INCAR contains all input parameters such as the algorithm used for geometry optimization, spin-polarized calculations, and many more.
- POSCAR has complete information about the system which includes lattice vectors and fractionals/cartesian coordinates.
- POTCAR contains the pseudopotential/projector augmented wave functions for each atomic species used in the calculation.
- KPOINTS contains the k-point coordinates and weights or the mesh size for creating the k-point grid.
- Output files are STDOUT, OSZICAR, IBZKPT, CONTCAR, CHGCAR, CHG, WAVECAR, TMPCAR, EIGENVAL, DOSCAR, PROCAR, PCDAT, XDATCAR, LOCPOT, ELFCAR, and PROOUT.
- OSZICAR or STDOUT contains information about convergence speed and about the current step.
- CONTCAR contains optimized geometry of the crystal structure.

For the interface to the G42-program, the files KPOINTS, POTCAR, and INCAR have to be provided beforehand, while the file POSCAR is provided by the G42-code. One of the important parameters during the global search is the minimum allowed distance between two atoms. Usually, we keep the minimum distance between two atoms 0.5 - 0.7 times the sum of the ionic radii in order to avoid unphysical geometries which can cause numerical instabilities in the *ab-initio* calculations. In order to estimate the atomic radii, a Bader charge analysis (163, 215) is performed. Then, the atomic and ionic radii are obtained from tabulated values of the corresponding atoms/ions, as a function of charge (226) (and employing a simple linear interpolation to obtain the radii, as the computed Bader charges are noninteger). We note that there is an ongoing discussion concerning the accuracy of the Bader charge analysis. However, we do not expect a big impact of the accuracy of the Bader charge analysis on the present calculations, as the derived charges and radii are only used to eliminate unrealistic conformations.

Part IV

Application to binary and elemental solids

6

Lithium

6.1 Introduction

Lithium is a soft, silver-white metal which belongs to the alkali metal group. It is the lightest metal and the least dense solid element at standard conditions. It is highly reactive and flammable as the other alkali metals. Because of its high reactivity, lithium never occurs freely in nature, and instead, only appears in compounds, which are usually ionic. The physical and electronic properties are explained by the nearly-free-electron model.

Lithium and its compounds have several industrial applications that include heat-resistant glass and ceramics, high strength-to-weight alloys used in aircraft, lithium batteries and lithium-ion batteries. About half of the production of lithium is consumed by the above usage.

It is a monovalent element, with one valence electron in the 2s orbital. It easily gives up this single electron to form a cation. It is a good conductor of heat, electricity and a high reactive element. However, lithium has a relatively low reactivity as compared to the other alkali metals because of the proximity of its valence electron to its nucleus; the remaining two electrons of lithium in the 1s orbital have much lower energy, and, therefore, they do not participate in chemical bonds.

At ambient condition, lithium crystallizes in a body-centered-cubic (bcc) structure like the other alkali metals. It shows interesting structures at low temperature and high pressures. With the help of x-ray diffraction, Barrett and Trautz suggested the existence of a hexagonal close packed (hcp) (242, 243, 244) structure at 77 K. This structure coexists with some fraction of the untransformed bcc phase. Using cold work some of the material could be converted to the face-centered-cubic (fcc) form. Neutron-scattering experiments performed below 70 K, and interpreted by Overhauser, led to the proposal and confirmation of a new modification. It is a hexagonal polytype and similar to the structure of samarium metal, the so-called *9R* structure (245). In an hcp packing, there are alternating layers stacked $ABAB$..... in the c direction whereas an fcc lattice has the stacking sequence $ABCABC$..... In contrast, the *9R* modification consists of a close-packing with a nine layer stacking sequence of $ABABCBCAC$. Lately, there have been some studies using neutron scattering (246, 247, 248) that show that 9R is predominantly found at low temperature, but there is also evidence of coexistence of some amount of bcc and some more closed-packed structures. Theoretical studies (249) showed that the low-temperature modification is not superconducting even at 6 mK. However, recent experiments showed that it becomes a superconductor below 0.4 mK (250) at ambient pressure.

Lithium is stable in the bcc modification up to 6.9 GPa, above which structural transformations occur. The crystal structure of the compressed lithium was detected as fcc, but the limited data would also be consistent with an hcp or *9R* structure. Neaton and Ashcroft (251, 252) suggested a dimerization of lithium at very high pressure beyond the fcc phase to an insulating αGa-type structure. It was the first study which suggested broken-symmetry structures at high pressure in such a simple monovalent metal. This signified that a build up of valence charge in the interstitial might be due to the core expulsion under strong compression. The prediction of such a novel structure brought back interest in experimental and theoretical investigations to discover the phases of lithium under high pressure. Later, it was discovered that the fcc phase transforms into a cubic structure with 16 atoms in the unit cell (cI16) (253, 254) at 42 GPa. There is one intermediate structure between these two phases, the so-called hR1 phase (255). Beyond the cI16 structure, there are suggestions for the existence of a broken-symmetry phase for Li above 60 GPa. This is suggested due to superconductivity (256) and Raman (257) measurements, but there is no clear evidence from x-ray diffraction data. In theory, apart from the paired dimer αGa-type structure, the orthorhombic Cmca-24 (258, 259) structure (260, 261) has been found to be energetically preferable with respect to the cI16 phase at very high pressure.

Recently, there has been an experimental study which yielded the phase diagram fig. 6.1 over a wide $P-T$ range (262, 263) by means of powder and single-crystal X-ray synchrotron diffraction. This study summarized the behavior of the solid phases and melting curve. It showed exciting features of the Li melting curve. In the range of 40 - 60 GPa, the melting temperature is 190 K which is the lowest melting temperature among the elemental metals. More spectacularly, lithium showed superconductivity (264, 265) at $T_c = 17$ K where the melting curve reaches a minimum in the same pressure range. At a temperature below 200 K and in the pressure range 45 - 60 GPa, the cI16 structure is stable. With more pressure, the cI16 structure is transformed into an orthorhombic C-face centered phase which has 88 atoms per unit cell, oC88. This phase is stable in a narrow pressure range. At 70 GPa and 150K, it changes into another C-face centered orthorhombic structure with 40 atoms per unit cell (oC40). There is one more detailed study in the 50 - 120 GPa range, see fig. 6.2. The oC40 phase has a wider stability range compared to oC88. Experimentally, it is observed that the sample becomes more dark when it transforms from oC88 to oC40. This is correlated to a metal-to-semimetal transition. As the oC40 phase is compressed further, it transforms to a C-faced centered orthorhombic phase with 24 atoms per unit cell (oC24). This structure is stable until 130 GPa. There is a narrow pressure range 94 - 110 GPa (see fig. 6.2) where lithium showed a metal-semiconductor-metal transformation (258, 263).

There has been one further theoretical study on lithium which predicted crystalline phases at high pressure, $Aba2-40$ (259) and $Cmca-56$ (60) which are stable for 60 - 80 GPa and 185 - 269 GPa, respectively.

Thus, it is an interesting task to investigate the energy landscape of lithium on the *ab-initio* level, and to perform a global search for structure candidates. The technical details of this procedure are described in the following section. The predicted structures

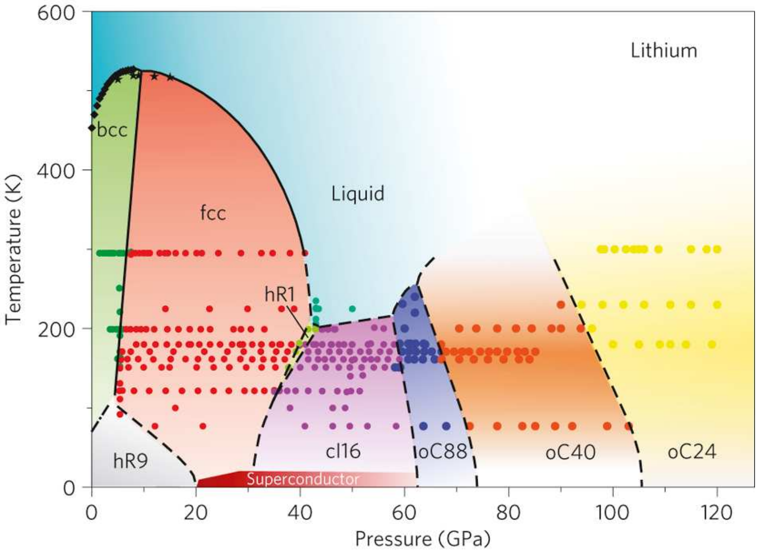

Figure 6.1: (Proposed) Phase diagram of lithium over a wide pressure-temperature range.

Phase diagram of lithium over a wide pressure-temperature range. We have taken this phase diagram from the literature.(262)

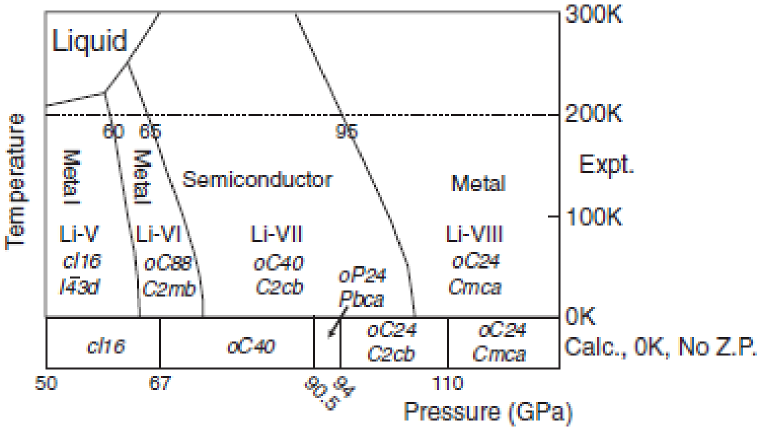
Liquid
300K
200K
Expt.
100K
0K
Calc., 0K, No Z.P.
60
65
95
Metal
Metal
Semiconductor
Metal
Li-V
cI16
I$\bar{4}$3d
Li-VI
oC88
C2mb
Li-VII
oC40
C2cb
oP24
Pbca
Li-VIII
oC24
Cmca
cI16
oC40
oC24
C2cb
oC24
Cmca
50
67
90.5
94
110
Temperature
Pressure (GPa)

Figure 6.2: The diagram shows the different modifications in the pressure range 50 - 120 GPa.

The diagram shows the different modifications in the pressure range 50 - 120 GPa. (263)

as well as their thermodynamic and kinetic stability are discussed in the section on results and discussion.

6.2 Methods

We employ a general structure prediction method based on the global exploration of the energy landscape, where the stable modifications are represented by locally ergodic regions of the landscape, in particular by the local minima. (41, 266) The method used for the global exploration of the energy landscape is as follows: First, a list of structure candidates is obtained via global optimization. Then each candidate structure is optimized locally, and the symmetry and space group are determined (222, 223). The global optimization consists of simulated annealing runs combined with subsequent stochastic quenches. During the global search, the *ab-initio* calculations are performed without gradient-based minimization. To analyze the symmetry and space group of the structure candidate, the software KPLOT (225) is used.

In this study, all energy calculations during the global and local optimization were performed on the *ab-initio* level using CRYSTAL09. (267) The system consisted of 4 or 8 lithium atoms in a variable periodically repeated simulation cell, where the initial cell volume for 4 and 8 atoms was 176.52 Å^3 and 353.05 Å^3, respectively. The atoms were initially placed at random positions inside the cell, and the initial temperature for the simulated annealing runs was 1 eV ($\cong$ 11604K). Each run consisted of 5000 Monte Carlo steps, where the temperature was reduced by a factor of 0.995 after every 250 steps. Subsequently, the temperature was set to 0K and a quench of 10000 steps was performed. During the stochastic simulated annealing and quench, the moves were chosen as: movements of individual atoms (80%) and changes of the lattice parameters (20%). The probability of the cell to shrink during a lattice move was set to 60%, in order to reach solid state densities more rapidly.

6.2.1 Details of the energy calculation at standard pressure

The global optimization calculations were performed on the level of the local density approximation (LDA), whereas the local optimizations using analytical gradients (268, 269) were performed using both LDA and the gradient corrected functional by Perdew, Burke, Ernzerhof (PBE). Gaussian-type orbitals were used as basis sets (during the global search [3s2p] with 0.15 as the exponent of the 3sp shell, and during the local optimization [3s2p] with 0.10 as the exponent of the 3sp shell as in Ref (270)) During the global exploration, a smaller 4×4×4 $\vec{k}$-point mesh was used, in order to improve the computational speed. For the local optimization, a 8×8×8 $\vec{k}$-point mesh was employed, and a smearing temperature of 0.001 E_h (1 E_h=27.2114 eV) was applied. Note that the final results as presented in the figures and tables are all obtained with high quality parameters.

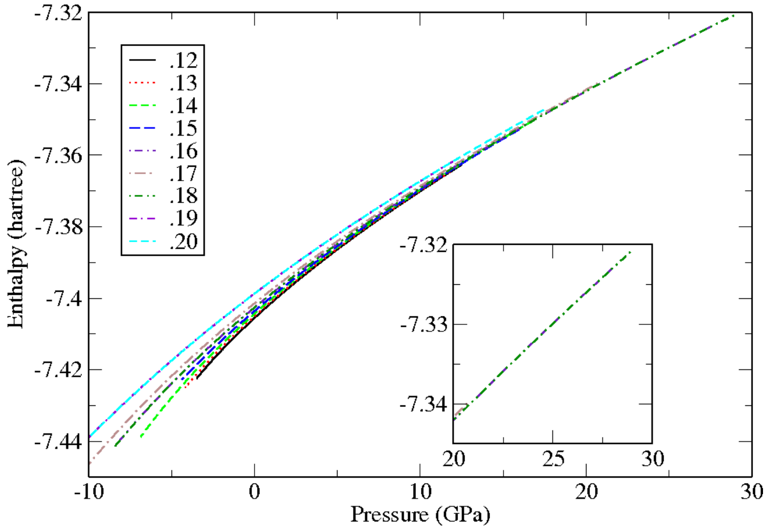

Figure 6.3: Enthalpy as a function of the diffuse sp exponent of the basis set for the fcc structure versus the pressure. The calculations were performed on the LDA level.

6.2.2 Details of the energy calculation at high pressure

The energy landscape exploration was performed at high pressure on the LDA level. We used during the global exploration a [3s2p] basis with 0.18 as the exponent of the 3sp shell. We employed a different basis-set for the high pressure landscape exploration because we had to ensure that it is stable at high pressure (see Fig. 6.3). Apart from this, we kept all parameters the same.

6.3 Results and Discussion

6.3.1 Standard pressure

We performed 136 global search runs at standard pressure, of which 94 runs employed 4 atoms per unit cell and 42 runs 8 atoms per unit cell, respectively. Besides the bcc-, fcc-, and hcp-structures, and several high-lying minima, we found the A15 structure as a promising candidate (see figure 6.4). The four modifications obtained from our search with the lowest energy after the local optimization were bcc, fcc, hcp, and A15 (c.f. Tables 6.1). According to the statistics (c.f. Tables 6.2), bcc-Li was the most likely outcome of the global optimization (41 times), followed by fcc-Li (32 times), while hcp-Li and A15-Li were found four times each.

The most interesting result is the prediction of a new modification exhibiting the A15 structure type. This structure is normally observed in binary compounds (with Cr_3Si as the reference), where the cations form infinite non-intersecting chains parallel to the Cartesian axes. This structure type had initially been suggested for elemental tungsten, (271) but later it was argued that W in the A15 structure is only possible

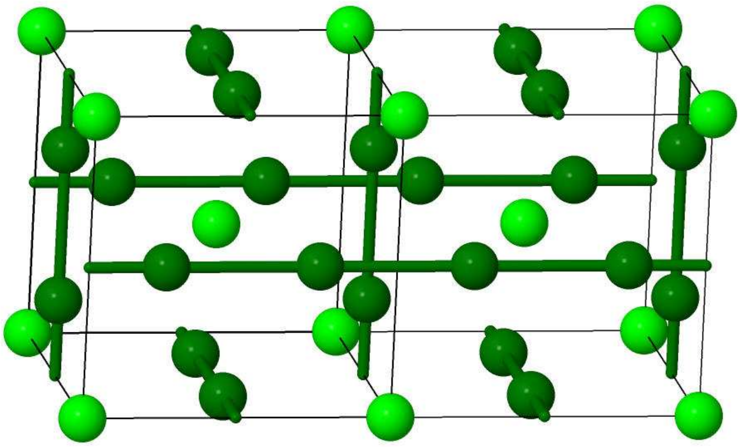

Figure 6.4: A15 structure for lithium. Light green spheres correspond to Li1 atoms and dark green spheres to Li2 atoms.

Table 6.1: Total energies at zero pressure of the relaxed structures of the most relevant modifications found and their statistics of occurrence during the global optimization. Energies are in hartree units (1 E_h=27.2114 eV), per atom. For comparison, the 9R^a structure is also shown.

structure type	space group	energy $[E_h]$ LDA	PBE
bcc	$Im\bar{3}m$ (229)	-7.4059	-7.5176
fcc	$Fm\bar{3}m$ (225)	-7.4062	-7.5180
hcp	$P6_3/mmc$ (194)	-7.4063	-7.5179
A15	$Pm\bar{3}n$ (223)	-7.4057	-7.5174
9R^a	$R\bar{3}m$ (166)	-7.4063	-7.5179
cI16^a	$I\bar{4}3d$ (220)	-7.3802	-7.4872
hR1^a	$R\bar{3}m$ (166)	-7.4028	-7.5136

[a] This structure was not observed in the searches, since it contains 3, 9, and 16 atoms per unit cell for hR1, 9R, and cI16 whereas cells containing 4 or 8 atoms were considered during the global optimization. Thus, only structures with 1,2,4 or 8 atoms in the primitive cell could be found (i.e. the divisors of 8).

Table 6.2: Statistics of structures found at standard and high pressure

Structure type	(at pressure in GPa)				
	0	16	32	48	64
bcc	41	2	3	1	0
fcc	32	1	1	0	0
hcp	4	0	0	0	0
A15	4	0	1	0	0
other modifications (with higher energies and irregular polyhedra)	2	3	2	0	0
Total number of runs	136	12	14	12	5

in the presence of impurities such as oxygen (272) – a still ongoing discussion (see e.g. Ref. (273)). There are two crystallographically different types of lithium atoms (analogous to Cr_3Si) viz., Li1 corresponds to Si atoms and Li2 corresponds to Cr atoms, respectively. In the Cr_3Si structure type, Cr (Li2) atoms form rods along the faces of the cube made up of Si atoms, parallel to the Cartesian axes. These rods are non-intersecting and create voids which are filled by Si (Li1) atoms. The coordination of the Li2 atoms is 2+4+8 (see Table 6.3). Two atoms are equidistant from the Li2 atom along the chain, four voids that are created by Li rods are occupied by the next neighbors (Li1), and the remaining eight neighbors are from the neighboring chains. The nearest neighbors of the Li1 atom are 12 Li2 atoms, which occupy the faces of the cube. The lattice constant is 5.347 Å. We are aware of only one computational study, an on-site-energy-only generalized cluster expansion investigation for a large set of elemental systems, (274) where this structure has been considered for lithium in the past.

The $E(V)$ curves for all important structures are displayed, on the LDA level, in table 6.1 and figure 6.5. We note that the energy of the A15 structure is very close to the energies of the other four structures (bcc, fcc, hcp, and 9R), and that they can be considered degenerate within the limitations of DFT-LDA (an energy difference of less than one milli-hartree is within the range of the numerical noise). This near-degeneracy of the various possible lithium phases is well known from previous calculations, e.g. Ref (270, 278). Experimentally, having several energetically competitive phases present can lead to the possible co-existence of various phases – fcc, hcp, 9R (a stacking variant of fcc and hcp) and possibly also A15 – at low temperature, with the bcc phase appearing at higher temperature. The A15 structure has so far not been observed, and it would be highly interesting to search for ways to synthesize such a structure for bulk lithium. Although the calculations suggest that the energy is degenerate with the observed phases at ambient pressure, it may be that the A15 structure is only stable within a very narrow temperature and pressure range, or can

Table 6.3: Interatomic Li-Li distances [Å] and volumes [Å^3] per atom of the known modifications and A15 at ambient conditions after local optimization on the LDA level. Energy and volume are given per atom.

modification	distance between Li atoms (in Å) experimental	 computed	Nearest neighbor	volume (Å^3)
bcc	3.013 (275)	2.922	8	19.217
fcc	3.104 (276, 277)	3.001	12	19.105
hcp	3.111 (242, 243, 244)	2.856	6	19.059
	3.116 (242, 243, 244)	2.886	6	
9R^a	3.101 (275)	2.969	6	19.058
	3.133 (275)	3.030	6	
A15		2.989 (Li1)	12	19.106
		2.673 (Li2)	2	
		2.989 (Li2)	4	
		3.274 (Li2)	8	
cI16^a		2.282	2	18.312
		2.306	3	
		2.338	6	
hR1^a		2.752	6	16.805
		2.931	2	

[a] This structure was not observed in the searches.

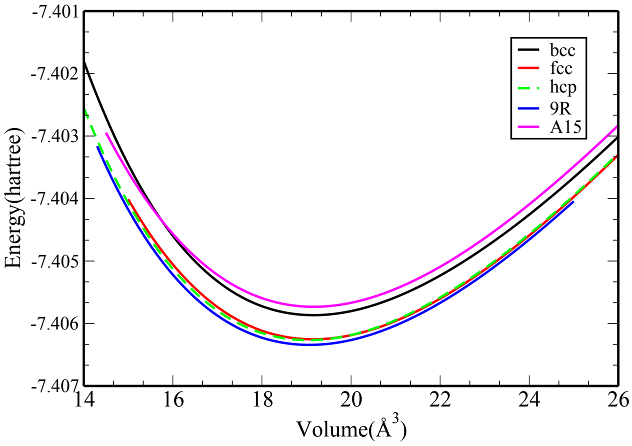

Figure 6.5: $E(V)$ curves for the structures in table 7.1, on the LDA level

only be synthesized using special synthesis techniques. One possibility could be to grow lithium on a substrate such as Ti_3Sb, which has the same structure type and similar lattice parameters (279) as the predicted lithium modification.

To ensure that the newly found A15 structure is stable, phonon frequencies were computed across the Brillouin zone using the FROPHO code, (280) which is based on the finite-displacement approach. (281) This work was performed with the help of Dr. D. L. V. K. Prasad. The required forces for the displaced 2×2×2 super cell structures were obtained from VASP with the PAW (projector augmented wave) approximation (282) and the PBE functional. The forces were considered converged when the electronic energy threshold of 10^{-8} eV had been reached. The computed phonon dispersion of lithium in the A15 structure at 0 GPa is presented in figure 6.6. The absence of imaginary frequencies indicates that the structure is dynamically stable against small displacements. The highest phonon frequency is 11.93 THz (398 cm^{-1}) and corresponds to the Li-Li bond (2.717 Å) stretching mode in the Li chain. The overall frequency range is comparable to that of fcc- and bcc-Li. (278)

As a further check, the stability of the structure against finite atom displacements was tested by changing the interatomic distances between lithium atoms along the chain by up to 0.4 Å; in all cases, the distorted structure returned to the original one upon relaxation. In addition, all atoms were randomly displaced by about 10% of the lattice constant ($\sim$ 0.5 Å) away from their positions in the A15 structure raising the energy of the distorted structure by about $0.0036E_h$ per atom ($\cong$ 1150K). Again, the original A15 structure was recovered after relaxation, clearly indicating the relatively high stability of this modification.

The band structure and density of states for this structure are displayed in figure 6.7. The A15 structure shows metallic character similar to the other ambient pressure structures. Near the Fermi energy, the band is mainly s-like. The Mulliken population charges show virtually the same charge for Li1 and Li2.

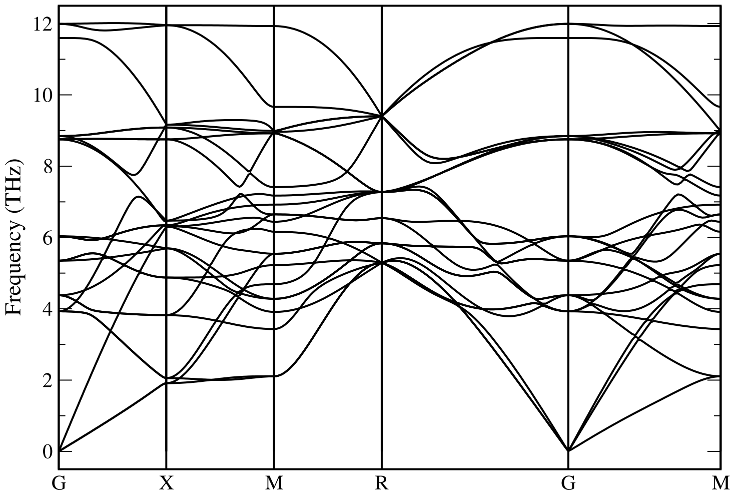

Figure 6.6: Phonon dispersion spectrum for lithium-A15 structure

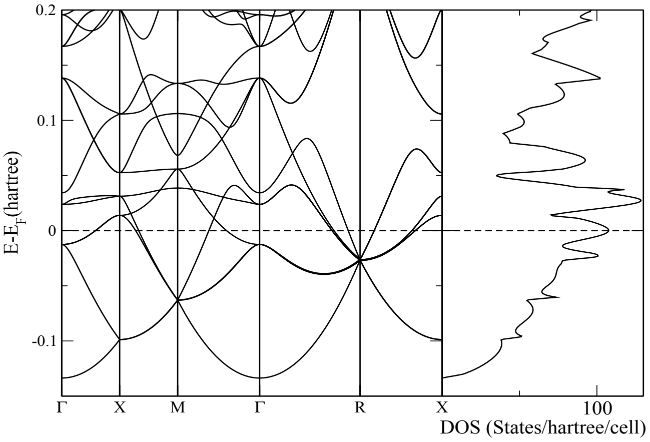

Figure 6.7: Calculated band structure and electronic density of states of lithium-A15 modification, on the LDA level

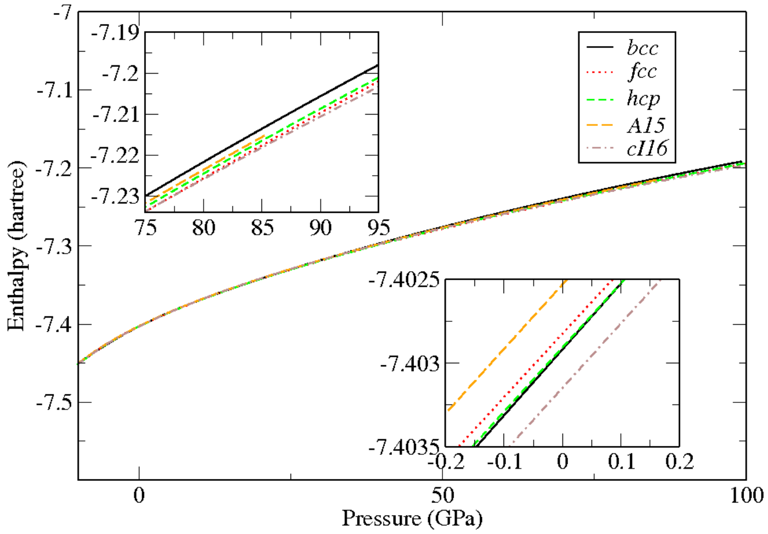

Figure 6.8: E(V) for known modification and cI16. The calculations were performed on the LDA level

The band structure and the phonon dispersion spectrum do not give any indications that the structure might exhibit instabilities such as Peierls distortions. Thus, we can conclude that the A15 structure, found by the global exploration of the energy landscape of lithium, is a new metastable structural candidate, in addition to the experimentally known structures. The A15 structure is unusual for elemental systems, but the calculations suggest that it is energetically competitive with the structures known to exist at ambient pressure.

6.3.2 High pressure

We performed 43 runs for global searches with various pressures using 4 and 8 atoms per unit cell. We found the same structure types as at standard pressure (c.f. Tables 6.2). However, we could not do enough simulations for a large statistical sample at high pressures, because the simulation times were quite long. In addition to the outcome of the global searches, we have included structure candidates known at high pressure in our study i.e., cI16 and hR1. We optimized these structure under pressure using LDA. We plotted the enthalpy as a function of pressure in fig. 6.8. It becomes apparent, that over 70 GPa, the cI16 structure is a stable structure. We also confirmed that the cI16 structure is obtained from the bcc structure by reducing the symmetry (its space group is a subgroup of the space group of the bcc structure): In figure 6.9, we optimized the cI16 structure at various fixed volumes. We could see a clear transition from cI16 to bcc: the fractional coordinate changes from 0.05 to 0.0 when increasing the volume (or reducing the pressure), where 0.0 corresponds to bcc.

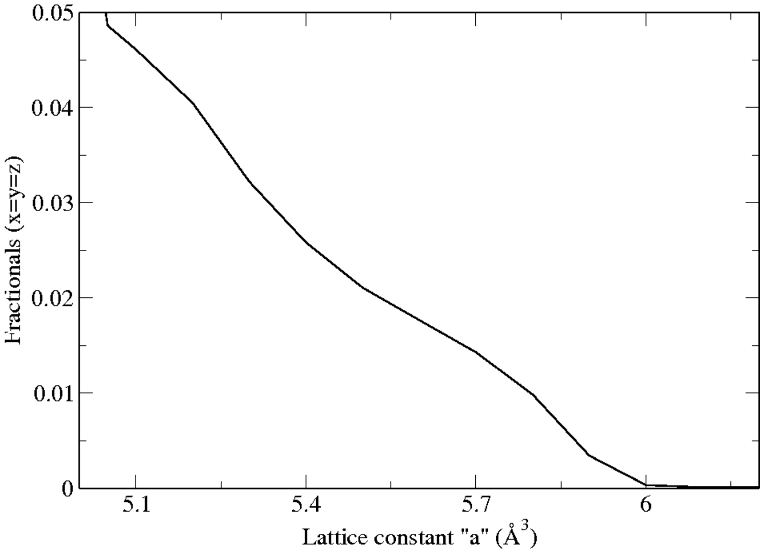

Figure 6.9: Change of fractional coordinate as a function of the lattice constant for the cI16 structure. The calculations were performed on the LDA level

6.4 Conclusion

We successfully performed a global exploration for elemental lithium on the *ab-initio* energy landscape at standard and high pressure. We found all those structures which are experimentally known at standard pressure, except for the 9R structure. We predicted a new modification, the A15 structure, as an interesting candidate. The energy of this structure is comparable to those of the known structures. In order to provide evidence of the kinetic stability, we performed phonon calculations and relaxations after finite atom displacements. Thus, this new hypothetical modification should be a promising synthesis target, although finding a route for the synthesis of this structure will pose a challenging task for the experimentalist. Our high pressure global search did not yield all high-pressure modifications. The number of runs was less as compared to the runs at standard pressure, because the number of atoms used for the simulation was larger. We have studied in detail some known modifications to understand their structural relationship. From this study, we confirmed that the cI16 modification is a derivative of the bcc structure. We plotted the $E(V)$ and $H(p)$-curves which confirmed that it is a stable modification at high pressure, with lower enthalpy than the structures which are stable at zero pressure.

7

Calcium carbide

7.1 Introduction

Calcium carbide is a very well known binary system which is commonly used to prepare acetylene (283) and calcium hydroxide. At the beginning of the 20th century, calcium carbide lamps (284) were used in the mines. Later, it was realized that the usage of these lamps was dangerous in coal mines where the presence of the flammable gas methane made them a serious hazard. There are some other industrial applications of calcium carbide such as in the desulfurization of iron, as a fuel in steel-making, and the production of calcium cyanamide (285).

Our motivation for studying CaC_2 was that it is a mixed covalent-ionic system thus allowing us to go beyond the study of purely ionic (e.g. LiF (286)) or purely covalent (e.g. BN (65)) systems. We note that in all experimentally known structures in this system, the carbon atoms combine to form C_2-dumbbells. Since the bonds between the carbon atoms in the dumbbells are covalent whereas the interaction between Ca and C_2 is "ionic", the global energy landscape of CaC_2 cannot be easily described by straightforward empirical potentials. Thus, it is necessary to perform the global search for structure candidates on the *ab-initio* level. Besides allowing us to deal with complex interactions, using *ab-initio* energies also enables us to dispense with the use of rigid C_2-building units during the global search, as had been commonly used for similar systems containing complex building blocks in the past (287), and to employ freely moving individual carbon atoms instead. In this fashion, one is able to identify structures that exhibit C-atom networks, which might occur at very high pressures.

Experimentally, four different modifications of CaC_2 are known (c.f. Fig. 7.1 (a), 7.1 (b), and 7.1 (c)). At room temperature, CaC_2-I crystallizes in the body-centered tetragonal system with space group $I4/mmm$ (no. 139) (288) and unit cell parameters a=3.87 Å and c=6.40 Å. The C_2-dumbbells are oriented along the [001] axis of the structure. With the C_2-dumbbells differently orientated, there are two more modifications viz., CaC_2-II with space group $C2/c$ (No. 15) (288) and CaC_2-III with space group $C2/m$ (No. 12) (288), both of which are assumed to be metastable. In both monoclinic structures, the C_2^{2-}-unit is surrounded by a distorted octahedron made of

Ca^{2+} ions. Finally, cubic CaC_2-IV (288) is found at high temperature. It can be visualized as a rock-salt structure with Ca^{2+} in the Na^+ positions and the center of gravity of the rotating C_2^{2-}-dumbbells in the Cl^- positions.

The following sections are organized as follows: the global search method is briefly explained in the next section. In the section "results", we present the outcome of the global searches performed on standard and elevated pressures. In the discussion section, the results are compared with the experimentally observed CaC_2 polymorphs and typical AX_2-type structures found in other chemical systems. Furthermore, the effect of the rotation of the C_2-dumbbell in all directions is analyzed, which gives insight to understand the stability of this material. Finally, the performance of the global optimization algorithm used is discussed.

7.2 Details for the global search

The technical details are given below for the global search. Regarding the size of the system, we have considered 2, 3 and 4 CaC_2 formula units per simulation cell, where one formula unit is composed of one Ca and 2 C atoms, since, from databases (289), it is known that most binary crystalline structures can be described by using up to four formula units per primitive cell. The initial volume of the simulation cell was chosen by multiplying with a factor in the range from 3 to 5 times of the ionic volume of the atoms. In this study, it was 883 $Å^3$ in the case of 2 formula units and 2650 $Å^3$ in the case of 4 formula units. Periodic boundary conditions were applied.

The global search was composed of simulated annealing and a subsequent stochastic quench which was based on the Metropolis algorithm (102). The initial temperature for the simulated annealing was 1.00 eV ($\sim$ 11604 K) and 6250 steps were used for 2, 3 and 4 formula units. The reduction in temperature during the simulation was exponential. Every 250 steps, it was multiplied by a factor of 0.995. The temperature was 0.88 eV ($\sim$ 10245 K) at the end of a simulated annealing run. After the simulated annealing, a quench was applied, i.e., a simulated annealing run with the temperature 0 eV. The selection of the simulated annealing and quench moves was based on the following criterion: movements of individual atoms (70%), atom exchange (10%), and change in lattice parameters (20%) were attempted. To accelerate shrinking of the cell, we set the probability to shrink the lattice constant to 60%. We note that there was no significant change by extending the length of the simulated annealing run to more than 15000 steps for the global optimization.

The calculations were performed for various pressures (0, 16, 32, 48, and 64 GPa), in order to search for possible high-pressure modifications.

There are some additional important parameters, e.g., the minimal allowed distance between two atoms and the reduction of the cell size. The minimal distance between two atoms was 0.7 times the sum of the ionic radii to avoid unphysical geometries which are responsible for numerical instabilities. The estimation of atomic/ionic radii was performed using a Mulliken population analysis. Later, the atomic and ionic radii were obtained from tabulated values of the corresponding atoms/ions, as a function of charge (226) (and employing a simple linear interpolation to obtain the radii, as the computed Mulliken charges are non-integer).

7.2.1 Description of basis set and pseudopotential

All energy calculations during the global search were performed on the *ab-initio* level with periodic boundary conditions using the CRYSTAL06 code (230). It is based on local Gaussian type orbitals. Since structure prediction is a very time consuming task involving many millions of energy calculations, one usually attempts to reduce the computational effort by employing simplified *ab-initio* energy functions. Here, we used two basis sets for the optimization. In the global optimization, calcium with a large core effective potential (290) was used together with a $[1s]$ basis set. For the $[1s]$ contraction we used the first two exponents of the $[1s]$ contraction as it was originally calibrated together with the pseudopotential (291). For carbon, we used a $[3s2p]$ basis set, which was derived from the 6-31G basis set (292), but with the outermost diffuse sp exponent replaced by 0.25, in order to speed up the calculation, and to achieve a higher numerical stability. In the subsequent local optimizations we used a small-core pseudopotential (293) for calcium, together with a $[3s2p]$ basis set. The tight $[2s]$ and $[2p]$ functions of this basis set were the same as in ref. (293), and one additional s-function (0.2) was added. For carbon, we used the same basis set as in the global search, but the outermost diffuse exponent was kept at the value 0.168714 instead of 0.25.

7.2.2 Local optimization

The local optimization is performed using analytical gradients (268, 269, 294, 295, 296), taking the symmetry of the structure into account. In order to gain an estimate of the validity of the *ab-initio* calculations, we have performed both Hartree-Fock and DFT (local density approximation, LDA, and the hybrid functional, B3LYP) calculations for all structures and systems during the local optimization. This local optimization is performed at zero temperature. These calculations require little CPU time and are therefore done with high-accuracy computational parameters.

7.2.2.1 Energy calculations

We note that the *ab-initio* total energy calculations for the global optimization were performed on the Hartree-Fock level, since the Hartree-Fock calculations are easier to converge for insulators due to the resulting larger size of the band gaps compared to DFT calculations. This is especially important as the atoms initially are at random positions that can be quite far apart (65), and the corresponding band structure looks therefore rather like that of a system with distant atoms and not with the typical density of solids.

Keeping the CPU time low plays a key role in the efficiency of the global search. This requires a careful calibration of many parameters in simulated annealing, e.g., the initial volume and temperature, the number of simulation steps and cooling schedule and the parameters of the *ab-initio* energy calculations. The initial volume and temperature are very large, i.e., the system is essentially in a gaseous state at the start. Converging the total-energy calculation both at such a random geometry and at all later stages of the simulated annealing and the quench, is a particularly difficult task for the system CaC_2 due to the mixed (covalent-ionic) nature of the bonds.

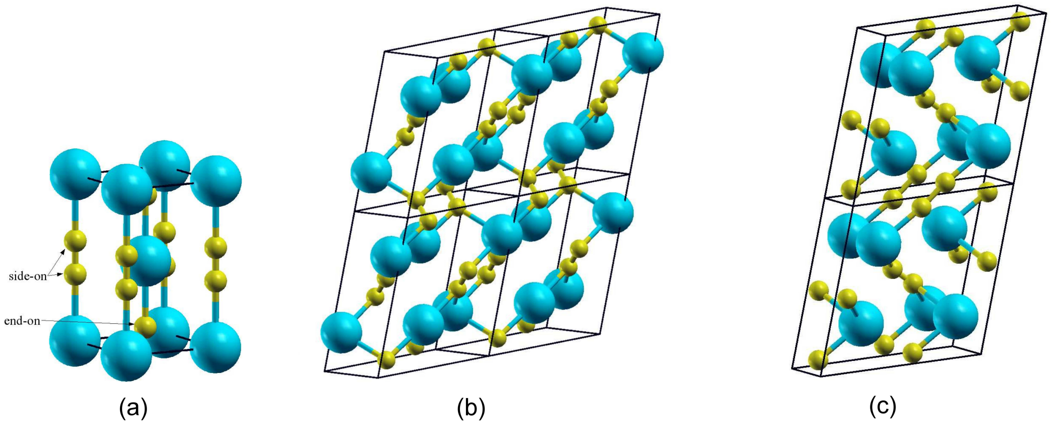

(a) (b) (c)

Figure 7.1: Experimentally known low-temperature modifications of CaC_2. (a) CaC_2-I (experimental + predicted), (b) CaC_2-II, and (c) CaC_2-III. Blue (big) spheres correspond to calcium, yellow (small) spheres to carbon atoms, respectively. The lines indicate the unit cells, with the z-axis pointing upwards. The label 'side-on' ('end-on') marks the C_2-dimer which is a side-on (end-on) neighbor of the central Ca atom.

In order to speed up the calculations during the global search, the self-consistent field cycles were terminated when the energy difference between two consecutive cycles was 10^{-4} E_h. A k-point mesh of the size 4×4×4 was used. In contrast, for the local optimization, default convergence criteria (10^{-7} E_h) and a larger k-point mesh (8×8×8) were used.

7.3 Results

7.3.1 Standard pressure

We performed 227 global searches for standard pressure. These global searches result in 10 different structure candidates for this system which have a space group different from P1. All polymorphs obtained from global searches showed the formation of C_2-bonds from initially widely separated carbon atoms. Three modifications symbolized by CaC_2-I, -V and -VI are energetically particularly stable (low-lying) at standard pressure. The total energies of these structures, after the local optimization, are displayed in table 7.1. These predicted structures are shown in Fig. 7.1 (a), 7.2 (a), and 7.2 (b) with XCRYSDEN (297), and their optimized structures are given in Table 7.2. In all structures, there is one common feature, isolated dumbbells are formed by the carbon atoms. The computed C-C bond length ranges from 1.272 Å to 1.280 Å for the low temperature structures CaC_2-I to -VI and CaC_2-VII (see Table 7.3, where the bond lengths after the local optimization are displayed).

Table 7.1: Total energies at zero pressure of the relaxed structures of the most important modifications found and their statistics of occurrence during the global optimization. Energies are in hartree units (1 E_h=27.2114 eV), per formula unit. A run is termed as successful, if it reaches a stable local minimum structure. Out of 227 runs at standard pressure 54 were successful. Similarly, among the 104 runs at elevated pressures, there were 39 successful runs.

name of modification (structure)	space group	energy [E_h]			number of times found (at pressure in GPa)				
		LDA	B3LYP	HF	0	16	32	48	64
CaC_2-I (Tetragonal)	*I4/mmm* (139)	-112.1717	-112.9470	-112.2114	11	1	3	2	0
CaC_2-V (Orthorhombic)	*Immm* (71)	-112.1735	-112.9499	-112.2141	18	3	3	5	1
CaC_2-VI (Monoclinic)	*C2/m* (12)	-112.1720	-112.9481	-112.2125	5	1	0	1	1
CaC_2-VII (Trigonal)	$R\bar{3}m$ (166)	-112.1532	-112.9215	-112.1821	0	2	4	1	4
other modifications (with higher energies and irregular polyhedra)					20	0	2	4	1
# of successful runs					54	7	12	13	7
Total # of runs					227	24	24	32	24

Table 7.2: The energetically most favorable structures in the CaC_2-system, plus several structures at higher energy derived from well-known structure types.

modification and space group	cell parameters and fractional coordinates (predicted, LDA)	(experimental at 83 K(288))	Energy (in hartree) per formula unit (LDA)
CaC_2-I(expt)		a=3.87 Å, c=6.40 Å	
CaC_2-I(predicted)	a=3.87Å, c=6.34Å		-112.1717
$I4/mmm$(139)	Ca(0, 0, 0)	Ca(0, 0, 0)	
Tetragonal structure	C(0, 0, 0.399)	C(0, 0, 0.407)	
CaC_2-V(predicted)	a=3.71Å, b=5.34Å,		-112.1735
$Immm$(71)	c=4.89Å		
Orthorhombic structure	Ca(0, 0, 0)		
	C(0, 1/2, 0.130)		
CaC_2-VI(predicted)	a=6.85Å, b=3.88Å,		-112.1720
$C2/m$(12)	c=3.95Å		
Monoclinic structure	β=114.3 °,		
	Ca(0, 0, 0)		
	C(0.595, 0.000, 0.628)		
CaC_2-II(expt) [a]	a=6.56Å, b=4.11Å	a=6.60Å, b=4.19Å	-112.1732
$C2/c$(15)	c=7.60Å	c=7.31Å	
Monoclinic structure	β=109.1 °	β=107.0 °	
	Ca(0, 0.325, 1/4)	Ca(0, 0.182, 1/4)	
	C(0.230, 0.145, 0.935)	C(0.282, 0.146, 0.056)	
CaC_2-III(expt) [a]	a=7.05 Å, b=3.80 Å	a=7.21Å, b=3.83Å	-112.1731
$C2/m$(12)	c=7.52 Å	c=7.37Å	
Monoclinic structure	β=106.6 °	β=107.2 °	
	Ca(0.204, 0.000, 0.249)	Ca(0.197, 0, 0.254)	
	C1(0.542, 0.000, 0.935)	C1(0.421, 0, 0.021)	
	and C2(0.080, 0.000, 0.566)	and C2(0.952, 0, 0.420)	
CaC_2-VII(predicted)	a=b=c=3.51Å		-112.1532
$R\bar{3}m$(166)	$\alpha=\beta=\gamma$=86.6 °		
Trigonal structure	Ca(0, 0, 0)		
	C(0.600, 0.600, 0.600)		
"$Ca(CN_2)$" configuration	a=b=c=4.55Å		-112.1678
$R\bar{3}m$(166)	$\alpha=\beta=\gamma$=49.4 °		
Trigonal structure	Ca(0, 0, 0)		
	C(0.447, 0.447, 0.447)		
"Cu (N C N)" configuration	a=b=3.78Å, c=8.09Å		-112.1653
$P6_3/mmc$(194)	γ=120.0 °		
Hexagonal structure	Ca(0, 0, 0)		
	C(1/3, 2/3, 0.328)		
FeS_2 (pyrite) configuration	a=b=c=5.81Å		-112.1654
$Pa\bar{3}$ (205)	Ca(0, 0, 0)		
Cubic structure	C(0.437, 0.437, 0.437)		
MgC_2 configuration	a=b=6.42Å, c=2.93Å		-111.7925
$P4_2/mnm$ (136)	Ca(0, 0, 0)		
Tetragonal structure	C(0.730, 0.730, 0)		

[a] Not found in the structure prediction, but instead experimental data was optimized.

Table 7.3: Interatomic C-C distances[Å] and volumes[Å^3] per formula unit of the most relevant modifications after local optimization on the LDA level, at standard pressure.

modification	C-C distance (in Å)		volume (Å^3)
	experimental	computed	
CaC_2-I	1.19	1.277	47.515
CaC_2-V		1.272	48.420
CaC_2-VI		1.274	47.805
CaC_2-II	1.19	1.274 [a]	48.364 [a]
CaC_2-III	1.18	1.275 [a]	48.254 [a]
	1.27		
CaC_2-VII		1.280	43.049

[a] Not found in the structure prediction, but instead obtained from the local optimization of experimental data

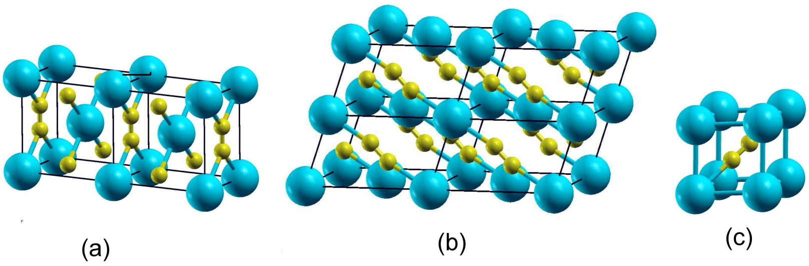
(a) (b) (c)

Figure 7.2: Newly predicted low-temperature modifications of CaC_2. For notation c.f. Fig. 7.1. Modifications (a) CaC_2-V and (b) CaC_2-VI are low-pressure modifications; (c) CaC_2-VII is a high-pressure modification.

Table 7.4: Interatomic distances[Å] between Ca and C atoms in the CaC_2-I, -II, -III, -V, -VI, and -VII modifications, with different types of coordination of Ca by C_2-dumbbells at zero pressure after local optimization on the LDA level.

modification	coordination of Ca by C-atoms	Distance from nearest carbon atom (in Å)	
		(experimental) [a]	(predicted)
CaC_2-I	2x,*end-on*	2.531	2.531
	8x,*side-on*	2.812	2.812
CaC_2-V	4x,*end-on*		2.589
	4x,*side-on*		2.747
CaC_2-VI	2x,*end-on*		2.551
	4x,*side-on*		2.668
CaC_2-II	2x,*end-on*	2.567	
	2x,*side-on*	2.602	
	2x,*side-on*	2.756	
	2x,*side-on*	2.795	
	2x,*side-on*	3.304	
CaC_2-III	*end-on*	2.556	
	side-on	2.753	
	side-on	2.765	
	2x,*end-on*	2.579	
	2x,*side-on*	2.676	
	2x,*side-on*	2.990	
CaC_2-VII	2x,*end-on*		2.576
	6x,*side-on*		2.813

[a] after local optimization of experimental data

The experimentally observed tetragonal structure (CaC_2-I) (298, 299) was identical with the first predicted structure, which is the room temperature modification. The orientation of the C_2-dumbbells is along the [001] axis of the tetragonal unit cell (see Fig. 7.1 (a)). Each Ca atom is surrounded by 4 C_2-units in a side-on way and 2 C_2-units in an end-on way.

We predicted two additional low-energy structures labeled as CaC_2-V and CaC_2-VI from our simulation. In CaC_2-V (see Fig. 7.2 (a)), the C_2-dumbbells are oriented along the [001] axis. Two C_2-units are side-on to Ca atoms. This breaks the tetragonal symmetry when compared to CaC_2-I, i.e., the C_4 axis of rotation is missing in the CaC_2-V structure, and the space group is *Immm*. Although the predicted CaC_2-VI polymorph shows the same space group as CaC_2-III, the two structures are not the same. This is most obvious from the fact that CaC_2-VI requires only two formula units per primitive cell, while CaC_2-III contains 4 formula units per primitive cell. In CaC_2-VI (see Fig. 7.2 (b)), the Ca_6-octahedra around the C_2-dumbbells are strongly distorted. Each Ca atom is surrounded by 2 end-on and 4 side-on C_2-dumbbells.

The experimental low-temperature modification CaC_2-III (299) is displayed in Fig. 7.1 (c). The LDA-optimized C-C distance in the C_2-dumbbell is about 1.275 Å. Again, the C_2-dumbbells are surrounded by a Ca_6-octahedron. Each Ca atom is enclosed by 3 C atoms in an end-on way and 6 C atoms in a side-on way. For completeness, we describe the modification CaC_2-II (299). It takes the form of the ThC_2 structure type (300) with C_2-dumbbells directed towards an edge of a Ca_6-octahedron and a small tilt angle. The octahedron itself is very strongly distorted (see Fig. 7.1 (b)). In CaC_2-II, a Ca atom is enclosed by 4 side-on and 2 end-on C_2-dumbbells (c.f. Table7.4).

7.3.2 Global search on elevated pressure

For the high pressures, viz. 16, 32, 48, and 64 GPa (c.f. Table 7.1), we have performed 104 global optimizations. Several new structures were found and some of the ones which are observed at standard pressure. The possible structures at 16 GPa are CaC_2-I, CaC_2-V, CaC_2-VI, and CaC_2-VII. Above 32 GPa pressure the CaC_2-VII structure (see Fig. 7.2 (c)) is predicted as the thermodynamically stable structure, the one with lowest enthalpy. The CaC_2-VII structure closely resembles the CsCl structure. The Ca atoms form a distorted cube with the C_2-units in the center (see Fig. 7.2 (c)) and, conversely, the centers of mass of the C_2-units form a distorted cube around the Ca atoms. Due to the distortions, the cubic symmetry of the “CsCl-type arrangement“ is reduced, resulting in the space group $R\bar{3}m$ (no. 166). Our results only apply to low temperature, of course. At elevated temperatures, we expect that the C_2-units will be able to rotate freely, and thus the CaC_2-VII structure will transform to a CsCl-type structure.

BaC_2 crystallizes in the CaC_2-I structure type at ambient conditions. In very recent high pressure experiments, a CaC_2-VII structure with space group $\mathrm{R\bar{3}m}$ (166) was observed at a pressure of 30 GPa. As Ba and Ca are both earth alkaline metals, this newly observed BaC_2 structure can be viewed as a confirmation of the existence of this structure type which we had predicted for CaC_2, and a strong hint that it should also exist for CaC_2.

With LDA and B3LYP functionals (see Fig. 8.3 (a) and 8.3 (b)), the energy-vs-volume curves are plotted for all relevant modifications. By the introduction of pressure, the high-coordinated structures become more favorable, which is in agreement with the rule that the coordination number increases with pressure - see e.g., Ref. (301). It is obvious from Fig. 8.4 (a) that the high-pressure structure would, at standard pressure, have the smallest volume per formula unit and thus the highest density, whereas CaC_2-I to -VI all have very similar volumes at standard pressure (see Table 7.3). The enthalpies are presented in Fig. 8.4 (a) and 8.4 (b) for LDA and B3LYP, respectively. The change in structure is observed from the structure CaC_2-VI to the structure CaC_2-VII, and the transition pressure computed with LDA and B3LYP is 24 and 34 GPa, respectively.

7.4 Discussion

7.4.1 Comparison with experiment

There are only standard pressure modifications of CaC_2 available for a comparison regarding structural data. According to table 7.3, there is good agreement between the experimentally observed bond-lengths and the theoretically computed ones. There is one exception, the CaC_2-III structure where two significantly different bond-lengths are found in experiments (1.18 Å and 1.27 Å at 83 K; and even 1.13 Å and 1.48 Å at 295 K). But, it was mentioned (288) that an artifact of the refinement is a probable reason for the inconsistency. In order to resolve this issue, we optimized the CaC_2-III structure resulting in a bond length of 1.275 Å, which is much more consistent with those found in the other modifications.

All structures, including the experimentally known structures (CaC_2-I, -II and -III) and the predicted low-temperature/low-pressure structures (CaC_2-I, -V and -VI), are some derivative of the rock-salt structure type: the centers of the C_2-dumbbells form an elongated and distorted octahedron around Ca atoms and conversely, the dumbbells are in the centers of elongated octahedra of Ca-atoms. The distances between Ca and the neighboring C atoms are displayed in table 7.4. The spatial orientation of the C_2-dumbbells is the main difference between these five structures. This is similar to the high-temperature modification CaC_2-IV that is described in the rock-salt type, where the centre of mass of the rotating C_2-dumbbells lie at the center of Ca-octahedra. It is observed that the three experimentally known low-temperature modifications (288) are found to coexist at 295 K (288). At a temperature of about 640 K (288), CaC_2-II transforms to CaC_2-I and CaC_2-III.

From our simulations, the CaC_2-V structure is the energetically most favorable structure. The differences in energies to the experimentally observed monoclinic structures (CaC_2-II and -III) are higher by about 0.4 mE_h per formula unit (≈ 4 meV/atom), corresponding to about 42 K. The predicted monoclinic structure (CaC_2-VI) is higher by about 1.5 mE_h per formula unit (≈ 14 meV/atom, i.e. by about 160 K), and the tetragonal structure (CaC_2-I) is higher by about 1.8 mE_h per formula unit (≈ 16 meV/atom) corresponding to about 190 K. We suggest that all five modifications, plus additional variants with alternative C_2 orientations should be able to exist at low temperature. We computed transition pressures with the LDA-functional, and predicted that there is a change in structure from CaC_2-V to CaC_2-I at about 5 GPa and at about 7 GPa from CaC_2-I to CaC_2-VI (see Fig. 8.3 (a) and 8.4 (a)) and finally at 30 GPa to CaC_2-VII.

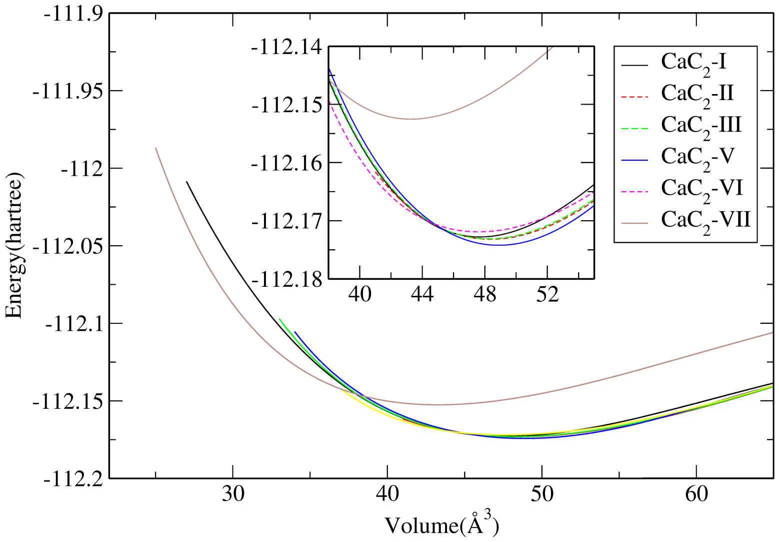

(a) DFT-LDA

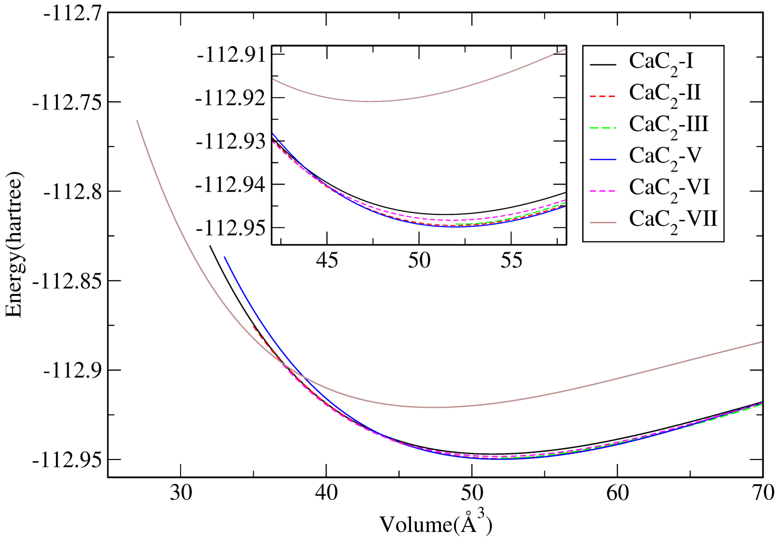

(b) DFT-B3LYP

Figure 7.3: E(V)-curves of the most relevant structures, at the LDA and B3LYP level. Energies per formula unit are given in hartree (E_h).

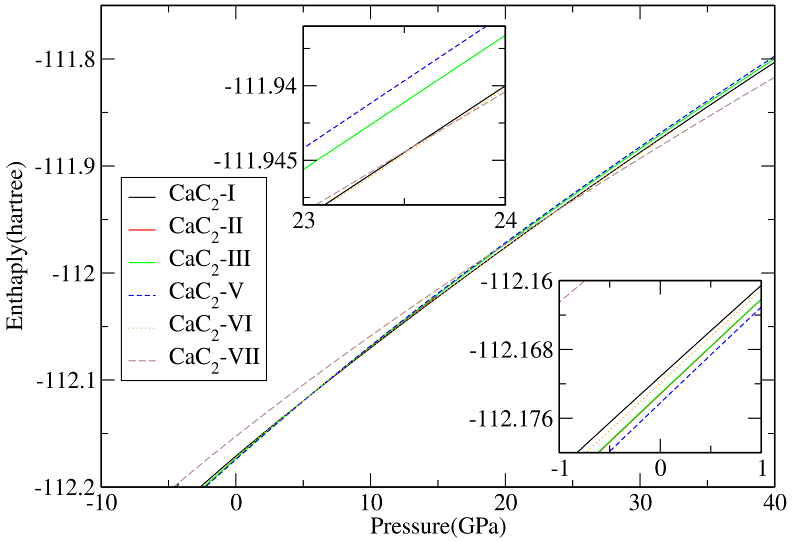

(a) DFT-LDA

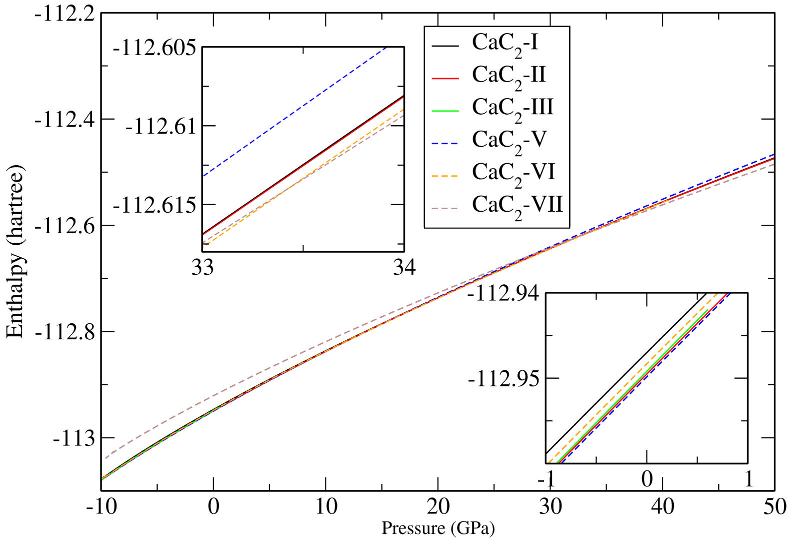

(b) DFT-B3LYP

Figure 7.4: Enthalpies per formula unit of the most relevant structures, at the LDA and B3LYP level. Inset upper left: high pressure range; inset lower right: standard pressure range.

7.4.2 Analyses of the barrier structures

As mentioned in the previous part, all the structures CaC_2-I to -VI are based on an essentially cubic close packed arrangement of the Ca atoms, where the C_2-units are located in the octahedral voids. All the structure types of CaC_2 are different because of the orientations of the C_2-units, leading to the many different low-temperature structures observed and predicted. To understand the stability of these modifications, we have studied the effect of the rotations of the C_2-dumbbells (302, 303). We have selected the CaC_2-I structure as a starting (and reference) configuration and one of the (equivalent) dumbbells. We rotated the C_2-unit and relaxed the structure via a local optimization. The rotation of the C_2-dumbbell can be described by a zenith angle (θ) and an azimuthal angle (ϕ) (see Fig. 8.1 (a)). When $\phi = 0°$, each C atom points towards the opposite face of the octahedron, and for $\phi = 45°$ each carbon atom points towards the opposite edge of the octahedron.

When we start with the CaC_2-I-type and then rotate the C_2 dumbbell by a very small angle ($\theta \leq 2°$ and ϕ=0°), we note that the subsequent local optimization goes back to the starting structure CaC_2-I. When the angle of rotation is larger than ($10° \leq \theta \leq 50°$), then the structure stabilizes in the CaC_2-VI structure after the subsequent local optimization. When the angle of rotation goes beyond 60°, then the local optimization leads to the structure CaC_2-V (see Fig. 8.1 (b)). The above result holds good for any angle ϕ. This explains that the structures CaC_2-I, CaC_2-V and CaC_2-VI are closely related but still distinct local minima. In contrast, the CaC_2-II and CaC_2-III structures are not accessible by a simple rotation of a single C_2 unit of the CaC_2-I structure.

The barrier estimation is possible, for transitions from the tetragonal (CaC_2-I) to the monoclinic (CaC_2-VI) or the orthorhombic (CaC_2-V) structure. The starting point was the tetragonal modification, where the C_2 dumbbell is oriented along the [001] direction. Then, the C_2 unit was tilted slowly and a local optimization was performed. When the C_2 dumbbell is rotated (and no optimization performed), then the energy increases monotonously with the tilt angle theta (up to $\theta = 90°$). Therefore, this energy can be used as an upper bound of the barrier. To have a transition from the tetragonal structure to the monoclinic structure, a tilt angle of 2° is required. The energy (for one formula unit) of the structure after such a tilt is 0.0001 hartree higher than that of the tetragonal structure, and this is an upper bound for the barrier. This barrier is very small, i.e., there is practically no barrier. To have a direct transition from the tetragonal to the orthorhombic structure, a tilt angle of 60° is required. The difference in energy after such a rotation is 0.039 hartree which is more than that of the tetragonal structure (for one formula unit). Again, this would be an estimated barrier which may be much larger than the real barrier (where many dumbbells might rotate in some connected fashion).

7.4.3 Comparison with CaC_2 candidates derived from common $A(X_2)$-structure types

In the literature (289), there are a number of “quasi-ionic“ structures $A(X_2)$ and $A(X_3)$ containing a fixed X_2-dumbbell or X_3-dumbbell. Clearly, it would be interesting to investigate, whether these structures have any resemblance to local minima on the energy landscape of CaC_2. Hence, we studied several such systems (c.f. Table 7.5). After replacing the cation (A) and anion (X) by Ca atoms and C_2-dumbbells, we have relaxed

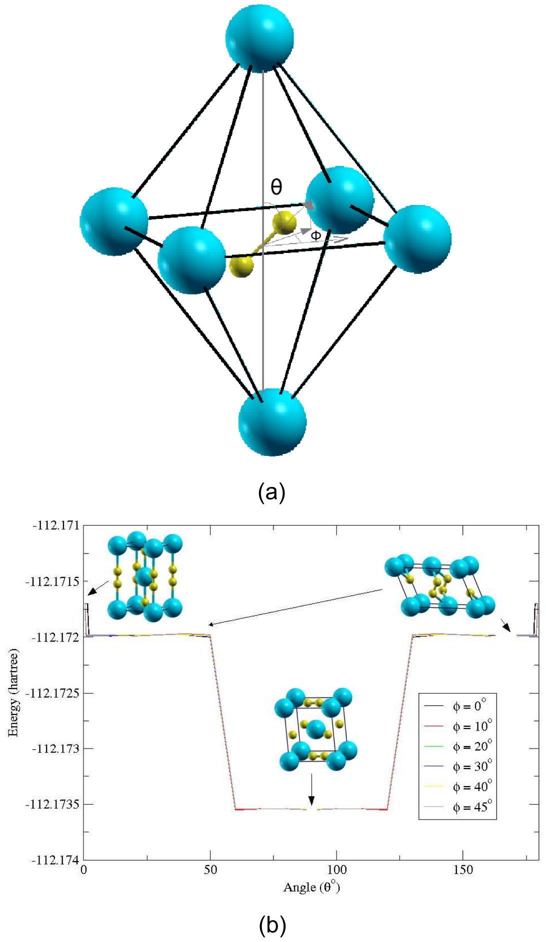

(a)

(b)

Figure 7.5: (a) Definition of the tilt angles θ and ϕ. (b) Rotation of the C_2-unit starting in the CaC_2-I-configuration. The curve shows the energy per formula unit after tilting the C_2-dumbbell by an angle ϕ (ϕ=0°, 10°, 20°, 30°, 40° and 45°) and rotating by an angle θ through 180°, and subsequently performing a local optimization. Three ranges of θ can be distinguished, [0°, 2°], [10°, 50°] and [60°, 90°], belonging to the basins of the CaC_2-I-, CaC_2-VI- and the CaC_2-V-modification. Note that the value of ϕ does not influence the outcome of the local minimization.

these structures, first keeping the space group fixed and then performing subsequently a full local optimization. We note that FeS_2 (marcasite) and RhN_2 relaxed to the CaC_2-I modification, and the structures based on BaC_2, KO_2, and NaN_3 transformed into CaC_2-V. All five structures above are not having any structural relation to CaC_2-I or CaC_2-V. The FeS_2 (pyrite)-based configuration remains in the same structure type, but the energy (see Table 7.5) is higher than those of the other structures. Thus, this structure may only exist at high temperatures; however, there it would compete with the CaC_2-IV structure. The one common feature in all the above structures is that the C_2-unit is octahedrally coordinated with Ca atoms after the local optimization.

CaC_2 in the $Ca(CN_2)$ structure type remains a trigonal structure both before and after full local optimization. The C_2-dumbbell is surrounded by 8 Ca-atoms and shows the same space group as CaC_2-VII. This structure has a lower enthalpy than the CaC_2-VII structure below 10 GPa; but, for higher pressure, CaC_2-VII is thermodynamically stable. In the case of Cu(NCN), the analogous CaC_2 structure transforms from an orthorhombic structure type before optimization to a distorted NiAs type after relaxation. We compared the ”Cu(NCN)“, ”$Ca(CN_2)$“, and ”FeS_2 (pyrite)“ type modifications with several of those found during the global search, i.e., CaC_2-VII, CaC_2-V, and CaC_2-I, with regard to the enthalpy as a function of pressure (see Fig. 8.2). We observed that not a single new modification deduced from the literature structures is thermodynamically stable, at least at low temperatures, compared to the predicted structures. Thus, we conclude that the structures obtained from our global search are representative for the thermodynamically stable low-temperature modifications.

7.5 Analysis of the performance of the global optimization procedure

So far, we have analyzed the outcome of the global search for possible modifications from a physical/chemical point of view by comparison with experiment and typical $A(X_2)$ structure types known from other chemical systems. We could conclude that we have most likely found the global minimum on the *ab-initio* energy landscape investigated, and in addition a typical sample of the many possible low-energy modifications that can be generated by varying the orientation of the C_2-units.

By performing additional simulated annealing runs, one would reach those minima, too. In general, the finite computation time available limits the volume of configuration space that can be explored using stochastic global optimization techniques and the cooling should be infinitely slow (304). However, the question arises, how large an additional computational effort would be necessary to substantially increase the number of new minima found, and whether this would be the most efficient use of computer resources.

In order to address this issue, we have performed an a-posteriori statistical analysis concerning the structures found. The calculation of posterior probability distribution functions had been suggested as a possible statistical analysis tool (305, 306, 307, 308). In the present work, in order to perform a statistical analysis, we sample subsets (called events) of the total set of runs (227 at standard pressure), each subset containing 10 randomly selected runs from among the total set. For each event, the ten runs were categorized into 3 groups viz. low-lying structure, duplicate, and not-a-low-lying

Table 7.5: Optimization of crystal structures taken from ICSD. Complex anions and cations were replaced by C_2-units and Ca-atoms, respectively. These modified structures were locally optimized using LDA. It was checked, whether the relaxed structure exhibited Ca_6-octahedra around the C_2-dumbbells.

Optimization of crystal structures taken from ICSD (289). Complex anions and cations were replaced by C_2-units and Ca-atoms, respectively. These modified structures were locally optimized using LDA. It was checked, whether the relaxed structure exhibited Ca_6-octahedra around the C_2-dumbbells.

ICSD compound	before local optimization		after local optimization			
	structure type	space group	structure type	space group	Energy	Ca_6-octahedron
BaC_2	ThC_2	*C2/c*	CaC_2-V	*Immm*	-112.1735	Yes
$Ca(CN_2)$	high temperature modification of NaN_3	$R\bar{3}m$	high temperature modification of NaN_3	$R\bar{3}m$	-112.1678	No (approximately cubic)
Cu (N C N)		*Cmcm*		$P6_3/mmc$	-112.1653	No (NiAS-type)[a]
FeS_2	Marcasite	*Pnnm*	CaC_2-I	*I4/mmm*	-112.1717	Yes
FeS_2	Pyrite	$Pa\bar{3}$	Pyrite	$Pa\bar{3}$	-112.1654	Yes
KO_2		*C2/c*	CaC_2-V	*Immm*	-112.1735	Yes
MgC_2		$P4_2/mnm$		$P4_2/mnm$	-111.7925	Yes
NaN_3	α-NaN_3	*C2/m*	CaC_2-V	*Immm*	-112.1735	Yes
RhN_2		*Pnnm*	CaC_2-I	*I4/mmm*	-112.1717	Yes

[a] Ca at the Ni place, C_2 at the As place

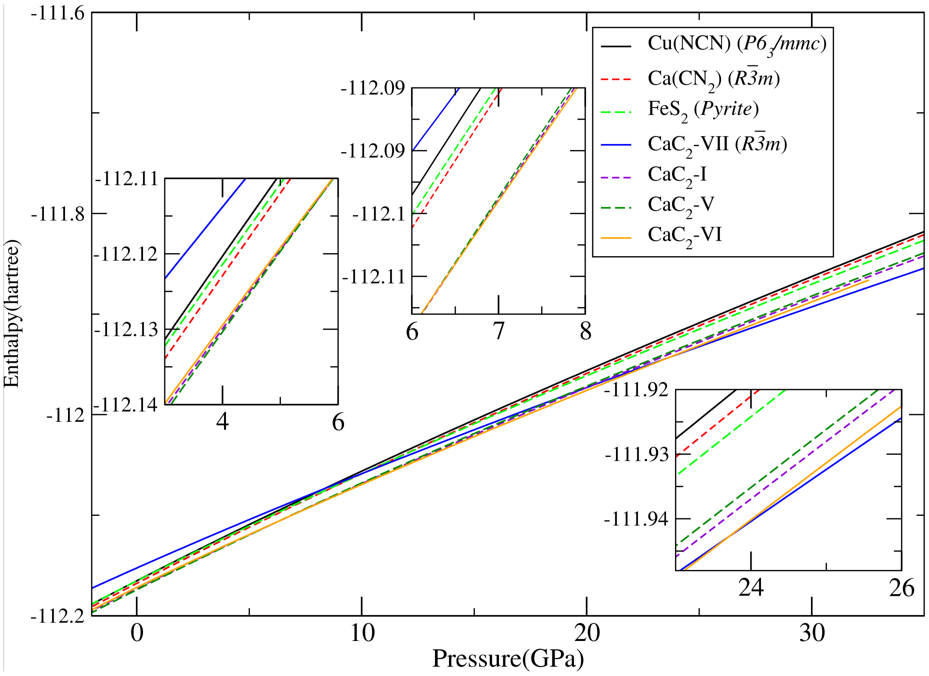

Figure 7.6: Enthalpy per formula unit of the three most relevant structures found during the global search and three additional ones based on well-known structure types, at the LDA level. Inset: upper left: 3 to 6 GPa; middle: 6 to 8 GPa; lower right: 23 to 26 GPa.

Table 7.6: Statistical analysis at different pressures

pressure	# of runs for one event	# of event	low-lying structures	duplicates	not-low-lying structures
0	10	1	1	1	8
		2	3	1	6
		3	3	1	6
		4	1	0	9
		5	2	0	8
		6	2	1	7
	100	1	3	20	77
		2	3	16	81
		3	3	15	82
high	10	1	2	2	6
		2	4	1	5
		3	3	3	4
		4	4	2	4
	100	1	4	35	61
		2	3	38	59

structure. The term low-lying structure is used when at the end of the run one of the energetically most favorable polymorphs is obtained. Other modifications (with higher energies and irregular coordination polyhedra) and unsuccessful runs, are placed into the category not-a-low-lying structure. If one of the runs ends up in a low-lying structure which had already been observed at the event under consideration, then it is counted as a duplicate. Six such events were analyzed, and the outcome is given in Table 7.6. The same analysis was repeated for three events consisting of 100 randomly chosen runs out of the total of 227 runs (c.f. Table 7.6).

We observe that out of 10 runs, 1-3 (average: 2) different low-lying structures were found. Similarly, out of 100 runs, 3 (average = 3) different low-lying structures were found, and the percentage of duplicates substantially increases. From this observation, we conclude that a substantially higher effort would be needed to find new low-lying minima.

We also performed the same statistical analysis at high pressure (16-64 GPa) using 10 and 100 (c.f. Table 7.6) global optimization runs as events. We observe that out of 10 runs, 2-4 (average: 3.25) and out of 100 runs, 3-4 (average: 3.5) different low-lying structures are found, respectively, and the percentage of duplicates again substantially increases when moving from 10 to 100 run events. Again, we can conclude that finding new low-lying minima would require a substantially larger computational effort.

Obviously, this statistical analysis can only serve as a rough estimate on the success rate of the global optimization procedure. But there is a clear trend that considerably more runs would be needed to identify additional relevant minima. However, since the structures of these minima apparently are all variants of a common structural theme (six/eight-fold coordination of Ca by C_2-units), performing further full global optimization runs does not appear to be very efficient. Instead, new minima could be generated systematically by selectively rotating C_2-units in the basic (rock salt / CsCl) structure, and then performing local optimizations to find the corresponding local minima.

For general comparison purposes, we have also performed 64 quench runs from random starting points. Such a set of stochastic local minimizations can serve as a reference for the efficiency of the global optimization procedure. However, in the present example, none of these runs reached one of the low-lying minima, demonstrating that the simulated annealing stage of the global search is definitely necessary.

7.6 Conclusions

We have shown that structure prediction, on the basis of simulated annealing as global optimization technique and *ab-initio* energy calculation in all steps of the search procedure, is feasible for the mixed covalent-ionic system CaC_2. The search was insofar restricted, as the structures with partially occupied sites or disordered structures were not included, and also structures with a very large number of formula units in the primitive cell (>4) could not be encountered. In all the polymorphs found, the carbon atoms had combined to form C_2-units. We found one experimentally known modification and several structures that are closely related to low-temperature modifications. Two new structures are predicted to be at least metastable at standard pressure: an orthorhombic structure (CaC_2-V), which was found to have the lowest energy of all structures considered, and another monoclinic modification (CaC_2-VI). At high pressure (above approximately 30 GPa), a transition is predicted from the quasi-six-fold coordinated structures to a quasi-eight-fold coordinated structure (CaC_2-VII) which is a distorted variant of the CsCl structure-type. In very recent high pressure experiments, CaC_2-VII structure was observed for BaC2.

8

Pernitride compounds

8.1 Introduction

In the earth's atmosphere, the most abundantly found element is nitrogen, constituting 78.08% by volume. Thus, nitrogen-rich compounds are very common, with nitrogen appearing in a variety of bonding situations. Among these are the nitrides, which are compounds of nitrogen where nitrogen has a formal oxidation state of 3. A class of nitrogen compounds which are related to, but distinct from nitride, are pernitrides, with N_2^{2-} or N_2^{4-}-units (N_2^{2-} is sometimes called diazenide), analogous to carbides C_2^{2-}. For completeness, there is an additional class of compounds, called azide, containing ($N_3{}^-$) units.

Metal nitrides and pernitrides show a wide range of excellent properties such as hardness, superconductivity, photoluminescence and various types of magnetism (309, 310, 311, 312, 313, 314). Hence, these compounds are attracting increasing interest in both experimental and theoretical studies. Pernitride compounds are not so common as nitrides. The experimentally known pernitrides are mostly from alkaline metals, alkaline earth metals, and some transition metals.

BaC_2 and BaO_2 are well known compounds for barium. Naturally this raised the question, whether a similar compound exists for the barium and nitrogen system. Barium nitride exists for two compositions, Ba_2N and Ba_3N. These are metal-rich compounds. On the other hand, the nitrogen-rich side might produce interesting N-N bonded species, more specifically the N_2^{2-} in BaN_2. This anion is closely related and isoelectronic to the oxygen molecule and to the C_2^{2-} anion of their oxide and carbide, respectively. (This is thought to be responsible for superconductivity in rare earth metal carbides and carbide halides (315, 316).) Experimentally, first nitrogen-rich nitrides were reported in 1892 (317). In the 1950s, the first high pressure experiments were performed for the preparation and characterization of BaN_2 (318, 319). The results showed the coexistence of Ba_3N_2 and BaN_2 (318, 319). Later in 2001, once again the same method was used to synthesize the barium pernitride. It crystallizes in the space group $C2/c$, similar to the ThC_2 structure type (320). Analogously, SrN_2 (321) was also synthesized the same way as BaN_2. In this reaction, Sr_2N is used as starting compound which reacts with N_2 under high pressure and high temperature.

During this synthesis, first SrN formed and later SrN_2. SrN crystallizes in a monoclinic structure with space group $C2/m$ whereas SrN_2 is formed in the CaC_2 structure type.

In 2003, a theoretical study was performed on CN_2 (322, 323), SiN_2 (323), and GeN_2 (323) which are not-yet synthesized systems. In this study, the compounds considered need the form $A^{4+}[N_2]^{4-}$ where A is C, Si, and Ge, and the anions form the same electronic configuration as S_2^{2-} in the pyrite structure in FeS_2. These structures were locally optimized and their physical properties were calculated. The distance between N-N atoms in SiN_2 and GeN_2 is 1.454 Å and 1.428 Å respectively, which is closely related to a single bond between nitrogen atoms in a N-N bond, whereas in the case of CN_2 one finds 1.34 Å which is in-between the length of a single and double bond between nitrogen atoms. The band gaps are calculated for CN_2, SiN_2, and GeN_2 to be 0.9, 5.5, and 1.5 eV, respectively. The bulk modulus has also been calculated for CN_2 to be 405 GPa (322). The experimentally known compositions of carbon and nitrogen are C_3N_4 (hardest compound) and $C_{11}N_4$ (324, 325, 326).

Later, a binary noble metal nitride, PtN_2, had been synthesized successfully at 45-50 GPa and temperatures more than 2000 K. Initially, it was wrongly formulated as PtN. But, afterwards theoretical (327) as well as experimental (328), studies showed that instead of PtN, PtN_2 (329) had been synthesized. It crystallized in the pyrite structure type. Similarly, Ir reacts with N_2 at high temperature and high pressure. IrN_2 is stabilized in the baddeleyite structure type (330). PtN_2 and IrN_2 are insulators at ambient conditions.

In 2008, palladium nitride was synthesized at a pressure above 58 GPa and a temperature somewhat below 1000 K (330). The other noble metal nitrides (IrN_2, OsN_2, RuN_2, and RhN_2) were also formed at high pressure and temperature conditions but PdN_2 decomposes at about ∼13 GPa. And theoretical studies also showed that PdN_2 stabilizes in the same structure type as PtN_2 (330). There was one independent study performed on OsN_2, which clearly shows that OsN_2 crystallizes in the marcasite structure type and is metallic in nature (331).

In 2010, theoretical work was performed on alkaline-earth metal pernitrides, viz., BeN_2, MgN_2, and CaN_2 (332). According to this study, BeN_2 and MgN_2 should crystallize in the ThC_2 type structure, and CaN_2 in the $ZnCl_2$ structure type, respectively. But recent experimental investigations on CaN_2 showed that the CaC_2-I structure type (333) is the stable one. Later in the same year, a theoretical investigation was performed on LaN_2 (334). In this system, the ThC_2 structure type should be the most stable modification at high pressure which is similar to the CaC_2 system. According to the electron count LaN_2 should be described as $La^{3+} + N_2^{2-} + e^-$.

In 2011, theoretical studies were performed on noble metal nitrides with the metals Ru, Rh, Re, and Au. It was proposed that RuN_2 and RhN_2 stabilize in the marcasite structure type (335), while ReN_2 should crystallize in an orthorhombic structure with symmetry $Pbcn$ (336). It should be a metallic and super-compressible solid. Its computed hardness is comparable to Si_3N_4 which is ∼17 GPa (337). Au belongs to the same row as Os, Ir, and Pt. So AuN_2 was the next candidate for a theoretical structural exploration. A theoretical study showed that AuN_2 would be quite difficult to synthesize because of it having a higher formation energy compared to other pernitrides (338). With the help of high pressure and high temperature, AuN_2 may show the same Au:N stoichiometric ratios or same other composition.

Some theoretical investigations have been performed on alkali metal diazenides viz., Li_2N_2 (339) and Na_nN_2 (333). Li_2N_2 crystallizes in the space group $Immm$. In the

Na_nN_2 study, different compositions of Na_n (n = 2,..,6) with N_2 were investigated, where some interesting structures were predicted, Na_2N_2 (in space group $Pmmm$) and Na_6N_2 (in space group Cm).

Finally, iron nitrides were first studied by Despretz (340) in 1829. The phase diagram of the binary Fe-N system (341) has been investigated in the middle of the twentieth century. There are four iron-rich compounds, among them two closely related daltonide compounds (Fe_4N and Fe_8N), the berthollide phase (Fe_3N) (342) and Fe_2N (343), which are exothermic. The next candidate in the phase diagram shows a 1:1 composition of Fe and N, which exists in crystalline powder form or in thin films. It is anti-ferromagnetic and crystallizes in the ZnS-type structure. The next composition is nitrogen-rich i.e., FeN_2 (344) which has also been theoretically studied. It is ferromagnetic and adopts the space group $R\bar{3}m$.

In this chapter, we are interested to globally explore the energy landscapes of CaN_2, LaN_2, and TiN_2 by applying the *ab-initio* search method presented in this thesis (see Chapter 5). These systems are also mixed covalent-ionic systems like CaC_2. These three systems had not been yet-synthesized at the start, but interestingly, recently CaN_2 (333) has been successfully synthesized. The following sections are organized as follows: the specific technical aspects of the global optimization are given in the method section. In the section "results", the outcome of the global explorations are presented for optimizations at standard and elevated pressures. In the discussion section, the results are compared with the predicted structure for pernitride system polymorphs and typical AX_2-type structures found in other chemical systems. Furthermore, we studied physical properties such as thermodynamical stability, bulk modulus, and conducting behavior of these pernitride compounds.

8.2 Method

The global search consists of simulated annealing runs and subsequent stochastic quenches. The temperature at the beginning of the simulated annealing is 1 eV (∼ 11 604 K), and 0.778 eV (∼ 9038 K) at the end of the run. We used for each run z = 2, 3, or 4 formula units per simulation cell of $(AN_2)_z$ (A = La, Ca, and Ti). Here, one formula unit is composed of one A and two nitrogen atoms. The initial volume of the simulation cell was selected to be much larger than the estimated cell size for a solid phase. This initial choice of the cell is based on the atomic and ionic radii. After selecting the volume of the cell, the initial position of the atoms were randomly chosen, such that the system will have enough freedom for rearrangements during the global search. The positions of the atoms and the cell parameters were changed during the run by controlling the movement of an individual atom (70 %), switching the positions of two atoms (10 %), and altering the lattice constants (20 %). When a change in the cell parameter was proposed, the probability to contract the lattice constant was set to 60 %, which proved to be useful in smoothly and efficiently reducing the cell volume while not restricting the global exploration. Every run is composed of 12500 simulated annealing moves which are followed by 10000 quench steps. The calculations were performed at different pressures (0, 16, 32, 48, and 64 GPa), to explore the possible candidates which can exist at high-pressure.

All the total energy calculations were performed at *ab-initio* level using the VASP (Vienna *Ab Initio* Simulation Package) (231, 232, 345, 346) which is a plane-wave code.

A generalized gradient approximation (GGA) of PBE type (347) and the projector-augmented wave (PAW) method (348) were used for both the global and the local optimizations. During the global search, a small 2×2×2 k-point mesh was used to improve the computational speed. For the local optimization, a larger 8×8×8 k-point mesh was employed and a smearing temperature of 0.001 eV was applied. The final results as presented in the figures and tables have all been obtained with the high-quality parameters.

The structures obtained at the end of the global optimization all show space group P1 due to the optimization which is not restricted in any way. We used the program KPLOT (225) to determine possible symmetries (see Chapter 4) after the global search and once again after the local optimization.

In addition, the candidates obtained from the exploration of the energy landscape and the most common experimentally known AB_2 structures listed in the ICSD database (289) were compared in this study. We computed energy-vs-volume curves and determined the bulk moduli by fitting Murnaghan-type equations of state to these curves for the locally optimized structures obtained from global searches or from the database. Furthermore, with the help of the $E(V)$-curves and the corresponding $H(p)$-curves, we determine possible phase transitions at high pressures. Finally, to understand the chemical bonding in these compounds, we performed Bader charge analyses (217).

8.3 Results

We performed energy landscape explorations and local optimizations of the structure candidates for CaN_2, LaN_2, and TiN_2. These searches were supplemented by local optimizations of selected commonly known $A(B_2)$ structure types. Furthermore, we performed local optimizations for SrN_2 and BaN_2 starting from structure types found during the global optimizations in the CaN_2, LaN_2, TiN_2 and CaC_2 systems and selected AB_2 structure types from the ICSD, for comparison.

8.3.1 SrN_2

25 different well-known AB_2 structure types were considered in order to find new structure candidates (c.f. Table 8.2). These structures were relaxed without applying any constraints. From all the above structure types, the tetragonal (CaC_2-I) structure and the orthorhombic (CaC_2-V) structure type were the lowest one in energy (c.f. Table 8.1) for the structure types considered (see Fig. 8.1(a) and Fig. 8.2(b)). Experimentally, SrN_2 crystallizes in the tetragonal structure type at standard pressure. We observe that when performing unconstrained optimizations of the structures, most of them remain in the same structure type as the starting one, with the exception of ThC_2, which changed to the CaC_2-I structure type. The distance between the two nearest nitrogen atoms is 1.24 Å.

As in the case of CaC_2, the tetragonal (CaC_2-I) structure type, the N_2 dumbbell lies along the [001] axis, and in the orthorhombic structure, it is perpendicular to the [001] axis. Each Sr atom in the CaC_2-I modification is enclosed by six N_2 units. The $E(V)$-

Table 8.1: Energetically most stable structures which are derived from well-known structure types for SrN_2 on the PBE level.

modification and space group	lattice parameters(in Å) and fractionals		N-N distance (in Å)	energy (eV) per formula unit(PBE)	volume (in $Å^3$)
	experimental	predicted			
"CaC_2-I" configuration *I4/mmm* (139)	a= 3.81, c= 6.28 La(0, 0, 0), N(0, 0, 0.402)	a= 3.85, c= 6.31 La(0, 0, 0), N(0, 0, 0.401)	1.254	-19.83762	46.72
"CaC_2-V" configuration *Immm* (71)		a= 3.98, b= 5.28, c= 4.74 La(0, 0, 0) N(0, 1/2, 0.867)	1.259	-19.52950	49.88
"MgC_2" configuration *P4$_2$/mnm* (136)		a= b= 4.39, c= 5.22 La(0, 0, 0), N(0.600, 0.600, 0)	1.238	-19.68955	45.51

and $H(p)$-curves were calculated for the optimized structures with two different functionals viz., PBE (GGA with PBE funtional) and GGA (GGA with PW91 functional) (Fig. 8.3 and 8.4). The CaC_2-I-type is the thermodynamically stable modification with the PBE functional whereas the CaC_2-V-type in the case of the GGA functional. This indicates that for SrN_2 there are two structures equally likely to occur from a theoretical point of view, suggesting that several modifications might exist and be accessible to experiments, similar to e.g. calcium dicarbide (see chapter 7) (288, 349).

8.3.2 BaN_2

The same procedure was followed for BaN_2 (c.f. Table 8.4 and 8.3). The ThC_2 type (see Fig. 8.1(b)) was found as the thermodynamically stable structural candidate,

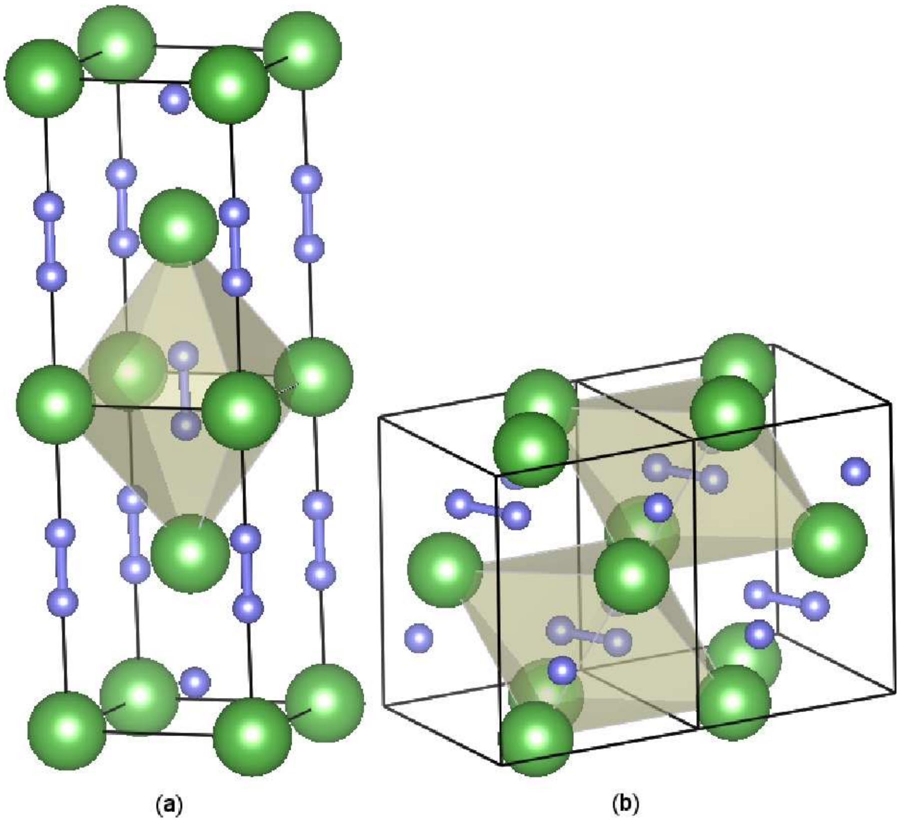

Figure 8.1: Experimentally known modifications of AN_2, where A is the cation (Sr, Ba, Ca, La, and Ti). (a) CaC_2-I and (b) CaC_2-II. Green (big) spheres correspond to metal, blue (small) spheres to nitrogen atoms, respectively. The lines indicate the unit cells, with the z-axis pointing upwards.

Experimentally known modifications of AN_2, where A is the cation (Sr, Ba, Ca, La, and Ti). (a) CaC_2-I and (b) CaC_2-II (288). Green (big) spheres correspond to metal, blue (small) spheres to nitrogen atoms, respectively. The lines indicate the unit cells, with the z-axis pointing upwards.

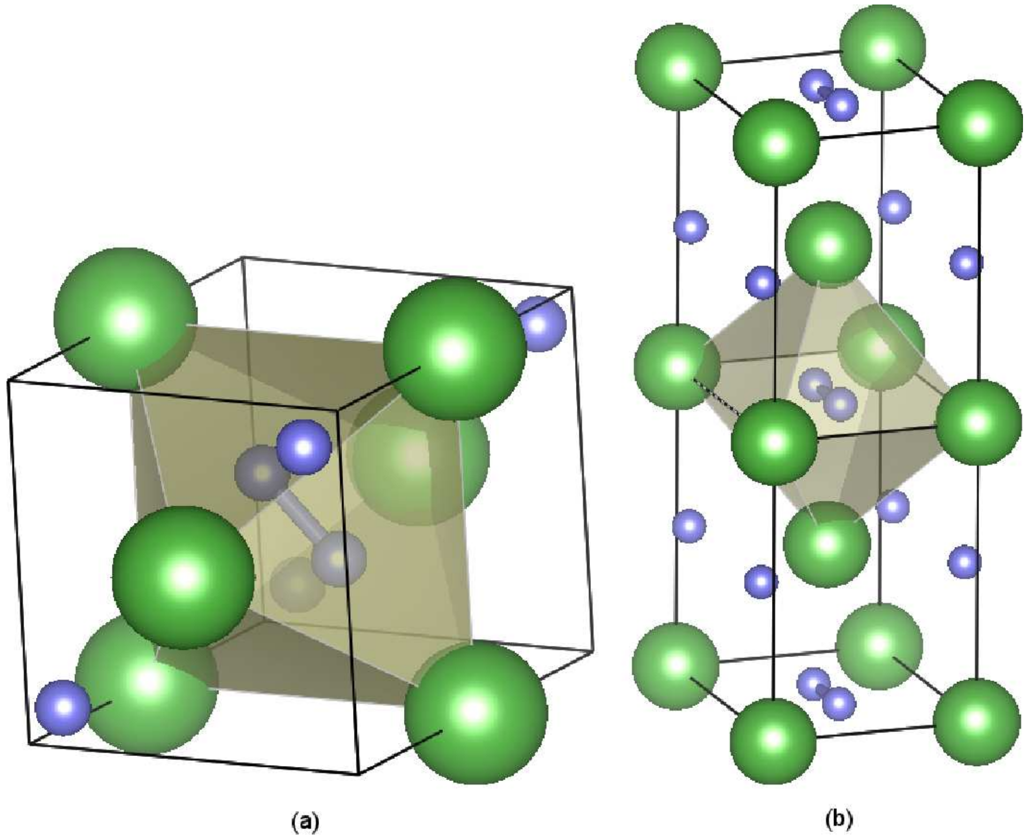

Figure 8.2: Predicted modifications for AN_2, where A is the cation (Sr, Ba, Ca, La, and Ti). (a) MgC_2-I and (b) CaC_2-V. Green (big) spheres correspond to metal, blue (small) spheres to nitrogen atoms, respectively. The lines indicate the unit cells, with the z-axis pointing upwards.

Table 8.2: Optimization of crystal structures taken from ICSD for SrN_2 with AB_2 structure type on the PBE level. The lowest energies are displayed by boldfaces.

name	Structure before optimization		Structure after optimization		energy(eV)
of	Structure	space	Structure	space	
compd	type	group	type	group	
SrN_2	Al_2Cu	$I4/mcm$ (140)	Al_2Cu	$I4/mcm$ (140)	-19.08906
	AlB_2	$P6/mmm$ (191)	AlB_2	$P6/mmm$ (191)	-16.19455
	CaC_2-I	$I4/mmm$ (139)	CaC_2-I	$I4/mmm$(139)	**-19.83762**
	CaC_2-II	$C2/c$ (15)	ThC_2	$C2/c$ (15)	**-19.6891**
	CaC_2-III	$C2/m$ (12)	ThC_2	$C2/c$ (15)	**-19.6891**
	CaC_2-V	$Immm$ (71)	CaC_2-V	$Immm$ (71)	**-19.52950**
	CaC_2-VII	$R\bar{3}m$ (166)	CaC_2-VII	$R\bar{3}m$ (166)	-19.18153
	CaF_2	$Fm\bar{3}m$ (225)	CaF_2	$Fm\bar{3}m$ (225)	-14.09131
	CaI_2	$P\bar{3}m1$ (164)		$P6/mmm$ (191)	-16.23583
	$CdCl_2$	$R\bar{3}m$ (166)	$CdCl_2$	$R\bar{3}m$ (166)	-19.18153
	Co_2Si	$Pnma$ (62)	Co_2Si	$Pnma$ (62)	-16.88936
	Cu_2Mg	$Fd\bar{3}m$(227)	Cu_2Mg	$Fd\bar{3}m$ (227)	-14.17465
	Cu_2S	$Fd\bar{3}m$ (227)	Cu_2S	$Fd\bar{3}m$ (227)	-14.17465
	$CuZr_2$	$I4/mmm$ (139)	CaC_2-I	$I4/mmm$ (139)	**-19.83762**
	Ga_2Sr	$P6/mmm$ (191)	Ga_2Sr	$P6/mmm$ (191)	-16.19455
	La_2Sb	$I4/mmm$ (139)	CaC_2-I	$I4/mmm$ (139)	**-19.83762**
	MgC_2	$P4_2/mnm$ (136)	MgC_2	$P4_2/mnm$ (136)	**-19.68955**
	NbS_2	$P6_3/mmc$ (194)	NbS_2	$P6_3/mmc$ (194)	-18.43622
	$PbCl_2$	$Pnam$ (62)		$Cmcm$ (63)	-14.21644
	$PbClF$	$P4/nmm$ (129)	$PbClF$	$P4/nmm$ (129)	-14.08754
	SiS_2	$I\bar{4}2d$ (122)	SiS_2	$I\bar{4}2d$ (122)	-16.60333
	$SiSr_2$	$I4_1/amd$ (141)	$SiSr_2$	$I4_1/amd$(141)	-18.90665
	ThC_2	$C2/c$ (15)	ThC_2	$C2/c$ (15)	**-19.86604**
	TiO_2(rutile)	$P4_2/mnm$ (136)	MgC_2	$P4_2/mnm$ (136)	**-19.68955**
	$ZnCl_2$	$Pna21$ (33)		$Pmna$ (62)	**-19.60341**

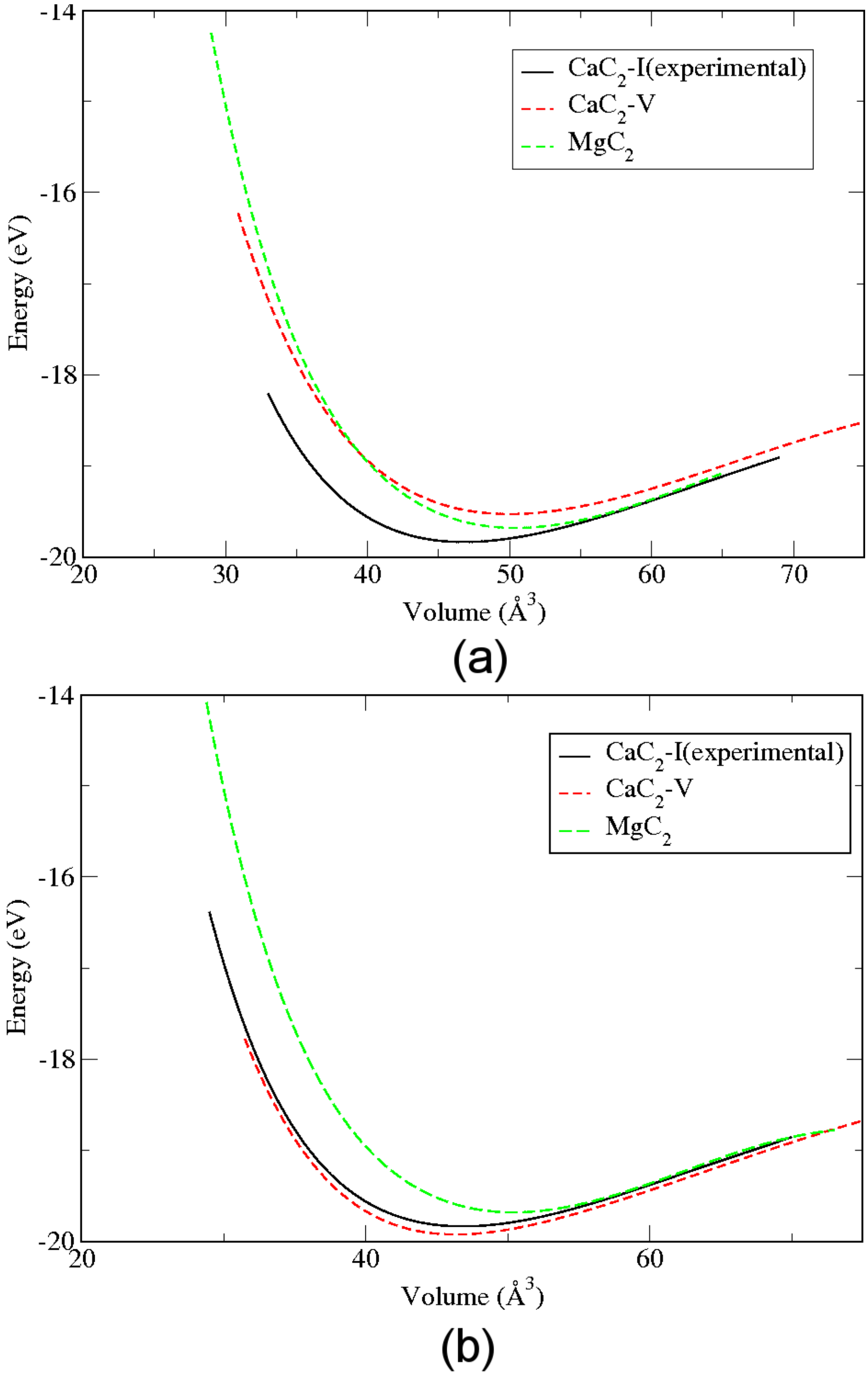

Figure 8.3: $E(V)$-curves of SrN_2 at (a) GGA and (b) PBE level. Energies per formula unit are represented in eV.

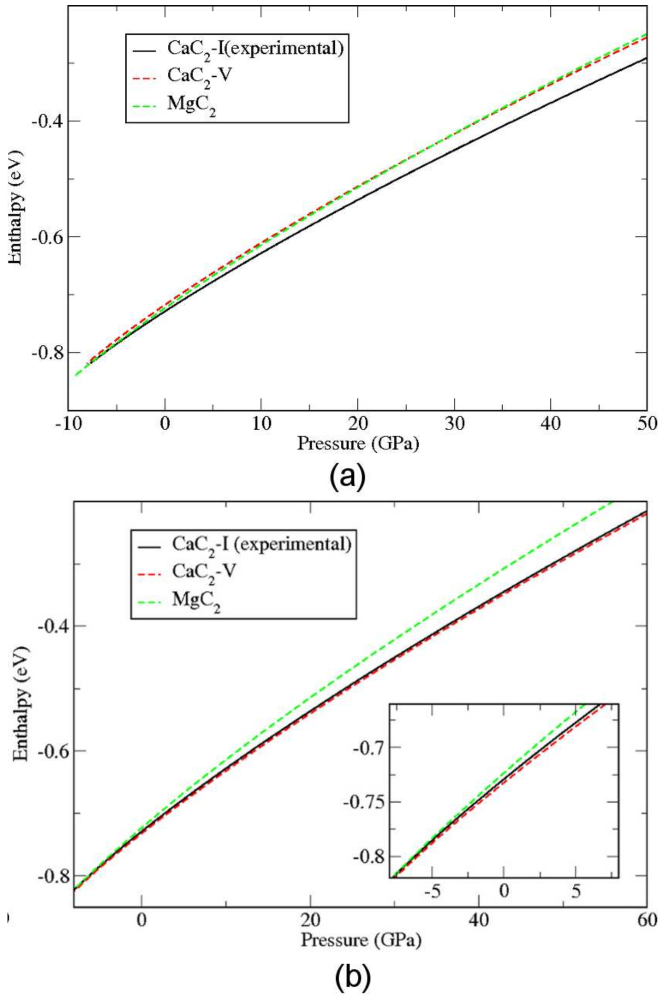

Figure 8.4: $H(p)$-curves of SrN_2 at (a) GGA and (b) PBE level. Energies per formula unit are represented in eV.

in agreement with experiment. Again, we plotted the $E(V)$- and $H(p)$-curves for all relevant structure candidates using PBE and GGA functionals. We noted in the BaN_2 system that the monoclinic, ThC_2-type structure is thermodynamically stable and there are three metastable modifications which are only slightly higher in energy. The energy difference between the experimentally known structure (ThC_2) and the tetragonal structure (CaC_2-I) is 0.3 eV/atom using the PBE functional. For both functionals, the ThC_2 structure type is the stable modification up to at least 20 GPa, whereas the CaC_2-I structure type is a metastable modification (see Fig. 8.5. The bond length of the N_2-unit in the ThC_2 modification is 1.23 Å.

8.3.3 CaN_2

Since at the beginning of this study CaN_2 was not known experimentally, before starting global optimizations, in a preliminary calculation, we selected a plausible structure candidate already observed in CaC_2, the CaC_2-I type structure, and compared its energy with the one of elemental calcium plus solid N_2. This formation energy being negative suggested that CaN_2 may be capable of existence. Based on these observations, 132 global optimization runs at ambient pressure were performed, which resulted in three promising structure candidates with symmetry higher than space group P1. In all the predicted structures with higher symmetry than P1, the calcium atom is surrounded by an octahedron formed by N_2 units.

The structures with the lowest energy were of a tetragonal (CaC_2-I), recently found in the experiment, and an orthorhombic (CaC_2-V) structure type (see Fig. 8.1(a) and Fig. 8.2(b)). Supplementing this global search with the minimization of structures analogous to those present in the database or found during global explorations in other carbides, peroxide or pernitride systems, showed that, in particular, the MgC_2 type structure candidate is also likely to be thermodynamically stable (c.f. Table 8.7 and 8.6). Further global optimization runs were performed at higher pressures, viz., 16, 32, and 48 GPa (c.f. Table 8.5), where, similar to the case of the CaC_2 and the LaN_2 system (see below), in addition to a number of new structures, several of those already observed during the searches at standard pressures are again found. After the local minimization stage, the $E(V)$- and $H(p)$-curves for all important structures were computed using the GGA/PBE type DFT functional and are shown in Fig. 8.5. From this, we conclude that the MgC_2 type modification is thermodynamically stable at low pressure, whereas the CaC_2-I type structure is a good structure candidate at elevated pressure. We note that the bond length of nitrogen atoms in the N_2 units increases from 1.242 Å to 1.258 Å after the phase transition (computed at the minimum of the E(V)-curve).

8.3.4 LaN_2

At standard pressure, 160 global searches were performed, resulting in 9 different structures with space group other than P1 (c.f. Table 8.5). In all the structure candidates, we observed that N_2 dumbbells formed from initially distant nitrogen atoms. There are four modifications which have comparably low energies at standard pressure, viz., the CaC_2-I (see Fig. 8.1(a)), the MgC_2 type (Fig. 8.2(a)), the ThC_2 (see Fig. 8.1(b)) and the CaC_2-III type. These four structures show an octahedral coordination of La

Table 8.3: Energetically most stable structures which are derived from well-known structure types for BaN_2 on the PBE level.

modification and space group	lattice parameters(in Å) and fractionals		N-N distance (in Å)	energy (eV) per formula unit(PBE)	volume (in $Å^3$)
	exptl.	predicted			
"CaC_2-I" configuration *I4/mmm* (139)		a= 4.14 c= 6.68 La(0, 0, 0) N(0, 0, 0.407)	1.239	-20.04876	57.32
"CaC_2-V" configuration *Immm* (71)		a= 4.31 b= 5.72 , c= 4.90 , La(0, 0, 0) N(1/2, 0, 0.373)	1.247	-19.72012	60.42
"ThC_2" configuration *C2/c* (15)	a= 7.17 b= 4.39 c=7.23, β=104.86 ° Ba(0, 0.198, 1/4) N(0.291, 0.143, 0.032)	a= 7.26 b= 4.46 c= 7.37 β=104.8 ° Ba(0, 0.789, 1/4) N(0.703, 0.852, 0.454)	1.230	-20.12775	57.56

Table 8.4: Optimization of crystal structures taken from ICSD for BaN_2 with AB_2 structure type on the PBE level. The lowest energies are displayed by boldfaces.

name	Structure before optimization		Structure after optimization		energy(eV)
of	Structure	space	Structure	space	
compd	type	group	type	group	
BaN_2	Al_2Cu	$I4/mcm$ (140)		$P4/mmm$(124)	-13.84225
	AlB_2	$P6/mmm$ (191)	AlB_2	$P6/mmm$ (191)	-15.88645
	CaC_2-I	$I4/mmm$ (139)	CaC_2(rt)	$I4/mmm$ (139)	**-20.04876**
	CaC_2-II	$C2/c$ (15)	ThC_2	$C2/c$ (15)	**-20.12775**
	CaC_2-III	$C2/m$ (12)	ThC_2	$C2/c$ (15)	**-20.12775**
	CaC_2-V	$Immm$ (71)	CaC_2-V	$Immm$ (71)	**-19.72012**
	CaC_2-VII	$R\bar{3}m$ (166)	CaC_2-VII	$R\bar{3}m$ (166)	-19.44838
	CaF_2	$Fm\bar{3}m$ (225)	CaF_2	$Fm\bar{3}m$ (225)	-14.21804
	CaI_2	$P\bar{3}m1$ (164)		$P6/mmm$ (191)	-15.88645
	$CdCl_2$	$R\bar{3}m$ (166)		$Fm\bar{3}m$ (225)	-14.21804
	Co_2Si	$Pnma$(62)	Co_2Si	$Pnma$ (62)	**-20.05729**
	Cu_2Mg	Fd-$3m$(227)	Cu_2Mg	Fd-$3m$ (227)	-14.21804
	Cu_2S	$Fd\bar{3}m$ (227)	Cu_2S	$Fd\bar{3}m$ (227)	-14.21804
	$CuZr_2$	$I4/mmm$ (139)	CaC_2(rt)	$I4/mmm$ (139)	**-20.04876**
	FeS_2	$Pa\bar{3}$ (205)	FeS_2	$Pa\bar{3}$ (205)	-19.42560
	Ga_2Sr	$P6/mmm$ (191)	Ga_2Sr	$P6/mmm$ (191)	-15.88645
	La_2Sb	$I4/mmm$ (139)	CaC_2(rt)	$I4/mmm$(139)	**-20.04876**
	MgC_2	$P4_2/mnm$ (136)	MgC_2	$P4_2/mnm$ (136)	**-19.95962**
	$PbCl_2$	$Pnam$ (62)		$Cmcm$ (63)	-14.28985
	$PbClF$	$P4/nmm$ (129)	$PbClF$	$P4/nmm$ (129)	-14.18913
	SiS_2	$I\bar{4}2d$ (122)	SiS_2	$I\bar{4}2d$ (122)	-16.762
	$SiSr_2$	$I4_1/amd$(141)	$SiSr_2$	$I4_1/amd$(141)	-19.18037
	ThC_2	$C2/c$(15)	ThC_2	$C2/c$(15)	**-20.12774**
	TiO_2(rutile)	$P4_2/mnm$ (136)	MgC_2	$P4_2/mnm$ (136)	**-19.95962**
	TiO_2(badd)	$P2_1/c$ (14)	ThC_2	$Cmmm$(65)	-16.88778
	$ZnCl_2$	$Pna2_1$ (33)		$Fm\bar{3}m$ (225)	-14.21804
	ZrO_2(badd)	$P2_1/c$ (14)	ThC_2	$C2/c$(15)	**-20.12774**

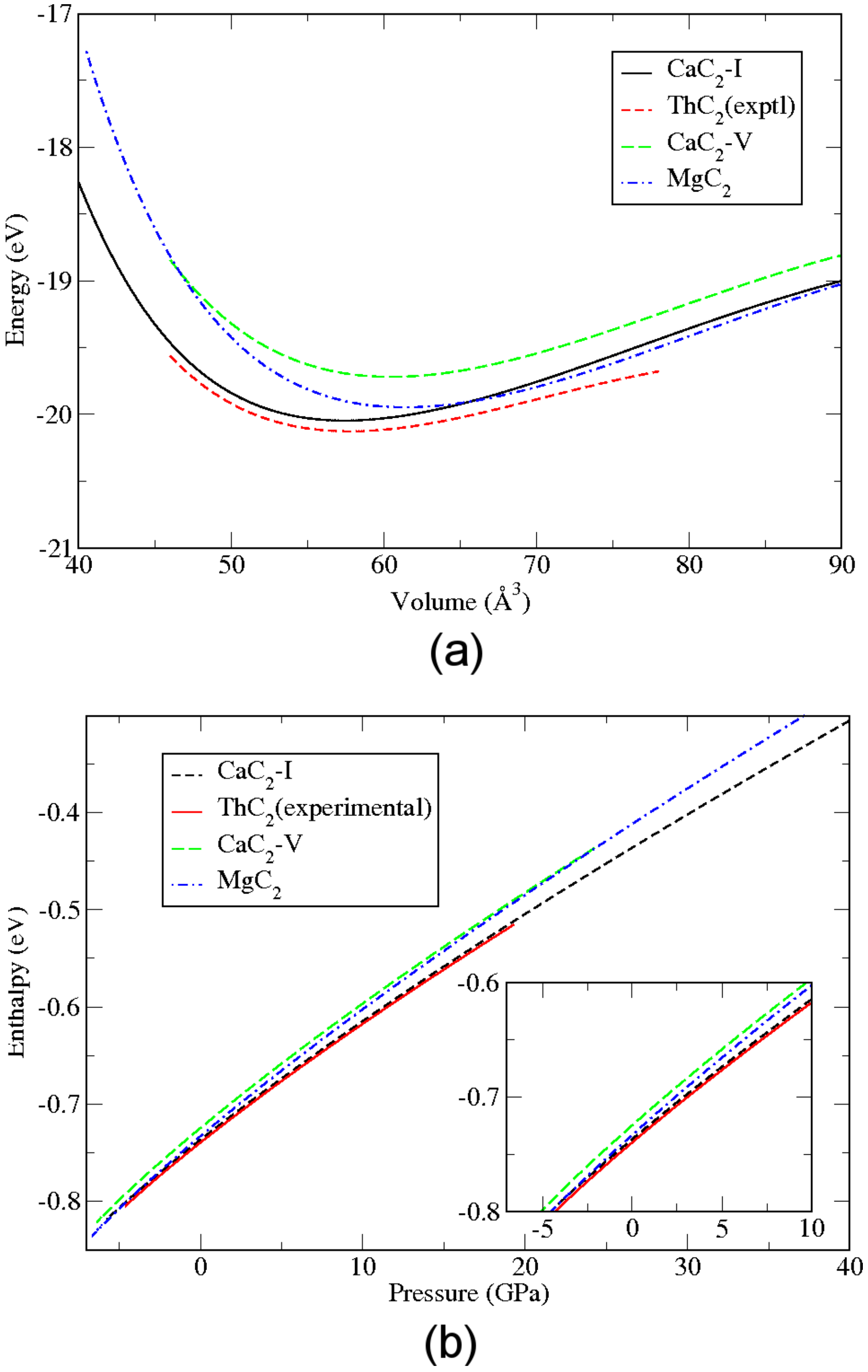

Figure 8.5: (a) E(V) and (b) H(p)-curves for the important structures of BaN_2 at PBE level. Energies per formula unit are represented in eV.

Table 8.5: The statistics of the most relevant modifications during the global optimization at various pressures.

name of the system	Structure type	space group	number of times found (at pressure in GPa)				
			0	16	32	48	64
CaN_2	"CaC_2-I"	*I4/mmm* (139)	12	6	1	1	0
	"CaC_2-V"	*Immm* (71)	4	2	1	0	0
	other modifications [a]		14	4	7	5	0
	successful runs		30	12	9	6	0
	Total runs		132	25	29	26	0
LaN_2	"CaC_2-I"	*I4/mmm* (139)	9	3	1	1	0
	"MgC_2"	*P42/mnm* (136)	13	5	0	0	0
	"ThC_2"	*C2/c* (15)	3	1	0	0	0
	"CaC_2-III"	*C2/m* (12)	4	2	2	0	0
	other modifications [a]		22	1	5	14	10
	successful runs		51	12	8	15	10
	Total runs		160	31	21	41	31
TiN_2	"CaC_2-I"	*I4/mmm* (139)	2	0	0	0	0
	"TiN_2-I"	*Pm2₁* (31)	15	4	1	1	0
	"CaC_2-V"	*Immm* (71)	2	0	0	0	0
	"ThC_2"	*C2/c* (15)	5	0	0	0	0
	"CaC_2-III"	*C2/m* (12)	4	0	2	0	0
	other modifications [a]		20	8	9	4	0
	successful runs		48	12	12	5	0
	Total runs		154	25	25	26	0

[a] With irregular polyhedra and higher in energies.

Table 8.6: Optimization of crystal structures taken from ICSD for CaN_2 with AB_2 structure type on the PBE level. The lowest energies are displayed by boldfaces.

name	Structure before optimization		Structure after optimization		energy(eV)
of compd	Structure type	space group	Structure type	space group	
CaN_2	Al_2Cu	$I4/mcm$ (140)	Al_2Cu	$I4/mcm$(140)	-19.51051
	AlB_2	$P6/mmm$ (191)	AlB_2	$P6/mmm$(191)	-16.77081
	CaC_2-I	$I4/mmm$ (139)	CaC_2(rt)	$I4/mmm$(139)	**-20.12208**
	CaC_2-II	$C2/c$ (15)	ThC_2	$C2/c$(15)	**-20.11887**
	CaC_2-III	$C2/m$ (12)	CaC_2-III	$C2/m$(12)	**-20.05048**
	CaC_2-V	$Immm$ (71)	CaC_2-V	$Immm$(71)	**-19.93767**
	CaC_2-VII	$R\bar{3}m$ (166)	CaC_2-VII	$R\bar{3}m$ (166)	-19.44461
	CaF_2	$Fm\bar{3}m$ (225)	CaF_2	$Fm\bar{3}m$ (225)	-14.44418
	CaI_2	$P\bar{3}m1$ (164)	CaI_2	$P\bar{3}m1$ (164)	-16.85026
	$CdCl_2$	$R\bar{3}m$ (166)	CaC_2-VII	$R\bar{3}m$ (166)	-14.69461
	Co_2Si	$Pnma$(62)	CaC_2(rt)	$I4/mmm$(139)	**-20.12208**
	Cu_2Mg	$Fd\bar{3}m$ (227)	Cu_2Mg	$Fd\bar{3}m$(227)	-14.86347
	CuNCN	$R\bar{3}m$(166)		$P6_3/mmc$(194)	-19.62057
	Cu_2S	$Fd\bar{3}m$ (227)	Cu_2S	$Fd\bar{3}m$ (227)	-14.87344
	$CuZr_2$	$I4/mmm$ (139)	CaC_2(rt)	$I4/mmm$(139)	**-20.12208**
	FeS_2	$Pa\bar{3}$ (205)	FeS_2	$Pa\bar{3}$ (205)	-19.65973
	Ga_2Sr	$P6/mmm$ (191)	Ga_2Sr	$P6/mmm$ (191)	-16.77081
	La_2Sb	$I4/mmm$ (139)	CaC_2(rt)	$I4/mmm$(139)	**-20.12208**
	MgC_2	$P4_2/mnm$ (136)	MgC_2	$P4_2/mnm$ (136)	**-19.98375**
	NbS_2	$P6_3/mmc$ (194)		$P6_3/mmc$ (194)	-19.62057
	$PbCl_2$	$Pnam$ (62)	$PbCl_2$	$Pnam$ (62)	-17.70491
	PbClF	$P4/nmm$ (129)	PbClF	$P4/nmm$ (129)	-15.09714
	SiS_2	$I\bar{4}2d$ (122)	SiS_2	$I\bar{4}2d$ (122)	-17.1235
	$SiSr_2$	$I4_1/amd$(141)	$SiSr_2$	$I4_1/amd$(141)	-19.26138
	ThC_2	$C2/c$(15)	ThC_2	$C2/c$(15)	**-20.11887**
	TiO_2(rutile)	$P4_2/mnm$ (136)	MgC_2	$P4_2/mnm$ (136)	**-19.98375**
	TiO_2(badd)	$P2_1/c$ (14)	ThC_2	$C2/c$(15)	**-20.11887**
	$ZnCl_2$	$Pna21$ (33)		$P6_3/mmc$ (194)	-19.62057
	ZrO_2(badd)	$P2_1/c$ (14)	ZrO_2(badd)	$C2/c$ (15)	**-20.11887**

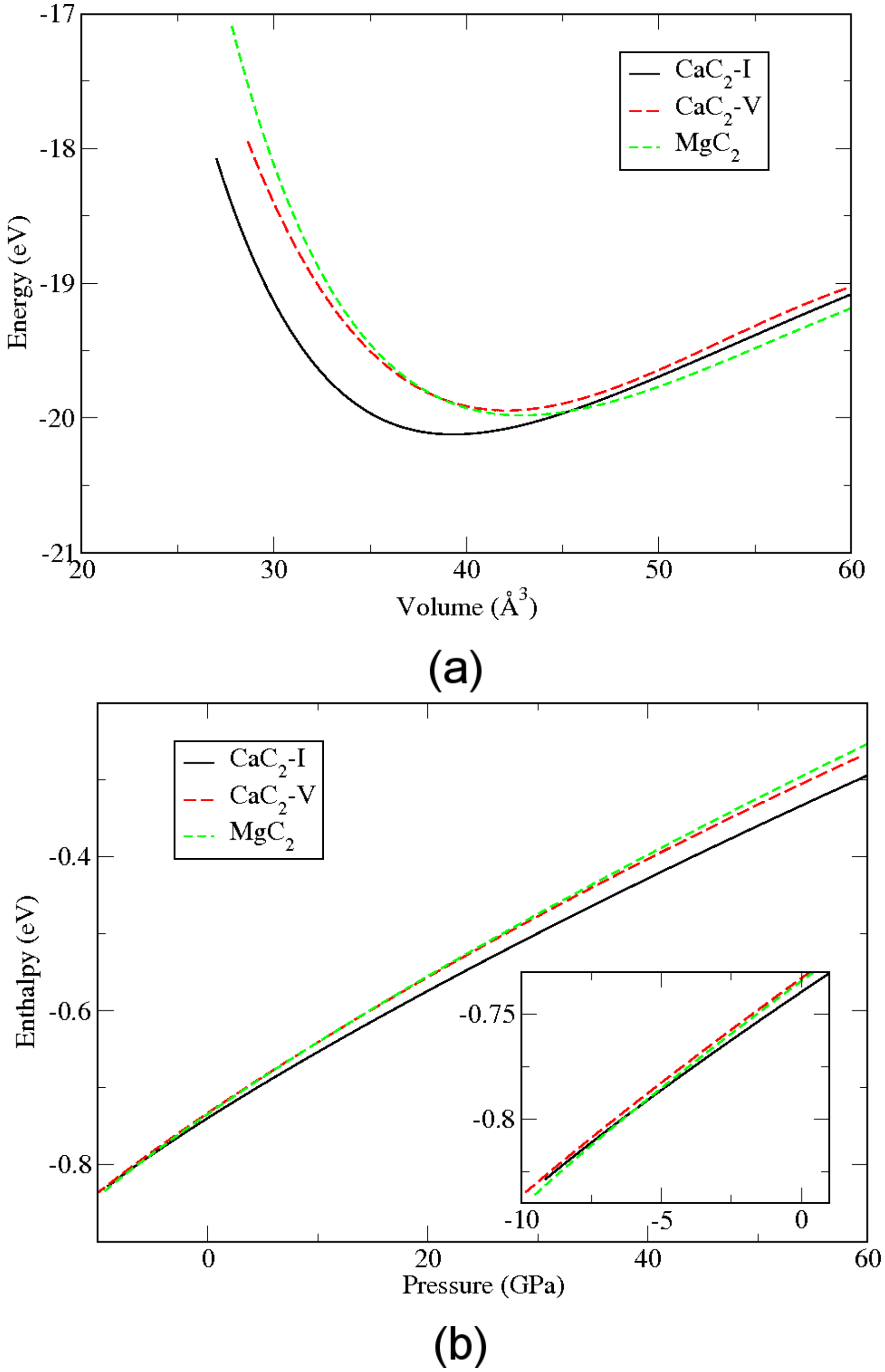

Figure 8.6: (a) E(V) and (b) H(p)-curves for the important structures of CaN_2 at PBE level. Energies per formula unit are represented in eV.

Table 8.7: Energetically most stable structures in CaN_2 and some more structures which are derived from well-known structure types on the PBE level.

modification and space group	lattice parameters(in Å) and fractionals	N-N distance (in Å)	energy (eV) per formula unit(PBE)	volume (in Å^3)
"CaC_2-I" configuration	a= 3.62, c= 6.01	1.258	-20.12208	39.41
I4/mmm (139)	La(0, 0, 0)			
	N(0, 0, 0.395)			
"CaC_2-V" configuration	a= 4.93, b= 4.62	1.263	-19.93767	42.22
Immm (71)	c= 3.70,			
	La(0, 0, 0),			
	N(1/2, 0.864, 0)			
"MgC_2" configuration	a= 4.191, c= 4.88	1.242	-19.98375	42.86
P42/mnm (136)	La(0, 0, 0)			
	N(0.395, 0.395, 0)			

by N_2 units. The other five structures found are considerably higher in energy and exhibit distorted $La(N_2)_{6-8}$ coordination polyhedra.

Furthermore, we performed 124 global optimization runs at various pressures, viz. 16, 32, 48, and 64 GPa (c.f. Table 8.5). We observed that several of the low pressure structures also exist at high pressures. In particular, the CaC_2-I type modification appears to be metastable up to high pressures. Finally, we selected a number of $A(B_2)$ type structures from our earlier landscape studies of the CaC_2-system (349) and from the ICSD-database for local minimizations. After local optimization of all the structures found, the total energies displayed in Table 8.9 were computed. The computed bond length of the N_2 units varied from 1.291 Å to 1.343 Å over the predicted modifications. We performed these calculations using PBE and PW91-functionals.

For all relevant modifications, the $E(V)$ and $H(p)$-curves computed by DFT with the PBE-functional are depicted in Fig. 8.7. Close to standard pressure, the thermodynamically stable candidates are the MgC_2 and the ThC_2 modification. The MgC_2-type structure is more favorable in the negative pressure range whereas the ThC_2 type is stable at slightly positive pressures. Since experience has shown that the actual transition pressures between two modifications can vary by several gigapascal depending on the computational method employed, it is not possible to definitely assign one of these two structures as the one present at ambient conditions.

Table 8.8: Energetically most stable structures in LaN_2 and some more structures which are derived from well-known structure types on the PBE level.

modification and space group	lattice parameters(in Å) and fractionals	N-N distance (in Å)	energy (eV) per formula unit(PBE)	volume (in $Å^3$)
"CaC_2-I" configuration *I4/mmm* (139)	a= 3.75 , c= 6.23 La(0, 0, 0) N(0, 0, 0.395)	1.314	-24.15885	43.72
"ThC_2" configuration *C2/C* (15)	a= 6.75 , b= 4.14, c= 6.53, β= 103.4° La(0, 0.785, 1/4), N(0.199, 0.632, 0.947)	1.299	-24.32581	44.44
"MgC_2" configuration *P42/mnm* (136)	a=b=4.29, c= 5.11 La(0, 0, 0), N(0.894, 0.894, 1/2)	1.291	-24.33338	47.07
"CaC_2-V" configuration *Immm* (71)	a= 5.12, b= 4.02 c= 4.56, La(0, 0, 0), N(1/2, 0, 0.853)	1.343	-23.92080	46.89

Table 8.9: Optimization of crystal structures taken from ICSD for LaN_2 with AB_2 structure type on the PBE level. The lowest energies are displayed by boldfaces.

name of compd	Structure before optimization		Structure after optimization		energy(eV)
	Structure type	space group	Structure type	space group	
LaN_2	Al_2Cu	$I4/mcm$ (140)	Al_2Cu	$I4/mcm$(140)	-22.96325
	AlB_2	$P6/mmm$ (191)	AlB_2	$P6/mmm$(191)	-20.73669
	CaC_2-I	$I4/mmm$ (139)	CaC_2(rt)	$I4/mmm$(139)	**-24.15885**
	CaC_2-II	$C2/c$(15)	ThC_2	$C2/c$(15)	**-24.32581**
	CaC_2-III	$C2/m$(12)	CaC_2-III	$C2/m$(12)	**-24.15885**
	CaC_2-V	$Immm$(71)	CaC_2-V	$Immm$(71)	**-23.92080**
	CaC_2-VII	$R\bar{3}m$(166)	CaC_2-VII	$R\bar{3}m$(166)	-23.03919
	CaF_2	$Fm\bar{3}m$ (225)	CaF_2	$Fm\bar{3}m$ (225)	-20.5332
	CaI_2	$P\bar{3}m1$ (164)		$P6/mmm$ (191)	-20.95268
	$CdCl_2$	$R\bar{3}m$ (166)		$Fm\bar{3}m$ (225)	-20.5332
	Co_2Si	$Pnma$(62)	Co_2Si	$Pnma$(62)	-21.9826
	Cu_2Mg	$Fd\bar{3}m$ (227)	Cu_2Mg	$Fd\bar{3}m$ (227)	-18.57192
	Cu_2S	$Fd\bar{3}m$ (227)	Cu_2S	$Fd\bar{3}m$ (227)	-18.57191
	$CuSr_2$	$I4/mmm$(139)	CaC_2(rt)	$I4/mmm$(139)	**-24.15885**
	$CuZr_2$	$I4/mmm$ (139)	$CuZr_2$	$I4/mmm$ (139)	**-24.15885**
	FeS_2	$Pa\bar{3}$ (205)	FeS_2	$Pa\bar{3}$ (205)	-23.43642
	Ga_2Sr	$P6/mmm$ (191)	Ga_2Sr	$P6/mmm$ (191)	-20.95268
	HgI_2	$P4_2/nmc$ (137)		$P4/mmm$ (123)	-21.59069
	La_2Sb	$I4/mmm$ (139)	CaC_2(rt)	$I4/mmm$(139)	**-24.15885**
	MgC_2	$P4_2/mnm$ (136)	MgC_2	$P4_2/mnm$ (136)	**-24.33338**
	NbS_2	$P6_3/mmc$ (194)	NbS_2	$P6_3/mmc$ (194)	-22.75316
	$PbCl_2$	$Pnam$ (62)		$Cmcm$ (63)	-23.97604
	PbClF	$P4/nmm$ (129)	PbClF	$P4/nmm$ (129)	-20.66454
	SiS_2	$I\bar{4}2d$ (122)	SiS_2	$I\bar{4}2d$ (122)	-18.66506
	$SiSr_2$	$I4_1/amd$(141)	$SiSr_2$	$I4_1/amd$(141)	-21.84387
	TiO_2(badd)	$P2_1/c$ (14)	ThC_2	$C2/c$(15)	**-24.32581**
	TiO_2(rutile)	$P4_2/mnm$ (136)	MgC_2	$P4_2/mnm$ (136)	**-24.33338**
	$ZnCl_2$	$Pna21$ (33)		$Pmna$ (62)	-19.35462
	ZrO_2(badd)	$P2_1/c$ (14)	ThC_2	$C2/c$(15)	**-24.32581**

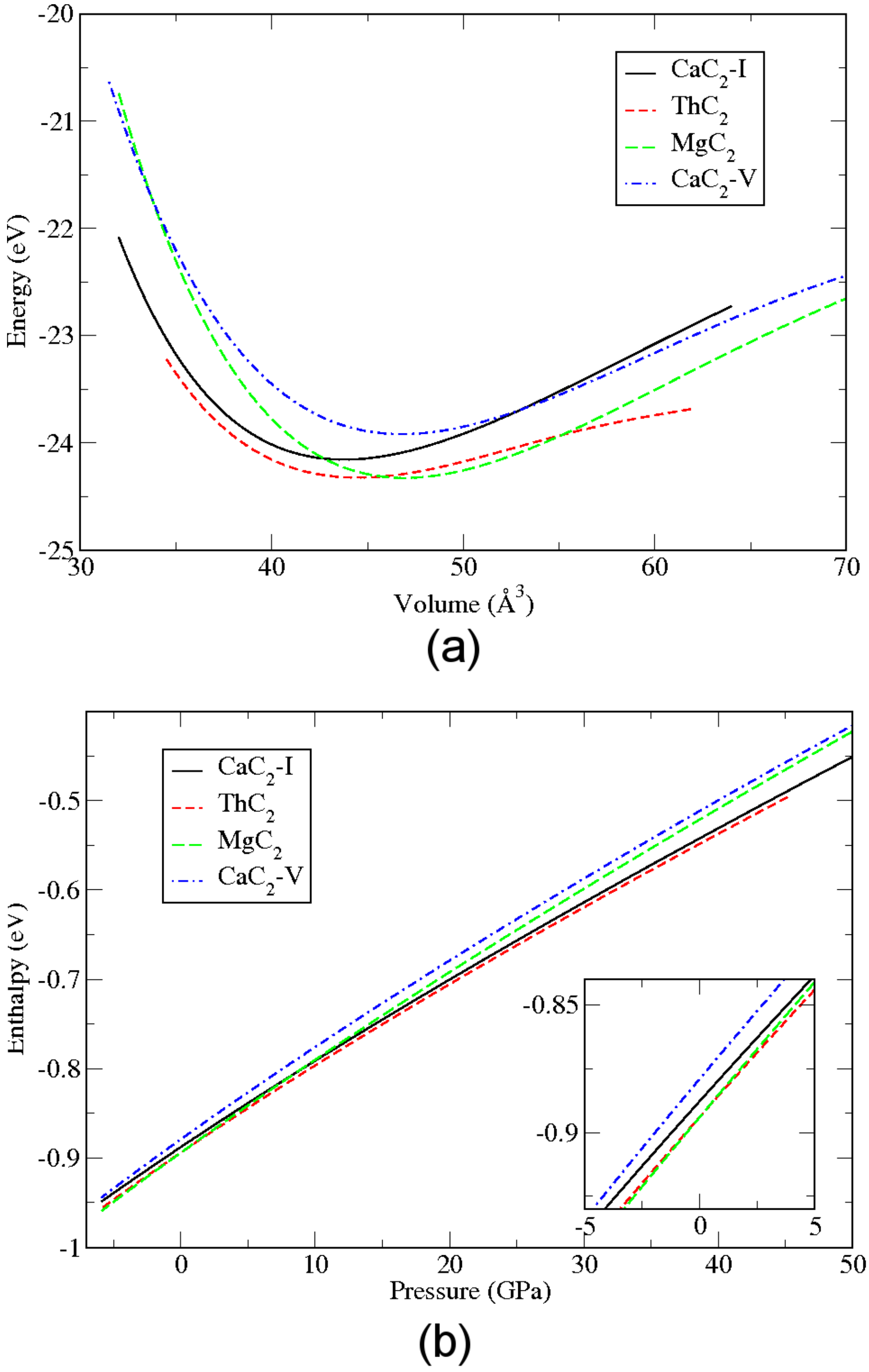

Figure 8.7: (a) E(V) and (b) H(p)-curves for the important structures of LaN_2 at PBE level. Energies per formula unit are represented in eV.

8.3.5 TiN_2

Titanium is present in various oxidation states e.g., +2, +3, and +4 in ionic compounds. Usually, titanium reacts with nitrogen to form titanium nitride with composition TiN at standard conditions, crystallizing in the rock-salt type crystal structure. Though TiN is a strong contender in the Ti/N-chemical system, nitrogen rich phases such as Ti_3N_4 (350) or TiN_2 might be capable of existence, respectively, at least as a metastable phase. Here, our aim is to study the potential existence of titanium pernitride TiN_2. We performed 154 simulated annealing runs in order to explore the energy landscape of TiN_2 at standard pressure. Four promising modifications were found as an outcome of the global searches, which includes the CaC_2-I, TiN_2-I (related to the $CdCl_2$ structure), MgC_2-, and CaC_2-V structure (see Fig. 8.1(a), Fig. 8.8, Fig. 8.2(a), and Fig. 8.2(b)), respectively. All the modifications show that N_2-dumbbells were formed that are surrounded by a Ti octahedron, except for the case of TiN_2-I. In the TiN_2-I modification, the N_2-unit sits inside a distorted square-pyramid formed by Ti cations. The bond length of N_2 varies from 1.26Å to 1.46 Å for all the (meta)stable modifications. Of these modifications, TiN_2-I and CaC_2-V were the ones with the lowest energy (c.f. Table 8.10 and 8.11). By again performing local minimizations of standard structure types taken from the ICSD-database and our earlier searches on AB_2-systems (349), we identified one further possible metastable modification, the MgC_2-type. We also performed global searches at high pressures (16, 32, and 48 GPa), which yielded mostly the TiN_2-I modification. After the local optimizations, the $E(V)$- and $H(p)$- curves for all relevant structures were plotted for two different functionals viz. PW91 and PBE (see Fig. 8.10). With this we see that, TiN_2-I is the thermodynamically stable structure at standard and slightly elevated pressure. At 14 GPa, the TiN_2-I-modification transforms into the CaC_2-V structure type. Again, we observe that with an increase in pressure, the system goes from lower coordination (see Fig. 8.3) of the N_2-unit to a higher one (301) (see Fig. 7.2(b)) similar as to the CaC_2 system (see chapter 7) (349).

8.4 Discussion

8.4.1 Information gained from local optimizations of structure candidates derived from known AX_2-structure types

In the literature, there are a large number of quasi-ionic AX_2 types of structures with X_2 existing as a dumbbell (and not as isolated atoms). So, it is interesting to examine whether the existing AX_2 structure types correspond to local minima on the energy landscape of AN_2 types of systems. Several such systems were studied by exchanging the cation with Ca, Sr, Ba, La, and Ti atoms, and the anionic units X_2 with N_2 dumbbells. We optimized these modified structures. During the local optimization, the structure was optimized with a full unconstrained relaxation. The results are presented in tables 8.2, 8.4, 8.6, 8.9, and 8.11.

We observed a common feature in all pernitride systems: the locally optimized structures derived from CaC_2-II, CaC_2-III, and ZrO_2 (badd) transform into the monoclinic structure type ThC_2. Several common AB_2 structures with isolated B-atoms were also included in our study for comparison. The structures taken from the $CuZr_2$-

Table 8.10: Energetically most stable structures in TiN_2 and some more structures which are derived from well-known structure types on the PBE level.

modification and space group	lattice parameters(in Å) and fractionals	N-N distance (in Å)	energy (eV) per formula unit(PBE)	volume (in Å^3)
"CaC_2-I" configuration $I4/mmm$ (139)	a= 2.85, c= 9.05 La(0, 0, 0), N(0, 0, 0.581)	1.460	-25.47611	36.65
"TiN_2-I" configuration $Pm2_1$ (31)	a=b= 3.62, c= 6.02 La(0, 0, 0), N(1/2, 1/2, 0.105)	1.258	-26.28087	34.05
"CaC_2-V" configuration $Immm$ (71)	a= 4.37, b= 4.16 c= 3.12 , La(0, 0, 0), N(1/2, 1/2, 0.105)	1.353	-25.88455	28.34
"MgC_2" configuration $P4_2/mnm$ (136)	a=b=3.75, c= 4.16 La(0, 0, 0), N(0.874, 0.874, 1/2)	1.333	-25.19346	29.32

Table 8.11: Optimization of crystal structures taken from ICSD for TiN_2 with AB_2 structure type on the PBE level. The lowest energies are displayed by boldfaces.

name of compd	Structure before optimization: Structure type	Structure before optimization: space group	Structure after optimization: Structure type	Structure after optimization: space group	energy(eV)
TiN_2	AlB_2	$P6/mmm$ (191)	AlB_2	$P6/mmm$ (191)	-22.2919
	CaC_2-I	$I4/mmm$ (139)	CaC_2(rt)	$I4/mmm$(139)	**-25.47611**
	CaC_2-II	$C2/c$ (15)	CaC_2-II	$C2/c$ (15)	**-26.27021**
	CaC_2-III	$C2/m$ (12)	CaC_2-III	$C2/m$ (12)	**-26.50148**
	CaC_2-V	$I4/mmm$ (139)	CaC_2-V	$Immm$(71)	**-25.88455**
	CaC_2-VII	$R\bar{3}m$ (166)	CaC_2-VII	$R\bar{3}m$ (166)	-24.62764
	CaF_2	$Fm\bar{3}m$ (225)	CaF_2	$Fm\bar{3}m$ (225)	-24.1039
	CaI_2	$P\bar{3}m1$ (164)	CaI_2	$P\bar{3}m1$ (164)	-23.81788
	Cu_2Mg	$Fd\bar{3}m$ (227)	MgC_2	$Fd\bar{3}m$ (227)	-19.98679
	Cu_2S	$Fd\bar{3}m$ (227)	Cu_2S	$Fd\bar{3}m$ (227)	-19.98680
	$CuZr_2$	$I4/mmm$ (139)	CaC_2(rt)	$I4/mmm$(139)	**-25.47611**
	Ga_2Sr	$P6/mmm$ (191)	Ga_2Sr	$P6/mmm$ (191)	-22.29105
	MgC_2	$P4_2/mnm$ (136)	MgC_2	$P4_2/mnm$ (136)	**-25.19346**
	NbS_2	$P6_3/mmc$ (194)	NbS_2	$P6_3/mmc$ (194)	**-25.78936**
	$PbCl_2$	$Pnam$ (62)	$PbCl_2$	$Pnam$ (62)	**-26.20261**
	$PbClF$	$P4/nmm$ (129)	$PbClF_2$	$P4/nmm$ (129)	-25.37726
	SiS_2	$I\bar{4}2d$ (122)		$Fd\bar{3}m$ (227)	-23.13742
	ThC_2	$C2/c$(15)	ThC_2	$C2/c$(15)	**-26.27021**
	TiO_2(rutile)	$P4_2/mnm$ (136)	MgC_2	$P4_2/mnm$ (136)	**-25.19346**
	TiO_2(badd)	$P2_1/c$ (14)	ThC_2	$C2/c$(15)	**-26.27021**
	$ZnCl_2$	$Pna2_1$ (33)	Co_2Si	$Pnma$(62)	**-26.20261**
	ZrO_2(badd)	$P2_1/c$ (14)	ThC_2	$C2/c$(15)	**-26.27021**

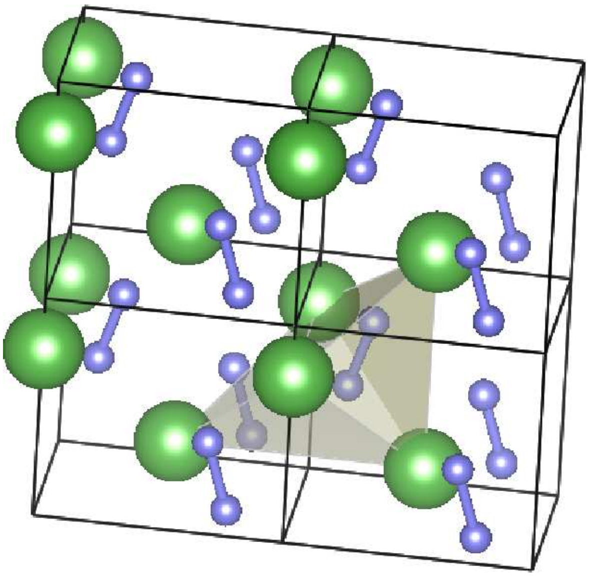

Figure 8.8: Predicted modifications for TiN_2. In the text, it is termed as TiN_2-I. Green (big) spheres correspond to titanium, blue (small) spheres to nitrogen atoms, respectively.

and La_2Sb-based modifications transform to the CaC_2-I type whereas TiO_2 (rutile) distorts into the MgC_2-type. As mentioned above, the ThC_2-type is the stable structure in the case of BaN_2 and LaN_2, and the CaC_2-I-type structure is lowest in energy in the case of SrN_2 and CaN_2. For SrN_2, BaN_2, and CaN_2, the MgC_2 and the CaC_2-V-type are metastable modifications. We also considered cubic and hexagonal structure types (pyrite, fluorite, hexagonal omega, chalcocite, Al_2Cu, and many more) for local optimization. These structures turned out to correspond to local minima which are quite high in energy.

8.4.2 Comparison among Metal Pernitrides

While comparing the SrN_2, BaN_2, CaN_2, LaN_2, and TiN_2 systems, we noted that the difference between energies of CaC_2-I, MgC_2, and CaC_2-V structure types is less compared to other structures for the SrN_2 and the CaN_2 system. From the energy-vs-volume and enthalpy-vs-pressure curves calculated using the PW91 and PBE functionals (see Fig. 8.3 and 8.4), it is likely that the CaC_2-V-type is the thermodynamically stable modification on PW91 level and the CaC_2-I type using the PBE functional. The experimentally known modification is CaC_2-I. Based on the enthalpies at zero temperature, the CaN_2 system stabilizes in the CaC_2-I structure type at ambient conditions and it transforms into the MgC_2 structure at negative pressure. In the BaN_2 system, we noted that the monoclinic structure, ThC_2 structure type, is thermodynamically stable and that the CaC_2-I, MgC_2, and CaC_2-V-types are metastable modifications

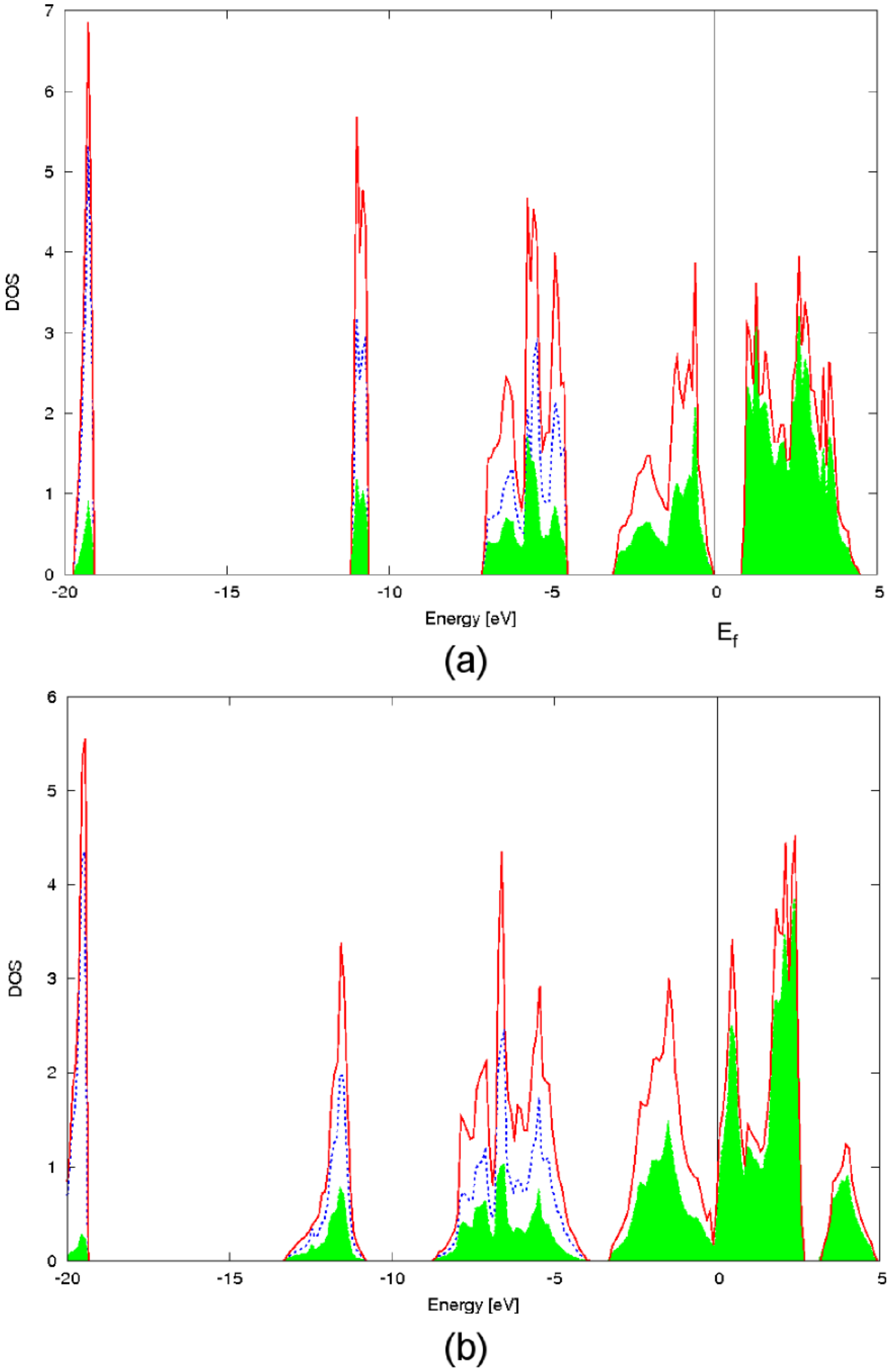

Figure 8.9: Density of states for TiN_2 at PBE level for (a)TiN_2-I and (b)CaC_2-V-modification. The total density of states is indicated by the red curve. And the contribution of the titanium atom is given as a shaded green area whereas nitrogen is displayed by the blue curve.

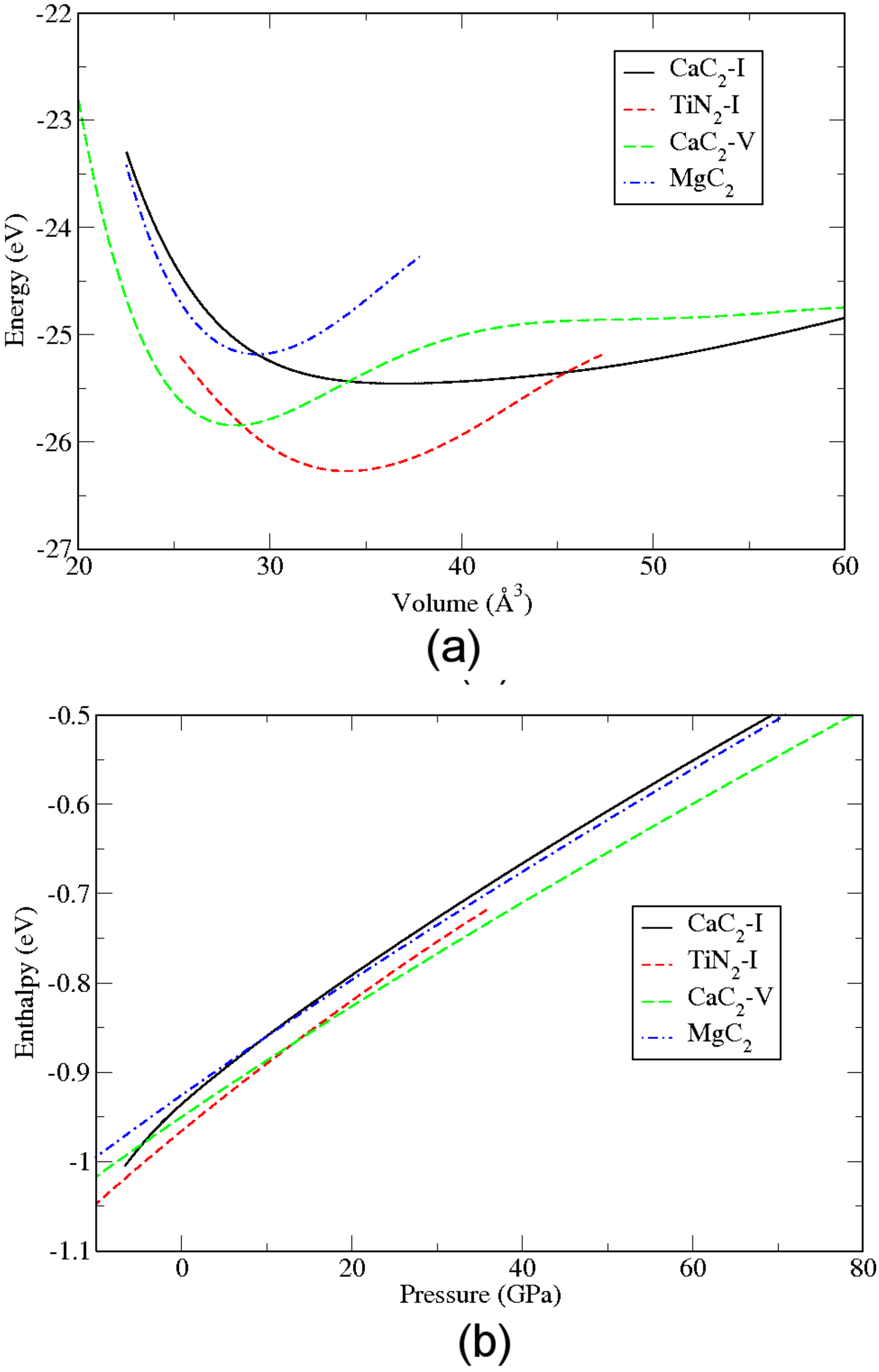

Figure 8.10: (a) E(V) and (b) H(p)-curves for the important structures of TiN_2 at PBE level. Energies per formula unit are represented in eV.

which are higher in energy. We computed the energy difference between the experimentally known structure ThC_2 and the tetragonal structure, CaC_2-I, 0.3 eV/atom using the PBE functional.

In LaN_2 (334), we observed that the structures seen in the global searches are among those published in a theoretical study in the literature, including the global minimum. LaN_2 should crystallize in the ThC_2 structure at ambient pressure, but at negative pressure, it transforms into the MgC_2-type. There exist also some metastable structures e.g., a CaC_2-I and a CaC_2-V type modification. In the case of the alkaline earth metals (Ca, Sr, and Ba) and the lanthanum pernitride system, we have seen one common feature, i.e., the ThC_2 and CaC_2-I structure types are derivatives of the rock-salt structure type: the center of each N_2 unit is surrounded by an elongated and distorted octahedron of cations and, conversely, the N_2 units form distorted octahedra around the cations. The main difference in these structures is the spatial orientation of the N_2 units. TiN_2 should crystallize in the TiN_2-I modification at standard conditions. At elevated pressure, it transforms into the CaC_2-V structure. In addition, there are two metastable modifications, the CaC_2-I and the MgC_2-type.

8.4.2.1 Bond length of the N_2-unit

We compared the bond length of N_2 units among the thermodynamically stable modifications for the five pernitride systems, which are in the range of 1.230 to 1.263 Å (c.f. Table 8.12), except for LaN_2. These bond lengths are much longer than the N-N triple bond and smaller than the N-N single bond. The length of an N-N double bond is 1.240 Å. For all systems, the bulk moduli of the various modifications have been calculated, and they are displayed in table 8.12. 65 and 46 GPa are the bulk modulus for SrN_2 and BaN_2, respectively, which is in good agreement with experimentally reported values. In LaN_2, the value of the bulk modulus of the ThC_2 and the MgC_2 modification is 89 and 126 GPa, respectively. The bulk modulus for the ThC_2 modification of the LaN_2 system is also comparable to published results from a theoretical study (334). In the case of the TiN_2 system, the bulk modulus of TiN_2-I and the high pressure modification CaC_2-V are 125 and 196 GPa, respectively. Finally, we performed a Bader charge analysis, which showed that the metal cation of the thermodynamically stable modifications should be assigned to the oxidation states +2 in all MN_2 systems, suggesting the claim that the N_2-dumbbell should exist as a N_2^{2-}-unit.

8.4.2.2 Trends of binding energies

As we mentioned in the introduction, all the experimentally known pernitride systems were synthesized at high pressure and high temperature. So, we were interested in the binding energies of these and/or newly predicted systems. They were computed as the difference between the total energy of the thermodynamically stable modification with the total energy of the pure metal and N_2 at zero pressure, and are displayed in table 8.13. We find a negative binding energy, which signifies that the compound is at least metastable and should not dissociate into the constituent elements at zero pressure. If we consider PdN_2, the existence of this system is only known in the range of 11 to 36 GPa (330). Thereafter, experimentally known pernitrides can exist at ambient conditions. For example, the binding energy is computed for CaN_2 in the CaC_2-I modification as -1.576 eV per formula unit, whereas for LaN_2 it is -2.733 eV

Table 8.12: Bulk modulus for various metal pernitrides on PBE and GGA level

name of compound	Structure type	N-N distance in Å	Bulk modulus in GPa		
			experimental	calculated	
				PBE	GGA
SrN_2	CaC_2-I	1.254	65 (334)	64	64
	MgC_2	1.238		75	76
	CaC_2-V	1.259		66	66
BaN_2	CaC_2-I	1.239		51	52
	ThC_2	1.230	46 (334)	47	47
	MgC_2	1.230		51	51
	CaC_2-V	1.247		50	51
CaN_2	CaC_2-I	1.258		82	81
	MgC_2	1.242		79	80
	CaC_2-V	1.263		89	89
LaN_2	CaC_2-I	1.314		115	113
	ThC_2	1.299	86[a]	87	87
	MgC_2	1.291		126	127
	CaC_2-V	1.343		115	116
TiN_2	CaC_2-I	1.460		26	26
	TiN_2-I	1.258		125	126
	CaC_2-V	1.353		196	221

[a] taken from the literature (334).

Table 8.13: Binding Energy in eV per formula unit on PBE level for MN_2 (where M = Sr, Ba, Ca, La, and Ti)

name of compound	Structure type	Binding Energy in eV per formula unit
CaN_2	CaC_2-I	-1.57623
	CaC_2-V	-1.39182
	MgC_2	-1.43790
SrN_2	CaC_2-I	-1.50679
	MgC_2	-1.35869
	CaC_2-V	-1.59177
BaN_2	CaC_2-I	-1.48129
	ThC_2	-1.56064
	MgC_2	-1.39214
	CaC_2-I	-1.17144
LaN_2	CaC_2-I	-2.56472
	ThC_2	-2.73344
	CaC_2-V	-2.73283
	MgC_2	-2.40917
TiN_2	TiN_2-I	-1.91137
	CaC_2-V	-1.51505
	CaC_2-I	-1.10661

per formula unit. In the TiN_2 system, the binding energy of the TiN_2-I modification lies in-between those of the CaN_2 and LaN_2 system. As CaN_2 has been synthesized at high pressure and temperature and the same has been suggested for LaN_2 (334), we propose that a possible way to synthesize TiN_2 may also be a high pressure - high temperature synthesis.

8.4.2.3 Electronic density of states for the TiN_2 modifications

In the literature, it is reported that SrN_2, BaN_2, CaN_2, and the proposed LaN_2 are metallic in nature. Thus, we have calculated the electronic density of states (DOS) for the TiN_2-I and the CaC_2-V-structure type for titanium pernitride. Fig. 8.9 shows that TiN_2-I has a bandgap of 0.8 eV and should be denoted as a semiconductor, whereas the CaC_2-V modification should be metallic. Apart from common features, e.g., such as the 2s states of N being filled (between -13 and -10 eV), the π bonding states of the $(N{=}N)^{2-}$ unit for TiN_2-I are located in the range from -7 to -5 eV, whereas for the CaC_2-V-type, they are found in the range from -9 to -4 eV. The contribution from the 3s orbital of Ti and the π^* states of the N_2-unit exist in the range of -3 to 0 eV in both modifications. Above the Fermi energy level, the density of states exhibits major contributions from the 3d orbital of the titanium atoms in both modifications. As we increase the pressure, TiN_2 transforms into the higher symmetry to the CaC_2-V modification, which is also responsible for the change in the electronic behavior from semiconducting to a metal.

8.5 Conclusions

We successfully performed a structure prediction study for MN_2 (M = Ca, La, and Ti) at different pressures using *ab-initio* energy calculations during both the global energy landscape exploration and the local optimization. In our study, SrN_2 and BaN_2 were also included for the comparison. To supplement the global search for new modifications, we also considered well-known AB_2-type modifications as a starting point for local optimizations. After proper replacement of anion and cation, we relaxed the structures and compared with structures obtained from global searches. In all systems, N_2 units are surrounded by the cations in an octahedral or distorted octahedral fashion, except for TiN_2-I, where N_2 is enclosed in a square pyramid formed by the titanium atoms. For CaN_2, the CaC_2-I and the MgC_2 modifications are stable at standard pressure and slightly negative pressure, respectively, and the same applies to SrN_2. For BaN_2 and LaN_2, the ThC_2 modification is stable. Finally, TiN_2 should transform from the TiN_2-I modification at standard pressure to the CaC_2-V modifications at high pressure. From a Bader charge analysis, we confirmed the existence of a N_2^{2-} unit in the thermodynamically stable modification in all three pernitride systems. With the exception of TiN_2 the pernitride systems investigated are metallic in nature; only the high-pressure phase of TiN_2 should be metallic. The binding energy of TiN_2 is slightly lower than the one of CaN_2, and we suggest that it may be synthesized at high pressure and temperature.

Part V

Summary

9

Summary

Nowadays, in theoretical solid-state chemistry one of the main aims is to develop and design a new methodology to predict the possible (meta)stable modifications of a chemical system especially at ambient and high pressure. This information is quite useful to plan the synthesis of new compounds, and to investigate their physical properties under standard and extreme conditions. It is also important for systems which have not-yet been synthesized, and those that are hard to synthesize because of the requirement of extremely high pressure or high temperature. In such situations, theory can give some assistance, by investigating the energy landscape of the chemical compound of interest at ambient and elevated pressure. And these exploration methods also give more insight about chemical systems which can have several stable or metastable modifications. And theory can help to determine the crystal structure of newly synthesized compounds and provide estimates about their stability.

The aim of this thesis is to develop energy landscape exploration methods that work efficiently on the *ab-initio* level, and to apply these techniques to explore the energy landscape of several chemical systems such as elemental solids and binary compounds. The starting point of our exploration is to use the fact that (meta)stable modifications of chemical compounds correspond to locally ergodic regions of the energy landscape. At low temperatures these regions are basins around local minima, and thus identifying these minima is the foundation of all structure prediction methods. Once these stuctures have been found, they are analyzed and their physical properties are computed.

The general exploration methodology can be split into two parts, the first part being the global search and the second one the local optimization. The global optimization method used in this work to determine structure candidates consists of simulated annealing runs and subsequent stochastic quenches, where the energy is computed using *ab-initio* methods. The CRYSTAL and the VASP programs were used for the energy calculations. As part of our work, we created an interface for our global optimization program (G42) to the VASP-code. Both VASP and CRYSTAL have certain advantages: VASP requires no optimization of basis sets, and each energy calculation is relatively fast. CRYSTAL can employ the Hartree-Fock approximation, which tends to yield faster convergence than DFT-based calculations. Since the efficiency of the global search is an important factor in the methodology, we reduced the simulation time by using less stringent parameters in the *ab-initio* calculations during the global optimization, such as a e.g., smaller k-point mesh, less diffuse basis set (in case of CRYSTAL), and higher tolerance of the Self Consistent Field (SCF) cycles than usually used for *ab-initio* calculations. After the global search, the symmetry and space group of the candidate was determined. Then, a local optimization was performed for this candidate on *ab-initio* level with strict simulation parameters, and again, the symmetry and space group are identified. The E(V) and H(p)-curves yielded the thermodynamical stability of the structure as function of pressure, and the transition pressures among the phases were determined. For estimating the kinetical stability, phonon calculations were performed. Finally, to understand the charge distribution of the system, Bader charge analyses (VASP) and Mulliken population analyses (CRYSTAL) were performed.

This methodology was successfully applied to various chemical systems viz., lithium, calcium carbide and the binary pernitrides MN_2 (M = Ca, La, and Ti). In the case of lithium, all experimentally known modifications (fcc, bcc, and hcp) at standard pressure were observed during the global explorations, except the 9R modification. The A15 structure was predicted as a new modification which is quite energetically competitive to the known modifications. Phonon calculations and relaxations after finite atoms displacements were performed in order to study the kinetical stability of the new structure. The results showed that the new predicted modification is quite stable and a good candidate for synthesis.

In the second project, global searches were performed for calcium carbide, which is a mixed covalent-ionic system. We found one experimentally known structure and several more which are closely related to known low-temperature modifications. Two newly predicted modifications are at least metastable at standard pressure: an orthorhombic structure, CaC_2-V, which is lowest in energy compared to all (experimentally and theoretically observed) modifications, and another monoclinic structure (CaC_2-VI), which is closely related to the experimentally known low-temperature modification CaC_2-II. A phase transition was predicted at about 30 GPa, with a transformation of the six-fold coordinated structure (CaC_2-VI) to an eight-fold coordinated one (CaC_2-VII), which is a variation of the CsCl structure type.

Finally, a global structure prediction study was performed for metal pernitride systems, MN_2 (M = Ca, La, and Ti) at various pressures. We also included SrN_2 and BaN_2 in our study, which had been synthesized some years ago, for comparison. In addition to global searches, we investigated, whether well-known AB_2-structure types also constitute local minima on the energy landscape. We noted that in all pernitride systems, the N_2 dumbbells are surrounded by the metal cations in an octahedral or distorted octahedral fashion. An exception is the TiN_2-I structure, where the N_2 units are enclosed in square-pyramids formed by the cations. In the CaN_2 and SrN_2 system, the CaC_2-I and MgC_2 modifications are thermodynamically stable at standard pressure and slightly negative pressure, respectively. The ThC_2 structure type is stable for BaN_2 and LaN_2. TiN_2 should transform from the TiN_2-I modification at standard pressure to the CaC_2-V structure type at 20 GPa. The pernitride systems are metallic in nature except TiN_2, which shows metallic behavior only at increased pressure in the CaC_2-V-modification. The existence of a N_2^{-2} unit in all thermodynamically stable modifications was confirmed using Bader charge analysis. TiN_2 may be a promising candidate for synthesis at high pressure and temperature as the binding energy of TiN_2 is slightly lower than the one of CaN_2, and CaN_2 has recently been synthesized at such thermodynamic conditions.

In conclusion, we successfully explored the energy landscape for lithium, calcium carbide, and metal pernitride systems at standard and high pressure conditions. We predicted new modifications for all systems. Recently, CaC_2-VII, the predicted high-pressure crystal structure for calcium carbide was found in the BaC_2 system.

References

[1] M. Jansen. Syntheseplanung in der Festkörperchemie Presentation at the 30th anniversary of the Fonds der Chemie. 3

[2] J. Maddox. *Nature*, **335**:201–201, 1988. 3

[3] M. L. Cohen. *Nature*, **338**:291–292, 1989. 3

[4] F. C. Hawthorne. *Nature*, **345**:297–297, 1990. 3

[5] C. R. A. Catlow and G. D. Price. *Nature*, **347**:243–248, 1990. 3

[6] J. C. Schön and M. Jansen. *Angew. Chem. Int. Ed. Eng.*, **35**:1286–1304, 1996. 3, 4, 9, 12, 17

[7] J. C. Schön and M. Jansen. *Angew. Chem. Int. Ed. Eng.*, **35**:1286–1304, 1996. 3, 9, 43

[8] J. C. Schön and M. Jansen. *Z. Krist.*, **216**:307–325, 2001. 3, 9, 10, 14

[9] J. C. Schön and M. Jansen. *Z. Krist.*, **216**:361–383, 2001. 3, 9, 10, 14

[10] M. Jansen. *Abh. Rhein. Westf. Akad. Wiss.*, **N420**:7–35, 1996. 3

[11] M. Jansen. *Angew. Chem. Int. Ed.*, **41**(20):3746–3766, 2002. 3, 4, 9, 17

[12] O. M. Yaghi, M. O'Keeffe, and M. Kanatzidis. *J. Solid. State. Chem.*, **152**:1–2, 2000. 3

[13] M. O'Keeffe, M. Eddaoudi, H. L. Li, T. Reineke, and O. M. Yaghi. *J. Solid. State. Chem.*, **152**:3–20, 2000. 3

[14] M. Jansen. *Angew. Chem.*, **114**:3896, 2002. 3

[15] Z.X. Shen, C.W. Ong, S.H. Tang, and M.H. Kuok. *J. Phys. Chem. Solids*, **55**(8):665 – 669, 1994. 3

[16] I. Kiyoshi. *J. Vac. Sci. Technil. A*, **7**(2):256–258, 1989. 4

[17] T. Jung and A. Westphal. *Mat. Sci. Eng: A*, **140**:528 – 533, 1991. 4

[18] D. Fischer and M. Jansen. *Angew. Chem. Int. ed.*, **41**:1755–1756, 2002. 4

[19] D. Fischer and M. Jansen. *J. Am. Chem. Soc.*, **124**:3488, 2002. 4

[20] V. A. Shchukin and D. Bimberg. *Rev. Mod. Phys.*, **71**:1125–1171, 1999. 4

[21] R. C. Jaeger. *"Film Deposition". Introduction to Microelectronic Fabrication.* Prentice Hall, Upper Saddle River, NJ, USA, 2002. 4

[22] J. Stangl, V. Holý, and G. Bauer. *Rev. Mod. Phys.*, **76**:725–783, 2004. 4

[23] P. W. McCray. *Nat. Nano*, **2**:259 – 261, 2011. 4

[24] D. Fischer and M. Jansen. *Z. Anorg. Allg. Chem.*, **629**:1934, 2003. 4

[25] D. Fischer, Ž. Čančarević, J. C. Schön, and M. Jansen. *Z. Allgem. Anorg. Chem.*, **630**:156–160, 2004. 4

[26] L. Liu and W. A. Bassett. *Elements, Oxides and Silicates. High-Pressure Phases with Implications for the Earth's Interior.* Oxford Univ. Press, New York, 1986. 4

[27] L. Stixrude, R. E. Cohen, and R. J. Hemley. **Theory of minerals at high pressures**. In R.J. Hemley, editor, *MSA Reviews in Mineralogy; Ultrahigh-Pressure Mineralogy*, **37**, pages 639–671. Mineralogical Society of America, Washington, D.C., 1998. 4

[28] M. T. Yin and M. L. Cohen. *Phys. Rev.Lett.*, **50**:2006–2009, 1983. 4

[29] M. L. Cohen. *Int. J. Quantum Chem.*, **29**:883–854, 1986. 4

[30] R. E. Cohen. *Geophys. Res. Lett.*, **14**:37–40, 1987. 4

[31] H. Cynn, D. G. Isaak, R. E. Cohen, M. F. Nicol, and O. L. Anderson. *Amer. Mineral.*, **75**:439–442, 1990. 4

[32] M. L. Cohen, Z. Reut, L. J. Sham, P. B. Allen, N. W. Ashcroft, and V. Heine. *Phil. Trans. Roy. Soc. London A*, **334**:501–513, 1991. 4

[33] R. E. Cohen. **First-Principles Predictions of Elasticity and Phase Transitions in High Pressure SiO_2 and Geophysical Implications.** In M.H. Manghnani and Y. Syono, editors, *High Pressure Research in Mineral Physics: Application to Earth and Planetary Science*, pages 425–432. AGU, Washington, D.C., 1992. 4

[34] F. C. Marton and R. E. Cohen. *Amer. Mineral.*, **79**:789–792, 1994. 4

[35] K. T. Thomson, R. M. Wentzcovitch, and M. S. T. Bukowinski. *Amer. Mineral.*, **79**:789–792, 1994. 4

[36] B. Winkler, C. J. Pickard, V. Milman, W. E. Klee, and G. Thimm. *Chem. Phys. Lett.*, **312**:536–541, 1999. 4

[37] J. C. Schön, M. A. C. Wevers, and M. Jansen. *Solid State Sci.*, **2**:449–456, 2000. 4

[38] J. C. Schön, M. A. C. Wevers, and M. Jansen. *J. Mater. Chem.*, **11**:69–77, 2001. 4

[39] B. Winkler, C. J. Pickard, V. Milman, and G. Thimm. *Chem. Phys. Lett.*, **337**:36–42, 2001. 4

[40] Ž. Čančarević, J. C. Schön, and M. Jansen. *Z. Anorg. Allgem. Chem.*, **631**:1167–1171, 2005. 4

[41] J. C. Schön and M. Jansen. *Z. Krist.*, **216**:307–325;361–383, 2001. 4, 9, 10, 60

[42] S. M. Woodley, P. D. Battle, J. D. Gale, and C. R. A. Catlow. *Phys. Chem. Chem. Phys.*, **1**:2535–2542, 1999. 4

[43] C. Mellot-Draznieks, J. M. Newsam, A. M. Gorman, C. M. Freeman, and G. Ferey. *Angew. Chem. Int. Ed. Eng.*, **39**:2270–2275, 2000. 4

[44] S. Kirkpatrick, C. D. Gelatt Jr., and M. P. Vecchi. *Science*, **220**:671–680, 1983. 4, 15, 17, 44

[45] V. Czerny. *J. Optim. Theory Appl.*, **45**(1):41 – 51, 1985. 4, 15, 17, 44

[46] J. Pannetier, J. Bassas-Alsina, J. Rodriguez-Carvajal, and V. Caignart. *Nature(London)*, **346**(1):343–345, 1990. 4

[47] J. C. Schön and M. Jansen. *Comp. Mater. Sci.*, **4**:43–58, 1995. 4, 5

[48] J. H. Holland. *Adaptation in Natural and Artificial Systems.* Univ. Mich. Press, Ann Arbor, 1975. 4, 19

[49] R. L. Johnston, editor. *Applications of Evolutionary Computation in Chemistry.* Springer, Berlin, Heidelberg, 2004. 4

[50] A. R. Oganov, C. W. Glass, and S. Ono. *Earth Planet. Sci. Lett.*, **241**:95–103, 2006. 4, 5

[51] S. M. Woodley. *Phys. Chem. Chem. Phys.*, **9**:1070–1077, 2007. 4

[52] A. Nayeem, J. Vila, and H. A. Scheraga. *J. Comput. Chem.*, **12**(5):594–605, 1991. 4

[53] D. J. Wales and J. P. K. Doye. *J. Phys. Chem.*, **101**:5111–5116, 1997. 4, 18

[54] J. C. Schön, H. Putz, and M. Jansen. *J. Phys.: Cond. Matt.*, **8**:143–156, 1996. 4, 12, 19, 20

[55] A. Laio and M. Parrinello. *Proc. Natl. Aca. Sci. U. S. A.*, **99**:12562–12566, 2002. 4

[56] R. Martonak, A. Laio, and M. Parrinello. *Phys. Rev. Lett.*, **90**:075503–075506, 2003. 4

[57] J. Kennedy and R.Eberhart. *Proceedings of IEEE International Conference on Neural Networks IV*, pages 1942 – 1948, 1995. 4, 15

[58] Z. J. Feng, C. Dong, R. R. Jia, X. D. Deng, S. X. Cao, and J. C. Zhang. *J. Appl. Crystallogr.*, **42**:1189–1193, 2009. 4

[59] J. Liu, L. Wang, L. He, and F. Shi. *Analysis of Toy Model for Protein Folding Based on Particle Swarm Optimization Algorithm.* Springer, Berlin, Heidelberg, 2005. 4

[60] J. Lv, Y. Wang, L. Zhu, and Y. Ma. *Phys. Rev. Lett.*, **106**:015503, 2011. 4, 58

[61] C. J. Pickard and R. J. Needs. *Phys. Rev. Lett.*, **97**:045504, 2006. 4

[62] J. C. Schön, K. Doll, and M. Jansen. *Phys. Status Solidi B*, **247**(1):23–39, 2010. 4

[63] K. Doll, J. C. Schön, and M. Jansen. *Phys. Chem. Chem. Phys.*, **9**:6128–6133, 2007. 5

[64] Ž. Čančarević, J. C. Schön, and M. Jansen. *Chem. Asian J.*, **3**:561–572, 2008. 5

[65] K. Doll, J. C. Schön, and M. Jansen. *Phys. Rev. B*, **3**:144110, 2008. 5, 69, 71

[66] K. Doll, J. C. Schön, and M. Jansen. *J. Chem. Phys*, **133**:024107, 2010. 5

[67] S. Neelamraju, J. C. Schón, K. Doll, and M. Jansen. *Phys. Chem. Chem. Phys.*, **14**:1223–1234, 2012. 5

[68] K. Doll and M. Jansen. *Ang. Chem. Int. Ed.*, **50**(20):4627 – 4632, 2011. 5

[69] D. Zagorac, K. Doll, J. C. Schön, and M. Jansen. *Phys. Rev. B*, **84**:045206, 2011. 5

[70] J. Callaway. Academic Press, New York, 1974. 9

[71] M. Goldstein. *J. Chem. Phys.*, **51**:3728–3739, 1969. 9

[72] F.H. Stillinger and T. A. Weber. *Phys. Rev. A.*, **25**:978–989, 1982. 9

[73] R. S. Berry. *Chem. Rev.*, **93**:2379–2394, 1993. 9

[74] D. J. Wales. *Energy Landscapes with Applications to Clusters, Biomolecules and Glasses.* Cambridge Univ. Press, 2004. 9, 10

[75] M. Jansen. *Turning points in Solid-State, Materials and Surface Science.* RSC Publishing, Cambridge, UK, 2008. 9

[76] J. C. Schön and M. Jansen. *Int. J. Mat. Res.*, **100**:135–152, 2009. 9

[77] J. C. Schön, K. Doll, and M. Jansen. *Phys Stat. Sol. (b)*, **247**:23–39, 2010. 9

[78] M.Jansen, K. Doll, and J. C. Schön. *Acta. Cryst. A*, **66**:518–534, 2010. 9

[79] K. A. Dill, S. Bromberg, K. Yue, K. M. Fiebig, D. P. Yee, P. D. Thomas, and H. S. Chan. *Science*, **4**:561–602, 1995. 10

[80] H. Putz, J. C. Schön, and M. Jansen. *Ber. Bunsenges.*, **99**:1148–1153, 1995. 12

[81] J. C. Schön and M. Jansen. *Pauling's Legacy: Modern Modeling of the Chemical Bond.* Elsevier, Amsterdam, 1999. 12

[82] J. C. Schön. *Ber. Bunsenges.*, **100**:1388–1391, 1996. 12, 20

[83] Ž. Čančarević. *Prediction of not-yet-synthesized solids at extreme pressures, and the development of algorithms for local optimization on ab-initio level.* Phd-thesis, University of Stuttgart, Fakultät 3: Chemie, University of Stuttgart, Stuttgart, Germany, September 2006. 13

[84] J. C. Schön and P. Sibani. *J. Phys. A: Math. Gen.*, **31**:8165–8178, 1998. 12

[85] R. Horst, P. M. Pardalos, and N. V. Thoai. *Introduction to Global Optimization, Second Edition.* Kluwer Academic Publishers, 2000. 14, 15

[86] P. Y. Papalambros and D. J. Wilde. *Principles of Optimal Design: Modeling and Computation.* Cambridge University Press., Cambridge, 2000. 14, 15, 19

[87] S. Boyd and L. Vandenberghe. *Convex Optimization.* Cambridge University Press., Cambridge, 2004. 14, 15, 19

[88] T. Weise. **Global Optimization Algorithms – Theory and Application**, 2008. 15, 16, 17

[89] J. Pearl. *Heuristics: Intelligent Search Strategies for Computer Problem Solving.* The Addison-Wesley series in artificial intelligence. Addison-Wesley Pub (Sd), Boston, MA, 1984. 15

[90] C. R. Reeves V. J. Rayward-Smith, I. H. Osman and George D. Smith, editors. *Modern Heuristic Search Methods.* The Addison-Wesley series in artificial intelligence. Wiley-VCH, John Wiley & Sons, Inc., Weinheim, New York, 1996. 15

[91] Helena R. Loureno, O. Martin, and T. Sttzle. **Iterated Local Search**. In F. Glover and G. Kochenberger, editors, *Handbook of Metaheuristics*, **57** of *International Series in Operations Research & Management Science*, pages 321–353. Kluwer Academic Publishers, Norwell, MA, 2002. 15

[92] C. Blum and A. Roli. *ACM Computing Surveys*, **35**(3):268–308, 2003. 15

[93] K. Hamacher and W. Wenzel. *Phys. Rev.E*, **59**(1):938–941, 1999. 15

[94] W. Wenzel and K. Hamacher. *Phys. Rev.Lett.*, **82**(15):3003–3007, 1999. 15

[95] P. Salamon, P. Sibani, and R. Frost. *Facts, Conjectures and Improvements for Simulated Annealing*. SIAM Monographs on Mathematical Modeling and Computation. Society for Industrial and Applied Mathematics, Philadelphia, USA, 2002. 15, 17, 18

[96] A. Neumaier. **Complete Search in Continuous Global Optimization and Constrain Satisfaction**. In A. Iserles, editor, *Acta Numerica 2004*, pages 271–369. Cambridge University Press., Cambridge, 2004. 15

[97] R. Battiti and T. Gianpietro. *ORSA J Comput*, **6**:126, 1994. 15

[98] R. Storn and K. Price. *J. Global Optim*, **11**:341, 1997. 15

[99] J. Crowley. *A representation for visual information*. Phd thesis, Carnegie-Mellon University, 1981. 15

[100] M. William and M. W. S. Land. **Evolutionary Algorithms with Local Search for Combinatorial Optimization**, 1998. 15

[101] T. M. Mitchell. *Machine Learning*, **4**. McGraw-Hill, 1997. 15

[102] N. Metropolis, A. W. Rosenbluth, M. N. Rosenbluth, A. H. Teller, and E. Teller. *J. Chem. Phys.*, **21**:1087–1092, 1953. 17, 18, 44, 70

[103] J. C. Schön and M. Jansen. *Modern methods of crystal structure prediction*, **chapter 4**. Wiley VCh, Weinheim, 2011. 17, 18

[104] S. Geman and D. Geman. *IEEE T. Pattern Anal*, **6**:721–741, 1984. 17

[105] E. L. Lawler, J. K. Lenstra, A. H. G. Rinnooy Kan, and D. B. Shmoys. *The Traveling Salesman Problem: A Guided Tour of Combinatorial Optimization*. Wiley Interscience, Chichester, UK, 1985. 17

[106] D. L. Applegate, R. E. Bixby, V. Chv́atal, and W. J. Cook. *The Traveling Salesman Problem: A Computational Study*. Princeton University Press, Princeton, USA, 2006. 17

[107] L. Ingber. *Control Cybern.*, **25**:33–54, 1996. 17

[108] Sato. *Proceedings of IEEE International Conference on Computer Aided Design (ICCAD) ICCAD-97*. Washington, USA, 1997. 18

[109] J. N. Gillet and Y. Sheng. *Proceedings of the 18th Congress of the International Commission for Optics*, **3749**. 1999. 18

[110] M. Iwamatsu and Y. Okabe. *Chem. Phys. Lett.*, **399**:396400, 2004. 18

[111] D. J. Wales. *Modern methods of crystal structure prediction*, **chapter 2**. Wiley VCh, Weinheim, 2011. 18

[112] D. Delamarre and B. Virot. *RAIRO - Rech. Oper. Oper. Res.*, **32**:43–73, 1998. 18

[113] A. Möbius, A. Neklioudov, A. Diaz-Sanchez, K. H. Hoffmann, A. Fachat, and M. Schreiber. *Phys. Rev. Lett.*, **79**:4297–4301, 1997. 18

[114] A. Möbius, K.H. Hoffmann, and J. C. Schön. *Complexity, Metastability and Nonextensivity*, **37**. International School of Solid State Physics, World Scientific Singapore, 2004. 18

[115] G. Ruppeiner, J. M. Pedersen, and P. Salamon. *J. Phys. I*, **1**:455–470, 1991. 18

[116] P. Salamon, J. Nulton, J. Robinson, J. M. Pedersen, G. Ruppeiner, and L. Liao. *Comp. Phys. Comm.*, **49**:423–428, 1988. 18

[117] J. A. Chandy, S. Kim, B. Ramkumar, S. Parkes, and P. Banerjee. *IEEE Trans. Comp. Aided Des. ICS*, **16**:398–410, 1997. 18

[118] T. Zimmermann and P. Salamon. *Int. J. Comp. Math.*, **42**:21–32, 1992. 18

[119] J. Ma, D. Hsu, and J. E. Straub. *J. Chem. Phys.*, **99**:4024–4035, 1993. 18

[120] A. Roitberg and R. Elber. *J. Chem. Phys.*, **95**:9277–9287, 1991. 18

[121] J. E. Straub and M. Karplus. *J. Chem. Phys.*, **94**:6737–6739, 1990. 18

[122] J. G. Kim, Y. Fukunishi, A. Kidera, and H. Nakamura. *Chem. Phys. Lett.*, **392**:3439, 2004. 18

[123] J. Pillardy, Y. A. Arnautova, C. Czaplewski, K. D. Gibson, and H. A. Scheraga. *Proc. Nat. Acad. Sci.*, **98**:12351–12356, 2001. 18

[124] Y. H. Shi and R. Eberhart. *CEC 1998: Proceedings IEEE Congr. on evolutionary computation*, page 69, 1998. 18

[125] A. Venkatnathan and G. A. Voth. *J. Chem. Theo. Comp.*, **1**:36–40, 2005. 18

[126] T. Huber and W. F. van Gunsteren. *J. Phys. Chem.*, **102**:5937–5943, 1998. 18

[127] B. A. Berg, H. Nogushi, and Y. Okamoto. *Phys. Rev. E*, **68**:036126, 2003. 18

[128] S. G. Itoh and Y. Okamoto. *Chem. Phys. Lett.*, **400**:308–313, 2004. 18

[129] J. Kim and T. Keyes. *J. Chem. Phys.*, **121**:4237–4245, 2004. 18

[130] B. A. Berg and T. Neuhaus. *Phys. Rev. Lett.*, **68**:912, 1992. 18

[131] D. D. Frantz, D. L. Freeman, and J. D. Doll. *J. Chem. Phys.*, **93**:27692784, 1990. 18

[132] C. Tsallis. *J. Stat. Phys.*, **52**:479–487, 1988. 18

[133] C. Tsallis and S. A. Stariolo. *Physica A*, **233**:395–406, 1996. 18

[134] G. Dueck and T. Scheuer. *J. Comp. Phys.*, **90**:161–175, 1990. 18

[135] P. Salamon, P. Sibani, and R. Frost. *Facts, Conjectures, and Improvements for Simulated Annealing.* SIAM Monographs, Philadelphia, 2002. 18

[136] F. Glover, E. Taillard, and E. Taillard. *Ann. Oper. Res.*, **41**:1–28, 1993. 18

[137] F. Glover. *Comput. Oper. Res.*, **13**(5):533, 1986. 18

[138] P. Hansen. *In Talk presented at the Congress on Numerical Methods in Combinatorial Optimization.* Academic Press, Capri, Italy, 1986. 18

[139] F. Glover. *J. Comput.*, **1(3)**:190 – 206, 1989. 18

[140] F. Glover. *J. Comput.*, **2(1)**:190 – 206, 1990. 18

[141] D. de Werra and A. A. Hertz. *OR Spektrum*, **11**:131–141, 1989. 18

[142] Roberto Battiti. **The Reactive Tabu Search**, 1994. 18

[143] D. Cvijovic and J. Klinowski. *Science*, **267**:664–666, 1995. 18

[144] M. Ji and J. Klinowski. *Proc. Roy. Soc. A*, **462**:3613–3627, 2006. 18

[145] D. Cvijović and J. Klinowski. *Science*, **267**(5198):664 – 666, 1995. 18

[146] S. Goedecker. *J. Chem. Phys.*, **120**:9911–9917, 2004. 18

[147] T. Huber, A. Torda, and W. F. van Gunsteren. *J. Comput. Aided Mol. Des.*, **8**:695–708, 1994. 18

[148] Z. Zhu, M. E. Tuckerman, S. O. Samuelson, and G. J. Martyana. *Phys. Rev. Lett.*, **88**:100201, 2002. 18

[149] W. Wenzel and K. Hamacher. *Phys. Rev. Lett.*, **82**:3003–3007, 1999. 18

[150] H. Merlitz and W. Wenzel. *Chem. Phys. Lett.*, **362**:271–277, 2002. 18

[151] K. Hamacher. *Europhys. Lett.*, **74**:944–950, 2006. 18

[152] K. Hamacher. *Physica A*, **378**:307–314, 2007. 18

[153] L. Cheng, W. Cai, and X. Shao. *Chem. Phys. Chem.*, **6**:261–266, 2005. 18

[154] R. J. Wawak, J. Pillardy, A. Liwo, K. D. Gibson, and H. A. Scheraga. *J. Phys. Chem. A*, **102**:2904–2918, 1998. 18

[155] G. Dueck. *J. Comp. Phys.*, **104**:86–92, 1993. 18

[156] L. Davis. *Genetic Algorithms and Simulated Annealing.* Pitman, London, 1987. 19

[157] D. E. Goldberg. *Genetic Algorithms in Search, Optimization, and Machine Learning.* Addison-Wesley Publishing Company, Reading. M.A., 1989. 19

[158] F. Jensen. *Introduction to Computational Chemistry.* John Wiley & Sons, Ltd., Chichester, 1999. 23, 25, 34

[159] C. J. Cramer. *Essentials of Computational Chemistry.* John Wiley & Sons, Ltd., Chichester, 2002. 23, 25, 28, 30

[160] Samrath L Chaplot, Ranjan Mittal, and Narayani Choudhury. *Thermodynamic Properties of Solids.* U.S. Dept. of the Interior, Bureau of Mines, 1984. 23, 36

[161] http://www.wikipedia.org/, 2012. 23, 26

[162] http://vergil.chemistry.gatech.edu/notes/, Mar 2005. 23, 24, 25

[163] R. F. W. Bader. *Atoms in Molecules: A Quantum Theory.* Oxford University Press, USA, 1994. 23, 36, 54

[164] R. S. Mulliken. *J. Chem. Phys.*, **23**(10):1833–1840, 1955. 23, 35

[165] M. Born and R. Oppenheimer. *Ann. Phys. (Leipzig)*, **84**, 1927. 24

[166] A. Szabo and N. S. Ostlund. *Modern Quantum Chemistry.* Free Press, New York, 1983. 25, 28, 30, 46

[167] I. N. Levine. *Quantum Chemistry.* Prentice Hall, Englewood Cliffs, New Jersey, 1991. 25, 28, 30

[168] C. C. J. Roothaan. *Rev. Mod. Phys.*, **32**:179–185, 1960. 25

[169] T. D. Crawford, H. F. Schaefer, and T. J. Lee. *J. Chem. Phys.*, **105**(3):1060–1069, 1996. 25

[170] J. A. Pople and R. K. Nesbet. *J. Chem. Phys.*, **22**(3):571–572, 1954. 25

[171] R. S. Mulliken. *Science*, **157**(3784):13–24, 1967. 26, 28

[172] J. E. Huheey. *Inorganic Chemistry.* Harper and Row Publishers, New York, USA, 3rd edition, 1983. 26, 28

[173] E. R. Davidson and D. Feller. *Chem. Rev.*, **86**(4):681–696, 1986. 28, 30

[174] A. R. Leach. *Molecular Modelling:*. Free Press, Singapore, 1996. 28, 30

[175] W. J. Hehre. *A Guide to Molecular Mechanics and Quantum Chemical Calculations*. Wavefunction, Inc., Irvine, California, 1996. 28, 30

[176] D. Moran, A. C. Simmonett, F. E. Leach, W. D. Allen, P. v. R. Schleyer, and H. F. Schaefer. *Journal of the American Chemical Society*, **128**(29):9342–9343, 2006. 28, 30

[177] D. S. Sholl and J. A. Steckel. *Density Functional Theory: A Practical Introduction*. Wiley-VCH, John Wiley & Sons, Inc., Weinheim, New York, 2009. 28, 30

[178] N. Argaman and G. Makov. *Am. J. Phys.*, **68**(1):69–79, 2000. 28

[179] P. Hohenberg and W. Kohn. *Phys. Rev. B*, **136**:864–871, 1964. 28

[180] W. Kohn and L. J. Sham. *Phys. Rev. A*, **140**:1133–1138, 1965. 28

[181] R. Dovesi. **Total Energy and Related Properties**. In C.Pisani, editor, *Quantum-Mechanical Ab-initio Calculation of the Properties of Crystalline Materials*, **67** of *Lecture Notes in Chemistry*. Springer-Verlag, Berlin Heidelberg New York, 1996. 29, 30

[182] C. Pisani, editor. *Quantum-Mechanical Ab-initio Calculation of the Properties of Crystalline Materials*, **67** of *Lecture Notes in Chemistry*. Springer-Verlag, Berlin Heidelberg New York, 1996. 29, 30

[183] R. Dovesi, B. Civalleri, R. Orlando, C. Roeti, and V. R. Sounders. *Ab Initio Quantum Simulation in Solid State Chemistry*, **21** of *Reviews in Computational Chemistry*. Wiley-VCH, John Wiley & Sons, Inc., Weinheim, New York, 2005. 29, 30, 48

[184] R. Dovesi, R. Orlando, B. Civalleri, C. Roeti, V. R. Sounders, and C. M. Zicovich-Wilson. *Z. Kristalogr.*, **220**:571–573, 2005. 29, 30, 46

[185] J. P. Perdew. *Electronic Structure of Solids 91*, **17**. Akademie Verlag, Berlin, 1991. 30

[186] J. P. Perdew, J. A. Chevary, S. H. Vosko, K. A. Jackson, M. R. Pederson, D. J. Singh, and C. Fiolhais. *Phys. Rev. B*, **46**:6671–6687, 1992. 30

[187] J. P. Perdew, K. Burke, and M. Ernzerhof. *Phys. Rev. Lett.*, **77**:3865–3868, 1996. 30

[188] J. A. Pople and R. K. Nesbet. *Journal of Chemical Physics*, **22**:571, 1954. 30

[189] J. C. Slater. *Phys. Rev.*, **36**:57–64, 1930. 31

[190] D. Belki and H. S. Taylor. *Phys. Scripta*, **39**(2):226, 1989. 31

[191] S. A. Cruz, C. Cisneros, and I. Alvarez. *Phys. Rev. A*, **17**:132–140, 1978. 31

[192] I. I. Guseinov. *Int. J. Quan. Chem.*, **90**(1):114–118, 2002. 31

[193] *Int. J. Quan. Chem.*, **57**(4):801–810, 1996. 31

[194] P. M.W. Gill. **25** of *Advances in Quantum Chemistry*, pages 141 – 205. Academic Press, 1994. 31

[195] S. F. Boys. *Proceedings of the Royal Society of London. Series A, Mathematical and Physical Sciences*, **200**(1063):542 – 554, 1950. 31

[196] L. E. McMurchie and E. R. Davidson. *J. Comput. Phys.*, **26**(2):218 – 231, 1978. 31

[197] J. A. Pople and W. J. Hehre. *J. Comput. Phys.*, **27**(2):161 – 168, 1978. 31

[198] S. Obara and A. Saika. *J. Chem. Phys.*, **84**(7):3963–3974, 1986. 31

[199] P. M .W. Gill and J. A. Pople. *Int. J. Quan. Chem.*, **40**(6):753–772, 1991. 31

[200] K. G. Dyall. *Theor. Chem. Acc.*, **112**:403–409, 2004. 31, 32

[201] W. J. Hehre, L. Random, P. v. R. Schleyer, and J. A. Pople. *Ab Initio Molecular Orbital Theory.* Wiley, New York, 1986. 31, 32

[202] J. Almlof, T. Helgaker, and P. R. Taylor. *J. Phys. Chem.*, **92**(11):3029–3033, 1988. 32

[203] Jr. T. H. Dunning. *J. Chem. Phys.*, **90**(2):1007–1023, 1989. 32

[204] C. Herring. *Phys. Rev.*, **57**:1169–1177, 1940. 32

[205] J. Callaway. *Phys. Rev.*, **97**:933–936, 1955. 32

[206] J. C. Slater. *Phys. Rev.*, **51**:846–851, 1937. 33

[207] R. M. Martin. *Electronic Structure : Basic Theory and Practical Methods.* Cambridge University Press, 2005. 33

[208] J. C. Slater. *Phys. Rev.*, **92**:603–608, 1953. 33

[209] H. Hellmann. *J. Chem. Phys.*, **3**(1):611, 1935. 34

[210] H. Hellmann and W. Kassatotschkin. *J. Chem. Phys.*, **4**(5):324–325, 1936. 34

[211] Volker Heine. **The Pseudopotential Concept**. **24**. Academic Press, 1970. 34

[212] I. G. Csizmadia. *Theory and Practice of MO Calculations on Organic Molecules*. Elsevier, Amsterdam, 1976. 35

[213] A. R. Leach. *Molecular Modelling: Principles and Applications*, **2nd**. Prentice Hall, London, 2001. 35

[214] K. I. Ramachandran, G. Deepa, and K. Namboori. *Computational Chemistry and Molecular Modeling Principles and Applications*. Springer-Verlag, Berlin Heidelberg, 2008. 35

[215] R. F. W. Bader. *Chem. Rev.*, **91**(5):893–928, 1991. 36, 54

[216] E. Sanville, S. D. Kenny, R. Smith, and G. Henkelman. *Journal of Computational Chemistry*, **28**(5):899–908, 2007. 36

[217] G. Henkelman, A. Arnaldsson, and H. Jonsson. *Comput. Mater. Sci.*, **36**(3):354–360, 2006. 36, 92

[218] M. Born and K. Huang. *Dynamical Theory of Crystal Lattices*. Oxford University Press, London, 1954. 38, 39

[219] G. Venkataraman, L. Feldkamp, and V.C. Sahni. *Dynamics of Perfect Crystals*. The MIT Press, Cambridge, 1975. 38, 39

[220] P. Bruesch. *Phonons: Theory and experiments I*. Springer-Verlag, Berlin, 1982. 38, 39

[221] S. L. Chaplot, R. Mittal, and N. Choudhury, editors. *Thermodynamic Properties of Solids: Experiment and Modeling*. Wiley VCh, Weinheim, 2010. 38, 39

[222] R. Hundt, J. C. Schön, A. Hannemann, and M. Jansen. *J. Appl. Cryst.*, **32**:413–416, 1999. 44, 60

[223] A. Hannemann, R. Hundt, J. C. Schön, and M. Jansen. *J. Appl. Cryst.*, **31**:922–928, 1998. 44, 60

[224] R. Hundt, J. C. Schön, and M. Jansen. *J. Appl. Cryst.*, **39**:6–16, 2006. 44

[225] R. Hundt. KPLOT: A Program for Plotting and Investigation of Crystal Structures, University of Bonn, Germany, 1979. 44, 60, 92

[226] J. Emsley. *The Elements*. Oxford University Press, Inc., Oxford, UK, 1992. 46, 54, 70, 149

[227] U. Chandra Singh and P. A. Kollman. *J. Comput. Chem.*, **5**:129–145, 1984. 46

[228] L. E. Chirlian and M. M. Francl. *J. Comput. Chem.*, **8**:894–905, 1987. 46

[229] D. S. Marynick. *J. Comput. Chem.*, **18**:955–969, 1997. 46

[230] R. Dovesi, V. R. Saunders, C. Roetti, R. Orlando, C. M. Zicovich-Wilson, F. Pascale, B. Civalleri, K. Doll, N. M. Harrison, I. J. Bush, Ph. D'Arco, and M. Llunell. *CRYSTAL2006*. Univ. Torino, Torino, 2006. 46, 53, 71

[231] G. Kresse and J. Furthmüller. *J. Comput. Mater. Sci.*, **6**:15, 1996. 46, 47, 53, 91

[232] G. Kresse and J. Furthmüller. *Phys. Rev. B.*, **55**:11169, 1996. 46, 47, 53, 91

[233] G. Kresse and J. Hafner. *Phys. Rev. B.*, **47**:558, 1993. 46, 47, 53

[234] G. Kresse and J. Hafner. *Phys. Rev. B.*, **49**:14251, 1994. 46, 47, 53

[235] http://cms.mpi.univie.ac.at/vasp/vasp. 47

[236] F. D. Murnaghan. *Proc. Nat. Acad. Sci.*, **30**:244–247, 1944. 49, 50

[237] A. Togo, F. Oba F, and I. Tanaka. *Phys. Rev. B*, **78**:134106, Oct 2008. 50

[238] A. Togo. *Phonopy*. Kyoto University, Sakyo, 2008. 51

[239] H.C. Hsueh, M.C. Warren, H. Vass, G.J. Ackland, S.J. Clark, and J. Crain. *Phys. Rev. B*, **53**:14806–14817, 1996. 50

[240] M. Born and J. E. Mayer. *Z. Phys. A Hadrons and Nuclei*, **75**:1–18, 1932. 53

[241] R. A. Buckingham. *Proc. R. Soc. A*, **168**(933):264–283, 1938. 53

[242] C. S. Barrett. *Phys. Rev.*, **72**:245–245, 1947. 57, 64

[243] C. S. Barrett and O. R. Trautz. *Trans. Am. Inst. Mining Metall. Petrol. Eng.*, **175**:579, 1948. 57, 64

[244] C. S. Barrett. *Acta Crystallogr.*, **9**:671–245, 1956. 57, 64

[245] A. W. Overhauser. *Phys. Rev. Lett.*, **53**:64–65, 1984. 57

[246] H. G. Smith. *Phys. Rev. Lett.*, **58**:1228–1231, 1987. 57

[247] H. G. Smith, R. Berliner, and J. Trivisonno. *Phys. Rev. B*, **49**:8547–8551, 1994. 57

[248] G. Ernst, C. Artner, O. Blaschko, and G. Krexner. *Phys. Rev. B*, **33**:6465–6469, 1986. 57

[249] A. Y. Liu and M. L. Cohen. *Phys. Rev. B*, **44**:9678–9684, 1991. 58

[250] J. Tuoriniemi, K. Juntunen-Nurmilaukas, J. Uusvuori, E. Pentti, A. Salmela, and A. Sebedash. *Nature*, **447**:187 – 189, 2007. 58

[251] J. B. Neaton and N. W. Ashcroft. *Nature (London)*, **400**:141, 1999. 58

[252] N. E. Christensen and D. L. Novikov. *Solid State Commun.*, **119**(89):477 – 490, 2001. 58

[253] M. Hanfland, K. Syassen, N. E. Christensen, and D. L. Novikov. *Nature (London)*, **408**:174, 2000. 58

[254] Y. Ma, , A. R. Oganov, and Yu Xie. *Phys. Rev. B*, **78**:014102, 2008. 58

[255] V G Vaks, M I Katsnelson, V G Koreshkov, A I Likhtenstein, O E Parfenov, V F Skok, V A Sukhoparov, A V Trefilov, and A A Chernyshov. *J. Phys.-Condens. Mat.*, **1**(32):5319, 1989. [link]. 58

[256] V. V. Struzhkin, W. Gan, H-K. Mao, and R. J. Russell. *Science*, **298**:1213 – 1215, 2001. 58

[257] A. F. Goncharov, V. V. Struzhkin, H-K. Mao, and R. J. Hemley. *Phys. Rev. B*, **71**:184114, 2005. 58

[258] C. J. Pickard and R. J. Needs. *Phys. Rev. Lett.*, **102**:146401, 2009. 58

[259] Y. Yao, J. S. Tse, and D. D. Klug. *Phys. Rev. Lett.*, **102**:115503, 2009. 58

[260] R. Rousseau, K. Uehara, D. D. Klug, and J. S. Tse. *Chem. Phys. Chem.*, **6**(9):1703–1706, 2005. 58

[261] J. S. Tse, D. D. Klug, and T. Iitaka. *Phys. Rev. B*, **73**:212301, 2006. 58

[262] C. L. Guillaume, E. Gregoryanz, O. Degtyareva, M. I. McMahon, M. Hanfland, S. Evans, M. Guthrie, S. V. Sinogeikin, and H-K. Mao. *Nat. Phys.*, **7**:211, 2011. 58, 59

[263] M. Marqués, M. I. McMahon, E. Gregoryanz, M. Hanfland, C. L. Guillaume, C. J. Pickard, G. J. Ackland, and R. J. Nelmes. *Phys. Rev. Lett.*, **106**:095502, 2011. 58, 59

[264] K. Shimizu, H . Ishikawa, D. Takao, T. Yagi, and K. Amaya. *Nature*, **447**:597 – 599, 2002. 58

[265] T. Matsuoka, S. Onoda, M. Kaneshige, Y. Nakamoto, K. Shimizu, T. Kagayama, and Y. Ohishi. *J. Phys.: Conference Series*, **121**(5):052003, 2008. 58

[266] J. C. Schön and M. Jansen. *Int. J. Mat. Res.*, **100**:135–152, 2009. 60

[267] R. Dovesi, V. R. Saunders, C. Roetti, R. Orlando, C. M. Zicovich-Wilson, F. Pascale, B. Civalleri, K. Doll, N. M. Harrison, I. J. Bush, Ph. D'Arco, and M. Llunell. *CRYSTAL2009.* Univ. Torino, Torino, 2006. 60

[268] K. Doll, V. R. Saunders, and N. M. Harrison. *Int. J. Quantum Chem.*, **82**:1–13, 2001. 60, 71

[269] K. Doll, R. Dovesi, and R. Orlando. *Theor. Chem. Acc.*, **122**(5-6):394–402, 2004. 60, 71

[270] K. Doll, N. M. Harrison, and V. R. Saunders. *J. Phys.-Condens. Mat.*, **11**:5007, 1999. 60, 63

[271] H. Hartmann, F. Ebert, and O. Bretschneider. *Z. Anorg. Allg. Chem.*, **198**(1):116–140, 1931. 61

[272] G. Hägg and N. Schönberg. *Acta Cryst.*, **7**:351, 1954. 63

[273] C. L. Chen, T. Nagase, and H. Mori. *J. Mater. Sci.*, **44**:1965–1968, 2009. 63

[274] M. H. F. Sluiter. *Acta Materialia*, **55**:3707, 2007. 63

[275] R. Berliner, O. Fajen, H. G. Smith, and R. L. Hitterman. *Phys. Rev. B*, **40**:12086–12097, 1989. 64

[276] B. Olinger and J. W. Shaner. *Science*, **219**:1071–1072, 1983. 64

[277] A. P. Frolov and K. P. Rodionov. *Fiz. Tverd. Tela.*, **16**:2297, 1974. 64

[278] P. Staikov, A. Kara, and T. S. Rahman. *J. Phys.-Condens. Mat.*, **9**:2135, 1997. 63, 65

[279] B.T. Matthias, V.B. Compton, and E. Corenzwit. *J. Phys. Chem. Solids*, **19**(12):130 – 133, 1961. 65

[280] A. Togo, , F. Oba, and I. Tanaka. *Phys. Rev. B*, **78**:134106, 2008. 65

[281] K. Parlinski, Z. Q. Li, and Y. Kawazoe. *Phys. Rev. Lett.*, **78**:4063–4066, 1997. 65

[282] G. Kresse and J. Furthmüller. *Comp. Mat. Sci.*, **5**:15, 1996. 65

[283] *Kirk-Othmer Encyclopedia of Chemical Technology*. John Wiley and Sons, Inc., New York, USA, 3 edition, 1978. 69

[284] Gregg Clemmer. *American Miners' Carbide Lamps: A Collectors Guide to American Carbide Mine Lighting*. Westernlore Publications, 1987. 69

[285] N. N. Greenwood and A. Earnshaw. *Chemistry of the Elements*. Butterworth-Heinemann, Oxford, 2 edition, 1997. 69

[286] K. Doll, J. C. Schon, and M. Jansen. *J. Chem. Phys.*, **133**(2):024107, 2010. 69

[287] C. Mellot-Draznek, S. Girard, G. Férey, J. C. Schön, Ž. Čančarević, and M. Jansen. *Chem. Eur. J.*, **8**:4102–4113, 2002. 69

[288] M. Knapp and U. Ruschewitz. *Chem. Eur. J.*, **7**:874–880, 2001. 69, 70, 74, 78, 93, 94

[289] ICSD-Fiz-Karlsruhe. **Inorganic Crystal Structure Database**. http://icsdweb.fiz-karlsruhe.de, 2005. 70, 81, 84, 92

[290] P. Fuentealba, L. v. Szentpaly, H. Preuss, and H. Stoll. *J. Phys. B*, **18**(7):1287–1296, 1985. 71

[291] J. Poppe. [link]. 71

[292] W. J. Hehre, R. Ditchfield, and J. A. Pople. *J. Chem. Phys*, **56**:2257–2261, 1972. 71

[293] M. Kaupp, P. v. R. Schleyer, H. Stoll, and H. Preuss. *J. Chem. Phys*, **94**:1360–1366, 1991. 71

[294] K. Doll. *Comp. Phys. Comm.*, **137**:74–88, 2001. 71

[295] K. Doll, R. Dovesi, and R. Orlando. *Theor. Chem. Acc.*, **115**(5):354–360, 2006. 71

[296] B. Civalleri, Ph. D'Arco, R. Orlando, V. R. Saunders, and R. Dovesi. *Chem. Phys. Lett.*, **348**:131–138, 2000. 71

[297] A. Kokalj. *Com. Mat. Sci.*, **28**:155–168, 2003. 72

[298] O. Reckeweg, A. Baumann, H. A. Mayer, J. Glaser, and H. J. Meyer. *Z. Anorg. Allg. Chem.*, **625**:1686–1692, 1999. 77

[299] U. Ruschewitz. *Coord. Chem. Rev.*, **244**:115–136, 2003. 77

[300] E. B. Hunt and R. E. Rundle. *J. Am. Chem. Soc.*, **73**:4777–4781, 1951. 77

[301] U. Müller. *Inorganic Structural Chemistry*. Wiley, Chichester, UK, 2 edition, 2007. 78, 110

[302] E. Ruiz and P. Alemany. *J. Phys. Chem.*, **99**:3114–3119, 1995. 81

[303] J. R. Long, R. Hoffmann, and H. J. Meyer. *Inorg. Chem.*, **31**:1734–1740, 1992. 81

[304] K. Mosegaard and M. Sambridge. *Inverse Prob.*, **18**(3):29–54, 2002. 83

[305] K. Mosegaard. *Inverse Prob.*, **14**(3):405–426, 1998. 83

[306] J. P. F. Alvarez, J. L. F. Martínez, and C. O. M. Pérez. *Math. Geosci.*, **40**(4):375–408, 2008. 83

[307] N. Armstrong and D. B. Hibbert. *Chemom. Intell. Lab. Syst.*, **92**:194–210, 2009. 83

[308] N. Armstrong and D. B. Hibbert. *Chemom. Intell. Lab. Syst.*, **92**:211–220, 2009. 83

[309] S. H. Jhi, J. Ihm, S. G. Louie, and M. L. Cohen. *Nature*, **399**:132–134, 1999. 89

[310] P. F. McMillan. *Nat. Mater.*, **1**(1):19 – 25, 2002. 89

[311] S. Yamanaka andK. I. Hotehama and H. Kawaji. *Nature*, **392**:580–582, 1998. 89

[312] M. Chhowalla and E. H. Unalan. *Nature Materials*, **4**(4):317–322, 2005. 89

[313] A. Leineweber, H. Jacobs, and S. Hull. *Inorg. Chem.*, **40**(23):5818–5822, 2001. 89

[314] Z. Wu, X. J. Chen, V. V. Struzhkin, and R. E. Cohen. *Phys. Rev. B*, **71**:214103, 2005. 89

[315] A. Simon, M. Bäcker, R. W. Henn, C. Felser, R. K. Kremer, Hj. Mattausch, and A. Yoshiasa. *Z. Anorg. Allg. Chem.*, **622**(1):123–137, 1996. 89

[316] S. Horstmann, E. Irran, and W. Schnick. *Angew. Chem., Int. Ed. Engl.*, **36**(17):1873–1875, 1997. 89

[317] M. L. Maquene. *Bull. Soc. Chim. Belg*, **7**:366–373, 1892. 89

[318] S. M. Ariya and E. A. Prokof'eva. *Sbornik Statei Obshchei Khim., Akad. Nauk SSSR*, **1**:9 – 18, 1953. 89

[319] S. M. Ariya and E. A. Prokof'eva. *A. Chem. Zbl.*, page 14290, 1956. 89

[320] G. V. Vajenine, G. Auffermann, Y. Prots, W. Schnelle, R. K. Kremer, A. Simon, and R. Kniep. *Inorg. Chem.*, **40**(19):4866–4870, 2001. 89

[321] G. Auffermann, Y. Prots, and R. Kniep. *Angew. Chem. Int. Ed.*, **40**(3):547–549, 2001. 89

[322] R. Weihrich, S. F. Matar, E. Betranhandy, and V. Eyert. *Solid State Sci.*, **5**(5):701 – 703, 2003. 90

[323] R. Weihrich, V. Eyert, and S.F. Matar. *Chem. Phys. Lett.*, **373**(5-6):636 – 641, 2003. 90

[324] D. M. Teter and R. J. Hemley. *Science*, **271**(5245):53–55, 1996. 90

[325] A.Y. Liu and M. L. Cohen. *Science*, **245**(4920):841–842, 1989. 90

[326] M. Mattesini and S.F. Matar. *Solid State Sci.*, **3**(7):943 – 957, 2001. 90

[327] J. von Appen, M. W. Lumey, and R. Dronskowski. *Angew. Chem. Int. E.*, **45**(26):4365 – 4368, 2006. [link]. 90

[328] J. C. Crowhurst, A. F. Goncharov, B. Sadigh, C. L. Evans, P. G. Morrall, J. L. Ferreira, and A. J. Nelson. *Science*, **311**(5765):1275 – 1278, 2006. 90

[329] E. Gregoryanz, C. Sanloup, M. Somayazulu, J. Badro, G. Fiquet, H. k. Mao, and R. J. Hemley. *Nat. Mater.*, **3**:294 – 297, 2004. 90

[330] J. C. Crowhurst, A. F. Goncharov, B. Sadigh, J. M. Zaug, D. Aberg, Y. Meng, and V. B. Prakapenka. *J. Mater. Res.*, **23**:1–5, 2008. 90, 116

[331] J. A. Montoya, A. D. Hernandez, C. Sanloup, E. Gregoryanz, and S. Scandolo. *App. Phys. Lett.*, **90**(1):011909, 2007. 90

[332] M. Wessel and R. Dronskowski. *J. Comput. Chem.*, **31**(8):1613–1617, 2010. 90

[333] S. B. Schneider, R. Frankovsky, and W. Schnick. *Angew. Chem. Int. Ed.*, **51**(8):1873 – 1875, 2012. 90, 91

[334] M. Wessel and R. Dronskowski. *J. Am. Chem. Soc.*, **132**(7):2421–2429, 2010. 90, 116, 117, 118

[335] R. Yu, Q. Zhan, and L.C. DeJonghe. *Angew. Chem. Int. Ed.*, **46**(7):1136–1140, 2007. 90

[336] Y. L. Li and Z. Zeng. *Chem. Phys. Lett.*, **474**:15, 2009. 90

[337] D. M. Teter. *MRS Bull.*, **23**(1):22–27, 1998. 90

[338] W. Chen, J. S. Tse, and J. Z. Jiang. *Solid State Commun.*, **150**(3-4):181–186, 2010. 90

[339] X. Zhang, A. Zunger, and G. Trimarchi. *J. Chem. Phys.*, **133**(19):194504, 2010. 90

[340] C. Despretz. *Ann. Chim. Phys.*, **42**:122, 1829. 91

[341] K. H. Jack. *Proc. Roy. Soc. London Ser. A*, **208**(1093):200 – 215, 1951. 91

[342] H. Jacobs, D. Rechenbach, and U. Zachwieja. *Journal of Alloys and Compounds*, **227**(1):10 – 17, 1995. 91

[343] K. H. Jack. *Proc. Roy. Soc. London Ser. A*, **195**(1040):34 – 40, 1948. 91

[344] M. Wessel and R. Dronskowski. *Chem. Eur. J.*, **17**(9):2598–2603, 2011. 91

[345] G. Kresse and J. Hafner. *Phys. Rev. B*, **49**:14251–14269, 1994. 91

[346] G. Kresse and J. Hafner. *Phys. Rev. B*, **47**:558 – 561, Jan 1993. 91

[347] J. P. Perdew, K. Burke, and M. Ernzerhof. *Phys. Rev. Lett.*, **77**:3865 – 3868, 1996. 92

[348] P. E. Blöchl. *Phys. Rev. B*, **50**:17953 – 17979, 1994. 92

[349] A. Kulkarni, K. Doll, J. C. Schön, and M. Jansen. *J. Phys. Chem. B*, **114**:15573–15581, 2010. 93, 106, 110

[350] M. Xu, S. Wang, G. Yin, J. Li, Y. Zheng, L. Chen, and Y. Jia. *Applied Physics Letters*, **89**(15):151908, 2006. 110

Part VI

Appendix

Appendix A

Ionic radii

Table A.1: Ionic radii and ionization potential for lithium and calcium as function of charge.

Ionic radii and ionization potential for lithium and calcium as function of charge. (226)

neme of the element	charge	ionic radii in Å	ionization energy in eV
Li	-1.0	1.52	-0.618
	0.0	1.23	0.0
	1.0	0.78	5.39
Ca	-2.0	1.97	100000.0
	-1.0	1.97	100000.0
	0.0	1.74	0.0
	1.0	1.41	6.111
	2.0	1.06	17.98

Table A.2: Ionic radii and ionization potential for carbon, nitrogen, lanthanum, and titanium as function of charge.

neme of element	charge	ionic radii in Å	ionization energy in eV
C	-4.0	2.6	25.0
	-3.0	2.1	15.0
	-2.0	1.6	5.0
	-1.0	0.7	-1.263
	0.0	0.7	0.0
	1.0	0.6	11.26
	2.0	0.43	35.63
	3.0	0.3	83.47
	4.0	0.18	147.94
N	-3.0	1.4	21.6
	-2.0	1.2	8.2
	-1.0	1.0	-0.07
	0.0	0.71	0.0
	1.0	0.25	14.54
La	0.0	1.88	0.0
	1.0	1.69	5.574
	2.0	1.42	16.628
	3.0	1.22	35.794
	4.0	1.10	85.72
Ti	-1.0	2.0	-0.079
	0.0	1.44	0.0
	1.0	1.32	6.83
	2.0	0.86	20.46
	3.0	0.69	48.6
	4.0	0.61	91.84

Appendix B

Basis set for lithium and carbon

Table B.1: Besis set for lithium in CRYSTAL09 input format

3	3			
0	0	6	2.	1.
840.0	0.00264			
217.5	0.00850			
72.3	0.0335			
19.66	0.1824			
5.044	0.6379			
1.5	1.0			
0	1	1	1.	1.
0.514	1.0	1.0		
0	1	1	0.	1.
0.15	1.0	1.0		

Table B.2: Besis set for carbon

6	3			
0	0	6	2.0	1.0
.3047524880D+04	.1834737130D-02			
.4573695180D+03	.1403732280D-01			
.1039486850D+03	.6884262220D-01			
.2921015530D+02	.2321844430D+00			
.9286662960D+01	.4679413480D+00			
.3163926960D+01	.3623119850D+00			
0	1	3	4.0	1.0
7.868272350	-0.1193324200	0.06899906660		
1.881288540	-.1608541520	0.3164239610		
0.5442492580	1.143456440	0.7443082910		
0	1	1	0.0	1.0
.1687144782	1.000000000	1.000000		

Appendix C

Pseudopotential for Calcium

Table C.1: Pseudopotential for carbon in CRYSTAL09 input format

220	1				
2.	0	1	1	1	0
0.898000	12.466000	0			
0.548000	5.146000	0			
1.119000	-7.709000	0			
0	0	2	2.0	1	
0.8382650	0.1068310				
0.4323130	-0.3872400				

Appendix D

List of publications

A. Kulkarni, K. Doll, J. C. Schön, and M. Jansen, "Structure prediction of binary pernitride compounds MN_2 (M = Ca, Sr, Ba, La, and Ti)" (in preparation)

A. Kulkarni, K. Doll, D. L. V. K. Prasad, J. C. Schön, and M. Jansen, "Alternative structure predicted for lithium at ambient pressure", Phys. Rev. B, **84**, 172101 (**2011**)

A. Kulkarni, K. Doll, J. C. Schön, and M. Jansen, "Global exploration of the enthalpy landscape of calcium carbide", J. Phys. Chem. B, **114**, 15573 (**2010**)

Part VII

Formalia

Eidesstattliche Versicherung

Ich versichere hiermit an Eides Statt, dass ich die vorliegende Arbeit selbständig verfasst und die verwendeten Hilfsmittel angegeben habe.

Curriculum Vitae

Personal Data

Name	Aniket Kulkarni
Date of Birth	08.08.1980
Place of birth	Ratnagiri
Maritual Status	Single

Schooling

1990 – 1996	NMV High School, Pune, India
1996 – 1998	S P College, Pune, India

University studies

1998 – 2002	**B.S in Physics** University of Pune (UoP), Maharashtra, India
2002 – 2006	**M.S in Physics** University of Pune (UoP), Maharashtra, India
2008 – 2012	**Ph.D. in Chemistry** Max-Planck-Institute for Solid State Research, Stuttgart, Germany

Work Experience

Jan – Dec 2007	**Research and Development Assistant** Jawaharlal Nehru Centre for Advanced Scientific Research Bangalore (India)
Sep – Dec 2006	**Project Student** Department of Physics, University of Pune (UoP), Pune (India)
Jun – Aug 2006	**Project Student** Persistent Systems Pvt. Ltd., Pune (India)